THE
PHYSICAL REVIEW
A Journal of Experimental and Theoretical Physics Established by E. L. Nichols in 1893
VOL. 60, NO. 10 NOVEMBER 15, 1941 SECOND SERIES

The Scattering of Fast Neutrons by Lead

HENRY F. DUNLAP* AND ROBERT N. LITTLE
Rice Institute, Houston, Texas
(Received July 10, 1941)

The scattering of D-D neutrons by lead has been investigated with a cloud chamber. The energy distribution of the inelastically scattered neutrons has been determined from 0.6 to 2.0 Mev, and it has been found that the distribution does not agree with the theoretical predictions of Weisskopf, and of Weisskopf and Ewing. The cross section for inelastic scattering has been determined, and is $1.31\pm0.53\times10^{-24}$ cm^2. It has been shown that elastic scattering is not spherically symmetric, and is very small for angles greater than about 50°.

IT has been known for several years that many elements emit gamma-rays when they are bombarded by fast neutrons, and it has been shown that, at least in some cases, these are due to the inelastic scattering of the neutrons as they traverse the scatterer.[1–5] The cross section for this gamma-ray production has been obtained by Lea, by Gibson, Grahame, and Seaborg, by Kikuchi, Aoki, and Husimi, and by Nonaka.[1,2,4,5] The first two experiments were performed with the nonhomogeneous neutrons from the Ra-Be reaction, while Kikuchi and collaborators, and Nonaka, have used the more nearly homogeneous neutrons from the deuteron-deuteron reaction. The cross section for gamma-ray production might be taken as a measure of the cross section for inelastic scattering. However, in some inelastic collisions—particularly those in which the high energy (14-Mev) neutrons from the Ra-Be source are involved—the residual nucleus may decay to the ground state by emitting several gamma-rays. Therefore a cross section for gamma-ray production is likely to be larger than a corresponding cross section for inelastic scattering. It was one purpose of the present experiments to determine by a somewhat more direct method a value for the inelastic scattering cross section of fast monochromatic neutrons falling on lead.

Recently, several authors have proposed theories of the interaction of energetic particles with a heavy nucleus which are based on thermodynamical considerations, treating the nucleus as a liquid drop.[6,7] According to Weisskopf,[6] monochromatic fast neutrons which have been scattered inelastically by a heavy element should exhibit a distribution of energies approximately Maxwellian. If the energy of the neutrons is initially P, the mean energy of the scattered neutrons should be given by $2(aP)^{\frac{1}{2}}$, where the constant "a" may be regarded as the average distance between the lowest levels of the scat-

* At present at Carnegie Institute, Department of Terrestrial Magnetism, Washington, D. C.
[1] D. E. Lea, Proc. Roy. Soc. **A150**, 637 (1935).
[2] Seaborg, Gibson, and Grahame, Phys. Rev. **52**, 408 (1937).
[3] D. C. Grahame and G. T. Seaborg, Phys. Rev. **53**, 795 (1938).
[4] Kikuchi, Aoki, and Husimi, Proc. Phys. Math. Soc. Japan **18**, 727 (1936).
[5] I. Nonaka, Phys. Rev. **59**, 681 (1941).
[6] V. Weisskopf, Phys. Rev. **52**, 295 (1937).
[7] V. Weisskopf and D. H. Ewing, Phys. Rev. **57**, 472 (1939).

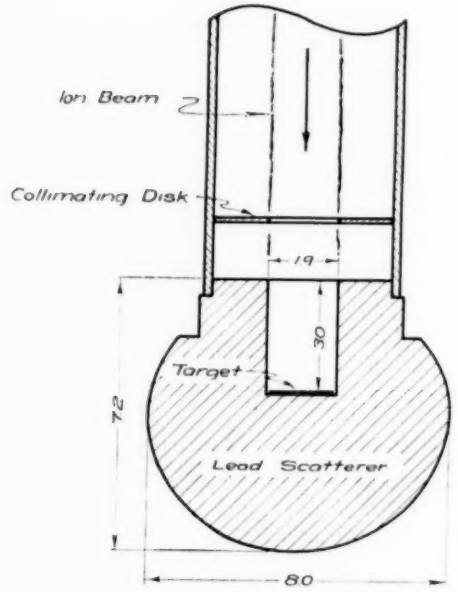

FIG. 1. Neutron source and scatterer. Dimensions are in cm. Cloud chamber 24 cm to right.

tering nucleus. The energy distribution of the inelastically scattered neutrons should be given by $N \leqq KEe^{-E/T}$, where N is the number of neutrons per unit energy interval emitted at energy E, K is a constant, e is the base of the natural logarithms, and T is the temperature of the residual nucleus after the neutron has been emitted. The value of T is given by the equation $T=(aP)^{\frac{1}{2}}=\frac{1}{2}E_{\text{mean}}$. Hence if the distribution of the inelastically scattered neutrons is determined experimentally, T may be determined from the mean energy of this distribution, and the theoretical relation compared with that obtained by experiment.

The other purpose of the experiments to be described was to determine the energy distribution of the neutrons inelastically scattered by lead, so as to test the above theory, and to determine the important quantity "a" for a lead nucleus.

It should be remarked that in Weisskopf's first paper,[6] the restriction was made that the incident neutrons should have a kinetic energy greater than or equal to 3 Mev. However, in a later paper by Weisskopf and Ewing,[7] the restriction was lowered to include neutrons with incident energies as low as 1 Mev. The neutrons used in the present experiments had a range of energies from 2.19 to 2.89 Mev, so this condition was well met.

EXPERIMENT

Deuterons of 100 kv were obtained with a Cockcroft-Walton voltage doubler. They bombarded a thick target of heavy paraffin wax surrounded by a lead scatterer as shown in Fig. 1. Some of the neutrons which passed through the lead produced recoil protons in a cloud chamber, placed at 90° to the deuteron beam, and with its center 30.8 cm from the center of the target. The cloud chamber, which was of light construction, had a diameter of 13.5 cm, an effective (illuminated) depth of 4 cm, and was mounted so that the axis of the chamber was parallel to the deuteron beam. Care was taken to stand well away from the chamber during expansions. No magnetic analysis was used on the deuteron beam, and with this apparatus, instantaneous unresolved deuteron currents of 400 μa were obtainable. The lengths of the recoil proton tracks, and their angles with respect to the direction of the incident neutrons, were measured. About 39,000 expansions were photographed in this work. On these photographs, 1014 recoil protons were observed which satisfied our criteria as to distinctness, and which recoiled within less than 12.5° of the direction of the incident neutrons. Our results are based on a study of these recoil protons. Of the 39,000 expansions photographed, about 23,000 were photographed with the apparatus as in Fig. 1, while the remaining 16,000 were photographed with a thin (1-mm) walled aluminum cup as the target holder.

Since theory predicts[6,7] that the neutrons will suffer large energy losses in inelastic collisions, the cloud chamber was first filled with methane, so that its comparatively low stopping power would enable tracks of low energy to be measured. The chamber pressure was atmospheric, and the vapor employed was ethyl alcohol. The apparatus was set up as in Fig. 1, and 248 recoil protons were measured in methane. The stopping power of the methane was then obtained by inserting a Th C′ source, and measuring the range of the alpha-particles emitted, whose range in standard air is 8.53 cm. This gave a stopping power of 1.01. Unfortunately, the walls of the

chamber became contaminated when this source was inserted, and it was necessary to take the chamber apart and clean it. This was done, the chamber reassembled, and 107 recoil protons were observed with a thin-walled aluminum cup in place of the lead scatterer as target holder. The stopping power of this methane was obtained by using Bonner's Q value of 3.31 Mev[8] for the deuteron-deuteron reaction. Bethe and Livingston have worked out a method for computing such Q values when the stopping power is known,[9] and this method may also be used to determine the stopping power if the Q value is known. This gave a stopping power of 0.96, a difference of about 5 percent from the previous value of 1.01. Such a variation becomes understandable when it is considered that the methane used comes from the commercial gas lines, which are themselves supplied at different times by different gas wells. If it is assumed that the stopping power of 0.96 is that of a gas with no ethane present, the addition of about 7 percent of ethane would give the stopping power of 1.01. A period of about a month elapsed between the times the gas was drawn from the mains, so that a variation of this amount in the percent of ethane present is not surprising.

However, since the data on the stopping power of the methane seemed slightly ambiguous, and since the data in methane seemed to indicate that the inelastically scattered neutrons would not have as low energies as was at first thought, it was decided that further data should be taken in a cloud chamber filled with a mixture of ethane and argon at atmospheric pressure. The vapor used was ethyl alcohol. When the chamber was filled with this mixture of ethane and argon, photographs were taken on alternate days with

TABLE I. *Compilation of data.*

Neutron Energy Mev	Observed Recoils with Pb	Observed Recoils Without Pb	Corrected Recoils with Pb	Corrected and Normalized Recoils Without Pb
		Methane		
0.5–0.6	4	0	4.4	0
0.6–0.7	12	3	13.9	4.2
0.7–0.8	11	2	13.5	3.9
0.8–0.9	9	4	11.8	5.2
0.9–1.0	12	1	16.8	2.3
1.0–1.1	10	2	15.1	4.9
1.1–1.2	12	0	19.1	0
1.2–1.3	8	1	13.8	2.9
1.3–1.4	7	1	13.0	3.1
1.4–1.5	13	2	26.2	6.7
1.5–1.6	14	3	31.0	11.1
1.6–1.7	10	3	24.6	12.5
1.7–1.8	13	1	35.4	4.6
1.8–1.9	9	3	27.4	16.2
1.9–2.0	9	4	32.0	18.6
2.0–2.1	11	8	45.0	59.6
2.1–2.2	16	7	77.8	54.9
2.2–2.3	16	10	95.0	103
2.3–2.4	14	25	106	249
2.4–2.5	18	25	164	453
2.5–2.6	16	1	225	31.4
2.6–2.7	4	1	86	48.0
2.7–2.8	0	0	0	0
		Ethane and Argon		
0.7–0.8	1	1	1.2	1.0
0.8–0.9	1	8	1.2	9.3
0.9–1.0	3	3	3.9	3.4
1.0–1.1	2	4	2.8	5.6
1.1–1.2	8	4	12.0	5.1
1.2–1.3	10	1	16.0	2.2
1.3–1.4	6	6	10.1	11.2
1.4–1.5	8	4	14.3	8.0
1.5–1.6	6	3	11.4	6.9
1.6–1.7	4	1	8.3	1.8
1.7–1.8	6	1	13.3	3.1
1.8–1.9	11	6	26.4	12.3
1.9–2.0	5	7	13.3	20.0
2.0–2.1	12	4	35.3	13.1
2.1–2.2	12	9	39.3	31.9
2.2–2.3	16	16	59.1	60.5
2.3–2.4	33	41	137	179
2.4–2.5	26	50	125	230
2.5–2.6	21	12	119	59.7
2.6–2.7	2	1	13.6	5.8
2.7–2.8	1	0	8.3	0

TABLE I.—*Continued.*

Neutron Energy Mev	Observed Recoils with Pb	Observed Recoils Without Pb	Corrected Recoils with Pb	Corrected and Normalized Recoils Without Pb
		Ethane		
0.7–0.8	2	2	2.3	2.3
0.8–0.9	3	3	3.7	3.7
0.9–1.0	3	1	3.8	1.3
1.0–1.1	2	4	2.8	5.5
1.1–1.2	2	0	2.9	0
1.2–1.3	1	0	1.5	0
1.3–1.4	6	3	9.9	5.0
1.4–1.5	3	2	5.2	3.5
1.5–1.6	3	1	5.5	1.8
1.6–1.7	4	2	7.8	3.9
1.7–1.8	2	2	4.1	4.1
1.8–1.9	6	4	13.3	8.9
1.9–2.0	3	0	7.3	0
2.0–2.1	7	3	16.6	8.0
2.1–2.2	6	7	17.2	20.1
2.2–2.3	13	11	40.9	34.7
2.3–2.4	22	41	77.2	144
2.4–2.5	33	38	132	152
2.5–2.6	16	15	71.7	67.3
2.6–2.7	6	0	29.3	0
2.7–2.8	1	0	5.9	0

[8] T. W. Bonner, Phys. Rev. **59**, 237 (1941).

[9] M. R. Livingston and H. A. Bethe, Rev. Mod. Phys. **9**, 289 (1937).

the lead scatterer and with the thin-walled aluminum cup as the target holder. The stopping power of this mixture was evaluated from the distribution obtained when there was no lead scatterer around the target, Bonner's Q value of 3.31 Mev was used just as before. Since the stopping power of the mixture seemed to change slightly about halfway through this run, the data were evaluated in two parts. For the first part we obtained the stopping power 1.30, and for the second part, the stopping power 1.31. Since the stopping powers are very nearly the same, these are listed together in our results under the title ethane and argon, although the appropriate stopping power was used in evaluating each part of this run. In all, 376 recoils were observed during this run, 194 being observed when there was lead surrounding the target, and 182 when there was no lead.

These results showed that it would be desirable to use a gas with an even higher stopping power in the cloud chamber. The cloud chamber was consequently rebuilt to obtain expansion ratios high enough for ethane, and further data were taken with ethane, and ethyl alcohol and water vapor in the chamber. Data were taken on alternate days with the lead scatterer and with the aluminum cup as the target holder, and the stopping power evaluated from the distribution obtained when there was no lead scatterer around the target. In all, 283 recoils were observed at this stopping power, 144 with the lead scatterer, and 139 without it.

Altogether, 586 tracks were measured with the lead, and 428 without it.

Our results are shown in Table I. The observed and corrected numbers of tracks are shown in each energy interval. The corrections are to allow for the varying probability of observation of a track of length L in a cloud chamber whose diameter is 13.5 cm, and to allow for the variation of neutron proton collision cross section with energy. If r is the radius of the chamber, then in general, we have that

$$P=[1/\pi r^2][\pi r^2-L(r^2-L^2/4)^{\frac{1}{2}}-2r^2\sin^{-1}(L/2r)]$$

where P is the number of tracks of length L observed in the chamber of area πr^2, divided by the number of tracks of length L that would have been observed in an equal area of a chamber whose radius was infinite. The observed number of tracks is multiplied by $1/P$. The neutron proton collision cross sections were taken from the work of Kittel and Breit,[10] and the factor we have used is the reciprocal of these cross sections, normalized to 1 at 0.5 Mev. In addition, after the above corrections were made, the corrected number of tracks obtained in each energy interval without the lead was multiplied by a factor such as to make the total number of tracks with the lead, and without it, equal. For example, the corrected number of tracks observed with the lead when methane was in the chamber was 1097, and the corrected number of tracks observed without lead was 688. The number of tracks in each energy interval obtained without the lead was therefore multiplied by the factor $1097/688=1.6$, and the result listed under the column headed "corrected and normalized recoils without lead." A similar procedure was carried out for the data obtained with ethane, and with ethane and argon in the chamber. This normalizing procedure assumes that the total number of neutrons entering the cloud chamber is nearly the same with the lead as without it. The measured tracks without the lead scatterer are mainly due to

TABLE II. *Total data, corrected and normalized.*

Neutron Energy Mev	Corrected Recoils with Pb	Normalized and Corrected Recoils Without Pb
0.5–0.6	4.4	0
0.6–0.7	13.9	4.2
0.7–0.8	17.0	7.2
0.8–0.9	16.7	18.2
0.9–1.0	24.5	7.0
1.0–1.1	20.7	16.0
1.1–1.2	34.0	5.1
1.2–1.3	31.3	5.1
1.3–1.4	33.0	19.3
1.4–1.5	45.7	18.2
1 5–1.6	47.9	19.1
1.6–1.7	40.7	18.2
1.7–1.8	52.8	11.8
1.8–1.9	67.1	37.4
1.9–2.0	52.6	38.6
2.0–2.1	96.9	80.7
2.1–2.2	134	107
2.2–2.3	195	198
2.3–2.4	320	572
2.4–2.5	421	835
2.5–2.6	416	158
2.6–2.7	129	53.8
2.7–2.8	14.2	0

[10] C. Kittel and G. Breit, Phys. Rev. **56**, 747 (1939).

neutrons coming directly from the source, but include some scattered by the aluminum cup and other bodies in the neighborhood. If we neglect neutrons scattered by the walls of the aluminum cup, the above assumption would be true if the lead scattered as many neutrons into the chamber as out of it. This is believed to be the case for elastically scattered neutrons, since as will be shown later they are mostly scattered through angles less than about 50°. The non-symmetrical distribution of the neutrons emitted in the deuteron-deuteron reaction will therefore not have much effect. It is true that inelastic scattering is thought to be spherically symmetrical, but since the neutrons that have been inelastically scattered are only about 12.5 percent of the total number, the non-symmetrical distribution of the neutrons coming from the deuteron-deuteron reaction will affect the total number but slightly. The total corrected number of tracks observed with the lead was 2230 on 23,000 photographs, and the total corrected number of tracks without the lead was 1797 on 16,000 photographs. Thus the number per photograph was 0.10 with the lead, and 0.11 without it. The agreement of these numbers supports the assumption that the total corrected number of tracks is not changed by the lead scatterer.

Table II shows all of our data, which have been corrected and normalized as described above. From these data, we obtain the distribution of the neutrons inelastically scattered by the lead as follows. The numbers of tracks in each energy interval obtained without the lead were subtracted from the number obtained with the lead in the corresponding energy interval. The differences obtained in this way were taken to be the number of neutrons inelastically scattered by the lead, and are given in Table III. Above 2.0 Mev, the number cannot be obtained in this way, since the number of elastically scattered neutrons begins to be appreciable. The lowest energy which a 2.19-Mev neutron could appear to have with our measurement criteria is 2.07 Mev. Since the probable error in the energy of a track due to all causes is about 100 kv, it is fairly certain that tracks with energies below 2.0 Mev are due to neutrons that have lost energy in an inelastic collision. Although the differences listed in Table III seem to show a group structure, with several rather sharp maxima and minima, this is thought to be statistical, as the fluctuations are barely outside the probable error. The data of Table III are accordingly given graphically in Fig. 2, plotted in 200-kv intervals to smooth out statistical fluctuations. The probable errors in the points are given by the vertical bars. The distribution has been extrapolated smoothly to the origin from 0.6 Mev. Since the neutrons from the deuteron-deuteron reaction are not exactly monochromatic (ranging from 2.19 to 2.89 Mev), the incident neutrons were all assumed to have the mean energy of 2.5 Mev, and the experimental distribution extrapolated to that energy. The behavior of the experimental curve beyond 1.8 Mev is somewhat doubtful. From 1.8 to 2.0 Mev the curve does seem to drop somewhat, but the probable errors are so large in this region that it might well be doubted if this has any real significance. Consequently the possibility that the distribution continues to rise as it approaches 2.5 Mev cannot be ruled out.

TABLE III. *Distribution of inelastically scattered neutrons.*

NEUTRON ENERGY Mev	NEUTRONS INELASTICALLY SCATTERED BY THE Pb
0.5–0.6	4.4
0.6–0.7	9.7
0.7–0.8	9.8
0.8–0.9	−1.5
0.9–1.0	17.5
1.0–1.1	4.7
1.1–1.2	28.9
1.2–1.3	26.2
1.3–1.4	13.7
1.4–1.5	27.5
1.5–1.6	28.8
1.6–1.7	22.5
1.7–1.8	41.0
1.8–1.9	29.7
1.9–2.0	14.0

According to Weisskopf, this distribution should be given approximately by

$$N \leqq KEe^{-E/T}$$

where the symbols have been defined previously. This curve is also shown in Fig. 2, plotted with two different values of T. In one, T was calculated from Weisskopf's theoretical relation,

$$2T = E_{\text{mean}}.$$

Here, E_{mean} is the mean energy of the neutrons

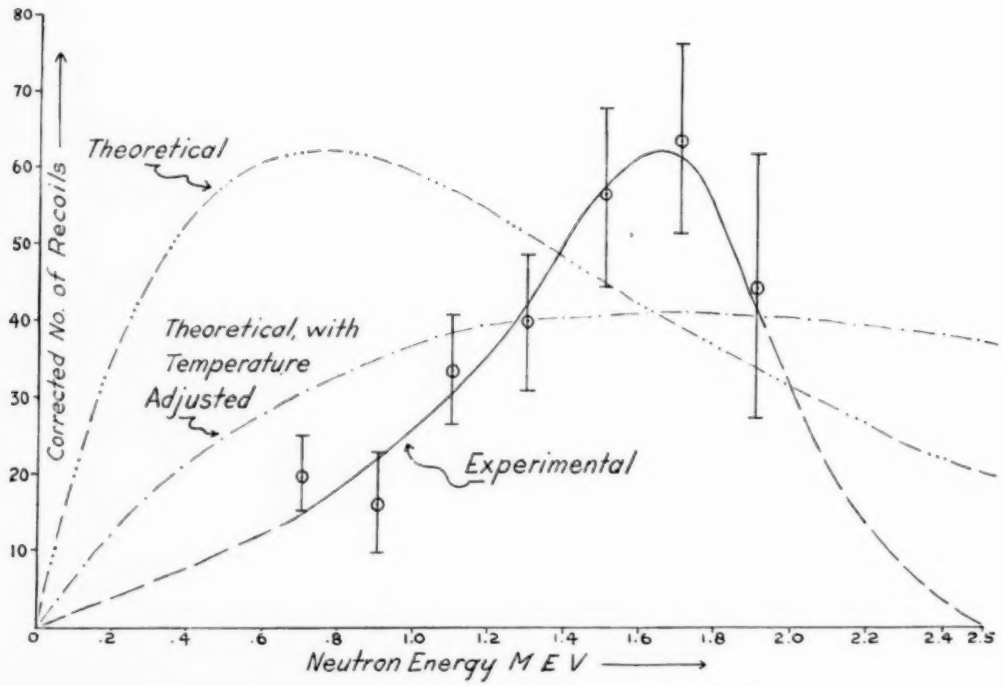

FIG. 2. Distribution of inelastically scattered neutrons.

inelastically scattered by the lead, taken to be 1.5 Mev under the assumption that the experimental distribution falls to zero as the energy approaches 2.5 Mev. In the other theoretical curve shown, T was arbitrarily adjusted so as to make the maxima of the experimental and theoretical distributions agree. The value of the constant K was also reduced by a factor of $\frac{2}{3}$ in order to come as close to all the experimental points as possible. It is interesting to note that the value of T necessary to make the maxima agree corresponds to a mean energy of the inelastically scattered neutrons of 3.4 Mev, which is larger than the energy of the incident neutrons!

In the light of the disagreement between the experimental and theoretical distributions, the value of the constant "a" seems to be of little interest. However, it was calculated from the theoretical relation

$$E_{\text{mean}}=2(aP)^{\frac{1}{2}}.$$

If P is taken as 2.5 Mev, this gives a value of "a"$=0.2$ Mev, while Weisskopf estimates that "a" should lie between 0.05 and 0.2 Mev.

It should be noted that Lea[1] has estimated that the average energy of the gamma-rays excited when Ra-Be neutrons pass through lead is of the order of 1.5 Mev, while Gibson, Grahame, and Seaborg[2] estimate that it is of the order of, or less than, 1 Mev. The mean energy of the neutrons emitted from a Ra-Be source is about 4.5 Mev,[11] so this means, that on the average, they lose about $1.3/4.5=0.29$ of their energy in an inelastic collision. This, of course, assumes that the excited nucleus loses its energy by emitting one large instead of several small gamma-rays, which may or may not be true. The mean energy of the neutron distribution we have observed comes at about 1.5 Mev, so that according to our results the neutrons should lose on the average $1.0/2.5=0.40$ of their energy. From the shape of the theoretical curve given in Fig. 2, it is evident that they should lose a much higher fraction of their energy.

If the distribution of inelastically scattered neutrons actually falls to zero at 2.5 Mev, the distribution is at least of the form expected, in spite of the fact that the most probable energy of an inelastically scattered neutron is considerably larger than thought. However, if, as seems possible from these results, the distribution

[11] J. R. Dunning, Phys. Rev. **45**, 586 (1934).

continues to rise as it approaches 2.5 Mev, the fact would have far-reaching theoretical implications. In particular, it would be difficult to reconcile such a result with the idea of the long existence of the compound nucleus. If the compound nucleus exists for a long time in comparison, say, to the transit time of the incident neutron across the nucleus, it is difficult to see how the incident neutron could be reemitted with a very high energy, since this energy would be shared by two hundred other particles. Our results could be understood, however, if the compound nucleus exists only long enough for the energy of the incident neutron to be shared by a few particles before the neutron is reemitted, with a comparatively high energy. In fact, a sort of "local heating" of the nucleus is implied both by these results, and by the gamma-ray results quoted above.

From these experiments, it is also possible to calculate the inelastic scattering cross section for 2.5-Mev neutrons from lead, provided that we assume that the scattering is spherically symmetrical. In that case, the cross section for inelastic scattering is given to a first approximation by the following formula:

$$B-A=(B-AK)e^{-nkx}. \tag{1}$$

Here, A is the corrected number of neutrons inelastically scattered by the lead (see Fig. 2); B is the corrected number of neutrons obtained when lead surrounded the target, the background having been subtracted, and the distribution from 0.6 to 0 Mev taken from Fig. 2; K is a factor arising from the asymmetry of the neutrons coming from the deuteron-deuteron reaction (to be discussed more fully later); e is the base of the natural logarithms; n is the number of lead nuclei per cc; k is the cross section for inelastic scattering; and x is the average thickness of lead through which the neutrons pass. We assume the total *number* of neutrons reaching the cloud chamber is unaffected by elastic scattering (as many scattered away from the chamber as toward it); we neglect the variation in solid angle which the chamber subtends at different parts of the scatterer (i.e., we assume that both the scattered and unscattered neutrons start at the center of the target. That this is permissible is shown by the fact that a calculation in which the single point source assumed for the scattered neutrons was replaced by four point sources symmetrically distributed in the scatterer gave a value of the inelastic scattering cross section only about 5 percent different from that obtained when a single point source at the center was assumed); and we assume that the scatterer is in the shape of a sphere, with a cylindrical hole above the target in it.

The spatial distribution of the neutrons emitted in the deuteron-deuteron reaction is given by

$$N_\theta=N_{90}(1+0.7\cos^2\theta),$$

where θ is the angle between the forward direction of the deuteron beam and the direction of the emitted neutron in a coordinate system in which the center of gravity is at rest, and N_θ is the number of neutrons emitted per unit solid angle at angle θ.[12–14] Neutrons will be scattered inelastically by the lead into the chamber from the forward and backward directions as well as at right angles to the deuteron beam. However, when the lead scatterer is not present, only neutrons emitted at right angles to the deuteron beam will reach the chamber. It is evident therefore, that the number of neutrons inelastically scattered into the chamber by the lead is larger than would be the case if the distribution of neutrons from this reaction were symmetric. To correct for this, we transform the above Eq. (1) into laboratory coordinates, and average it over the surface of a sphere from $\varphi=162.4°$ to $\varphi=0°$. The value $\varphi=180°-162.4°=17.6°$ corresponds to the angle between the center of the target, and the edge of the cylindrical cavity above the target. In laboratory coordinates, the distribution of the neutrons will be given by

$$N_\varphi=C[1+0.7\cos^2\{\varphi+\sin^{-1}(v_{c.g.}\sin\varphi/v_0)\}]\times\sin\varphi d\varphi. \tag{2}$$

Here, N_φ is the number of neutrons given off between the angles φ and $\varphi+d\varphi$, φ is the angle between the forward direction of the deuteron

[12] Kempton, Browne, and Maasdorp, Proc. Roy. Soc. **A157**, 386 (1936).
[13] Haxby, Allen, and Williams, Phys. Rev. **55**, 143 (1939).
[14] Huntoon, Ellett, Bayley, and Van Allen, Phys. Rev. **58**, 97 (1940).

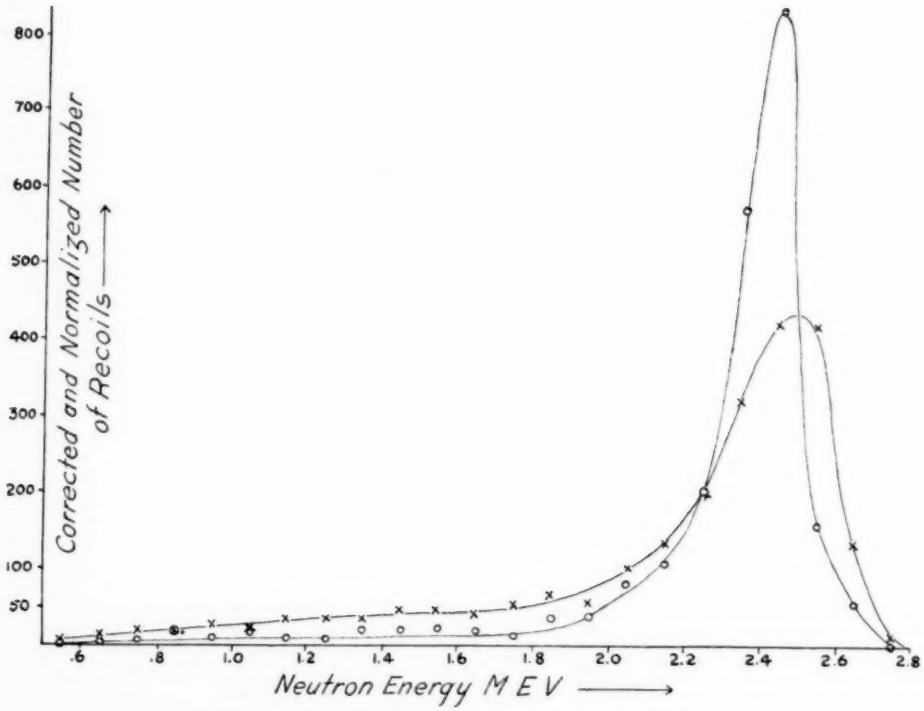

FIG. 3. x = data obtained with lead. o = data obtained without lead.

and the direction of the emitted neutron in laboratory coordinates, C is a constant, $v_{c.g.}$ is the velocity of the center of gravity of the system, easily calculated from the masses of the particles involved and the bombarding energy, v_0 is the velocity of the emitted neutron in the center of gravity system, also easily calculated from the masses and the known Q value for the reaction. The average value desired is just

$$N' = \left[\int_0^{162.4^\circ} N_\varphi\right] \Big/ \left[\int_0^{162.4^\circ} 2\pi \sin\varphi d\varphi\right]. \quad (3)$$

The numerator of Eq. (3) may be integrated after a trigonometric substitution, and we obtain the value $N' = 1.2$. The number of neutrons that would have been scattered into the chamber if the distribution had been symmetric is just $(1/1.2)A$. Hence, in Eq. (1), we subtract $(1-1/1.2)A$ from both A and B. Let $(1-1/1.2) = K$. Since KA is subtracted from both A and B, it has no effect on the left-hand side of Eq. (1). Using all the experimental results, and assuming that the distribution approaches zero as the energy approaches 2.5 Mev, we obtain the value $k = 1.31 \pm 0.53 \times 10^{-24}$ cm^2 from Eq. (1). If, however, the distribution continues to rise as the energy approaches 2.5 Mev, the value $k = 1.81 \pm .61 \times 10^{-24}$ cm^2 is obtained for the inelastic scattering cross section. These values may be compared with the value of Seaborg, Gibson, and Grahame[2] of $1.22 \pm 0.17 \times 10^{-24}$ cm^2, and the value obtained by Lea[1] of $2.16 \pm 0.22 \times 10^{-24}$ cm^2, both of which where obtained with the unhomogeneous neutrons emitted from a Ra-Be source, and while studying the gamma-rays emitted. Recently Nonaka,[5] using deuteron-deuteron neutrons of about 2.5 Mev, obtained a value of $0.63 \pm 0.2 \times 10^{-24}$ cm^2 from a study of the gamma-rays emitted from the lead scatterer. However, it should also be noted that Nonaka's value depends on an assumed efficiency of a Geiger counter. As these efficiencies depend in general upon the gamma-ray energy, which is unknown in his case, his small value may be somewhat in error.

The fact that cross sections obtained from a study of the gamma-rays emitted from the scatterer might be expected to be larger than those obtained from a direct study of the scattered neutrons (since several gamma-rays

may be emitted per inelastic collision) tends to give more weight to the assumption that the distribution falls to zero as the energy approaches 2.5 Mev, as this assumption yielded the smaller value of scattering cross section.

It is planned at present to expose some photographic plates to monochromatic 4-Mev deuteron-deuteron neutrons scattered by lead. At these higher energies, it should be possible definitely to settle the point as to whether or not the distribution of the inelastically scattered neutrons continues to rise as it approaches the energy of the incident neutrons.

Conclusions concerning elastic scattering of neutrons by lead may also be drawn from these experiments. At present, data concerning elastic scattering of neutrons by lead are scanty. Weisskopf and Ewing[7] quote some unpublished results of Bacher which indicate that at least 95 percent of the scattering of neutrons from lead is inelastic. There is some theoretical evidence that elastic scattering is especially large in the forward direction,[15] and recently a preponderance of small angle scattering of an unspecified nature has been reported.[16,17] By small angles, we mean angles under about 50°. Our data also show that considerable elastic scattering takes place, since the main group of the curve is considerably broader with the lead scatterer than with the aluminum cup. This is what would be expected if elastic scattering were appreciable, since the energy of the neutrons emitted in the deuteron-deuteron reaction depends on the angle of emission according to the following equation

$$E_n-(\sqrt{2}/2)(E_nE_i)^{\frac{1}{2}}\cos\varphi-(E_i+3Q)/4=0,$$

where E_n is the energy of the neutron which comes off at angle φ with respect to the incident deuteron in laboratory coordinates, E_i is the energy of the incident deuteron, and Q is the energy evolved in the reaction. This broadening is well shown in Fig. 3, which is a graph of the data given in Table II. Note that in addition to being broadened, the maximum of the 2.5-Mev group of neutrons is shifted appreciably to higher energies by the presence of the lead, which is again what would be expected to occur if elastic scattering took place, since there is more lead in front of the target than behind it, and since the more energetic neutrons come off in the forward direction.

The fact that the neutron spectrum does not extend beyond 2.8 Mev shows that elastic scattering cannot be spherically symmetrical. If it were, then neutrons would be scattered through angles as great as 90°, and the 2.89-Mev neutrons given off in the forward direction with respect to the deuteron beam would be able to reach the cloud chamber. On the other hand, the highest energy neutrons observed, which are 2.8-Mev, would have come off at 39° with respect to the incident deuterons. This means that elastic scattering at angles greater than $90°-39°=51°$ is not appreciable. This is in qualitative agreement with theory,[15] and also agrees with the results and Wakatuki and Kikuchi,[16,17] provided the assumption is made that the large cross sections for scattering in the forward direction which they observed are due to elastic scattering. Since they used an electroscope as the detector of their scattered neutrons, they were unable to distinguish between elastic and inelastic scattering. If this interpretation is made of the results of Wakatuki and Kikuchi, the assumption we have made that inelastic scattering is spherically symmetrical is justified, since the cross sections they observed were constant for the scattering angle greater than about 50°.

In conclusion, it is a pleasure to acknowledge the continued interest and suggestions of Professor Wilson, Professor Bonner, and Dr. Bennett, and to thank Professor Heaps for several helpful discussions of the problem. The assistance of Mr. Van der Henst and Mr. De Vries is also gratefully acknowledged.

[15] G. Placzek and H. A. Bethe, Phys. Rev. **57**, 1075 (1940).
[16] T. Wakatuki and S. Kikuchi, Proc. Phys. Math. Soc. Japan **21**, 656 (1939).
[17] T. Wakatuki, Proc. Phys. Math. Soc. Japan **22**, 430 (1940).

The Interaction of Slow Neutrons with Nuclei*

HENRY CARROLL
Pupin Physics Laboratories, Columbia University, New York, New York

(Received July 14, 1941)

The influence of the molecular binding of the proton has been investigated by measuring the total cross section per proton, for neutrons absorbed by cadmium (C neutrons), of a series of gaseous hydrocarbons of the form C_nH_{2n+2}. The measurements were also extended to include gaseous hydrogen (H_2), "ordinary" water (H_2O), and solid paraffin. The results show that the cross section per proton increases rapidly from the value for the free proton, varying roughly as the square of the reduced mass of the system. The bound proton cross section as measured for the highest hydrocarbon (paraffin) approaches a limiting value of 2.4 times that for the free proton. The dependence of neutron scattering on structure was investigated from measurements on one of the hydrocarbons, cetane ($C_{16}H_{34}$) in its liquid and solid states. The marked increase in the cross section of the liquid state over the solid state indicates that a large amount of coherent scattering must be present. The total cross sections of the deuteron in "heavy" water (D_2O), and of helium, neon, argon, krypton, oxygen, and nitrogen in the gaseous state, were also measured.

INTRODUCTION

FERMI[1] has pointed out that the proton cross section for slow neutrons should depend upon the binding of the proton within the molecular structure. For sufficiently energetic neutrons, this binding effect should disappear. The expression for neutron-proton scattering as developed by Wigner, Bethe and Peierls[2] has significance only when the proton may be considered "free," but for the slow neutrons absorbed in cadmium used in these experiments, the proton cross section is considerably larger than the "free" proton cross section and the use of this expression without modification is not valid.

The theoretical development by Fermi[1] and its extensions by Bethe[3] and Arley[4] show that the proton cross section for zero energy neutrons, calculated with the Born approximation should vary approximately as the square of the reduced mass of the system composed of the neutron and scatterer. In general, however, the above theory predicts the upper limit of the theoretically calculated cross section rather than the experimentally observed cross section, since binding effects will place some restrictions on the transfer of momentum.

Cadmium absorption neutrons (C neutrons) emerging from paraffin at room temperature ($\sim$300°K) have been shown to have energies corresponding to thermal velocities with a most probable energy of 0.025 ev.[5] As this energy is small compared to the binding energy of the protons for C neutrons, the effect of the proton binding should be large.

To investigate the effect of binding on the proton cross section,[6] a gaseous hydrocarbon series of the form C_nH_{2n+2} was selected and a systematic study of the change in cross section per proton was made as the number of protons per molecule increased. The choice of this series offered a twofold advantage in that:

(a) The series consists of substances whose chain-like molecular structure is similar.

(b) The choice of gases avoids solid state difficulties which result in interference effects from crystalline structure[7,8] and intramolecular binding. In fact, subsequent measurements on a liquid and solid hydrocarbon (cetane) show that a large change in the slow neutron cross section

* Publication assisted by the Ernest Kempton Adams Fund for Physical Research of Columbia University.

[1] E. Fermi, Ricerca Scient. **7**, 13 (1936).

[2] H. A. Bethe and R. F. Bacher, Rev. Mod. Phys. **8**, 117 (1936).

[3] H. A. Bethe, Rev. Mod. Phys. **9**, 124 (1937).

[4] N. Arley, Kgl. Danske Vid. Sels. Math.-fys. Medd. **16**, 1 (1938).

[5] Dunning, Pegram, Fink, Mitchell and Segrè, Phys. Rev. **48**, 704 (1935).

[6] A preliminary report on this work was given in Phys. Rev. **54**, 541 (1938).

[7] H. G. Beyer and M. D. Whitaker, Phys. Rev. **57**, 976 (1940).

[8] F. Rasetti, Phys. Rev. **58**, 321 (1940).

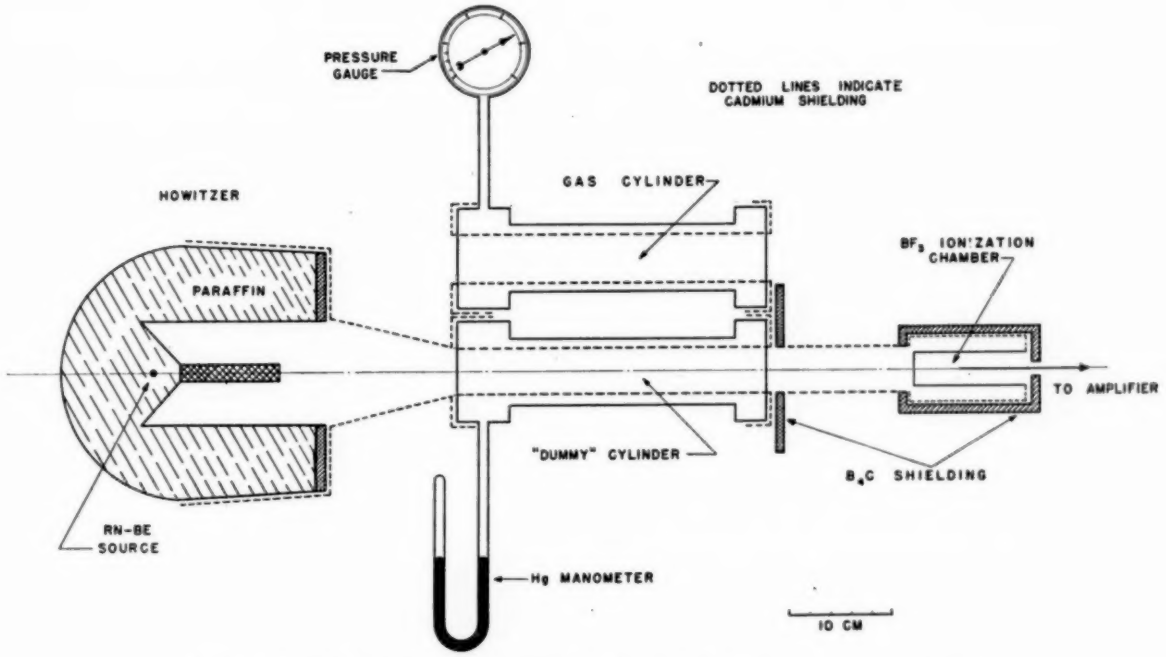

FIG. 1. General schematic arrangement of apparatus for gaseous measurements.

may accompany changes of structure. The use of gaseous substances of low molecular weight, however, offers a further complication due to the higher thermal velocities of the scattering nuclei. This, in the case of light molecules, will necessitate a small correction downward of the experimentally measured cross sections. (See Discussion of results, Section C.) The series investigated was gaseous hydrogen (H_2), methane (CH_4), ethane (C_2H_6), propane (C_3H_8), and butane (C_4H_{10}).

In addition, the cross section per proton for water and solid paraffin in two forms, one of "ordinary" paraffin, which is a mixture of hydrocarbon molecules, whose average molecule was assumed to be $C_{22}H_{46}$ and the other, a pure, single hydrocarbon, normal dotriacontane, ($C_{32}H_{66}$),[9] were measured.

Following the study of the behavior of the proton cross section, measurements were made of the cross section of the neighboring light nuclei, the deuteron, and the alpha-particle. Measurements on deuterium and helium are particularly useful, since the results are related to single isotopes. From the theoretical standpoint, the neutron-proton interaction requires the solution of a two-body problem which is capable of exact mathematical treatment. Beyond this, however, the neutron interaction with more complex particles necessitates the solution of a three-body problem. The mathematical difficulties arising in the general three-body problem are insuperable, though attempts have been made in the special case of the neutron-deuteron problem,[10] which represents a modified three-body problem. Furthermore, according to the generally accepted ideas of nuclear forces and application of the Pauli exclusion principle, the α-particle is to be considered a saturated system, and consequently, its neutron nuclear cross section is of particular interest. The deuteron cross section was measured with deuterium oxide (D_2O) of high purity, and the helium cross section was measured with helium gas as a scatterer.

Previously, the neutron nuclear cross sections of a large number of the elements of the periodic table have been measured,[11,12] but none of these

[9] The sample of normal dotriacontane was kindly supplied by Dr. F. D. Rossini of the National Bureau of Standards.

[10] L. Motz and J. Schwinger, Phys. Rev. **58**, 26 (1940).
[11] Dunning, Pegram, Fink and Mitchell, Phys. Rev. **48**, 265 (1935).
[12] M. Goldhaber and G. H. Briggs, Proc. Roy. Soc. **A162**, 127 (1937).

surveys has included any of the inert gas cross sections, as the substances used in previous experiments were in either the solid or liquid state. In these experiments, neutron measurements have been extended to include the cross sections of neon, argon and krypton in the gaseous form.

The cross sections of oxygen and nitrogen have been previously measured with compounds of these substances in solid form, or the elements

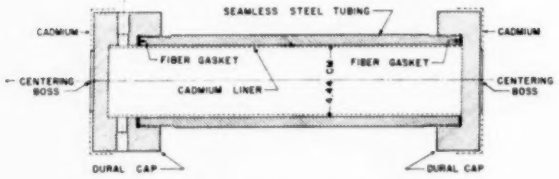

FIG. 2. High pressure gas cylinder details.

in liquid form. Interference effects[7,8] mentioned above made it desirable to redetermine these cross sections for the pure elements, and measurements were made on molecular oxygen and nitrogen in the gaseous form.

APPARATUS

The general experimental arrangement is shown in Fig. 1.

A. Neutron source and detector

The neutron sources used throughout all experiments were of the radon-beryllium type commonly used in this laboratory, whose maximum strength was about 650 millicuries.[13] To obtain slow neutrons, these bulbs were placed in a paraffin "howitzer."[14] Collimation was greatly improved and room scattering into the detector was greatly reduced by the use of hollow metal plaques and channels one cm thick, filled with powdered B_4C.[15] This supplemented the use of sheet cadmium shielding.

In order to approximate as nearly as possible the ideal arrangement which calls for a parallel beam of neutrons, a special ionization chamber was designed and constructed which offered a shielded opening to the neutron beam of only 3 cm diameter. The length of the chamber was 10 cm and its operating pressure of 2 atmospheres of boron trifluoride insured absorption of an appreciable fraction of the transmitted neutrons. Since the distance from source to scatterer was 40 cm and from scatterer to ionization chamber 35 cm, the solid angle subtended at the scatterer by the chamber was only 0.006 steradian.

The ionization chamber was operated from a stabilized power supply at 2000 volts to insure rapid ion collection. The ionization pulses were recorded by a linear amplifier and scale-of-two thyratron system operating a Cenco impulse counter.[16]

B. Gas measurement system

The gas cylinder finally adopted (see Fig. 2) consisted of a seamless steel tube 29 cm long threaded at both ends and closed with flat Duralumin caps 7.00 mm thick. Fiber gaskets and Apiezon Q in the cap threads insured a gas tight seal at pressures running up to 3000 lb. per sq. in. Good collimation was obtained by the use of cadmium diaphragms and B_4C plaques whose axes coincided with the cylinder axis.

In order to correct for neutron attenuation by the cylinder end caps, the experimental arrangement consisted of duplicate cylinders, one of which was evacuated and served as a "dummy." The other gas cylinder was provided either with a two-meter open tube mercury manometer, or a series of calibrated pressure gauges.[17]

During a cycle of measurements, it was

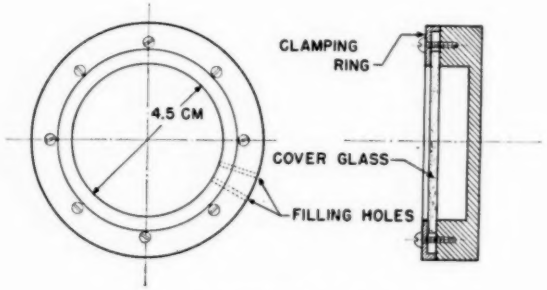

FIG. 3. Liquid cell details.

[13] The radon was obtained through the cooperation of Dr. G. Failla and Dr. J. J. Duffy of the Memorial Hospital, New York.
[14] G. A. Fink, Phys. Rev. **50**, 738 (1936).
[15] The boron carbide was supplied by the Norton Company of Worcester, Massachusetts.
[16] J. R. Dunning, Rev. Sci. Inst. **5**, 387 (1934).
[17] Kindly loaned by Professor C. F. Kayan of the Department of Mechanical Engineering.

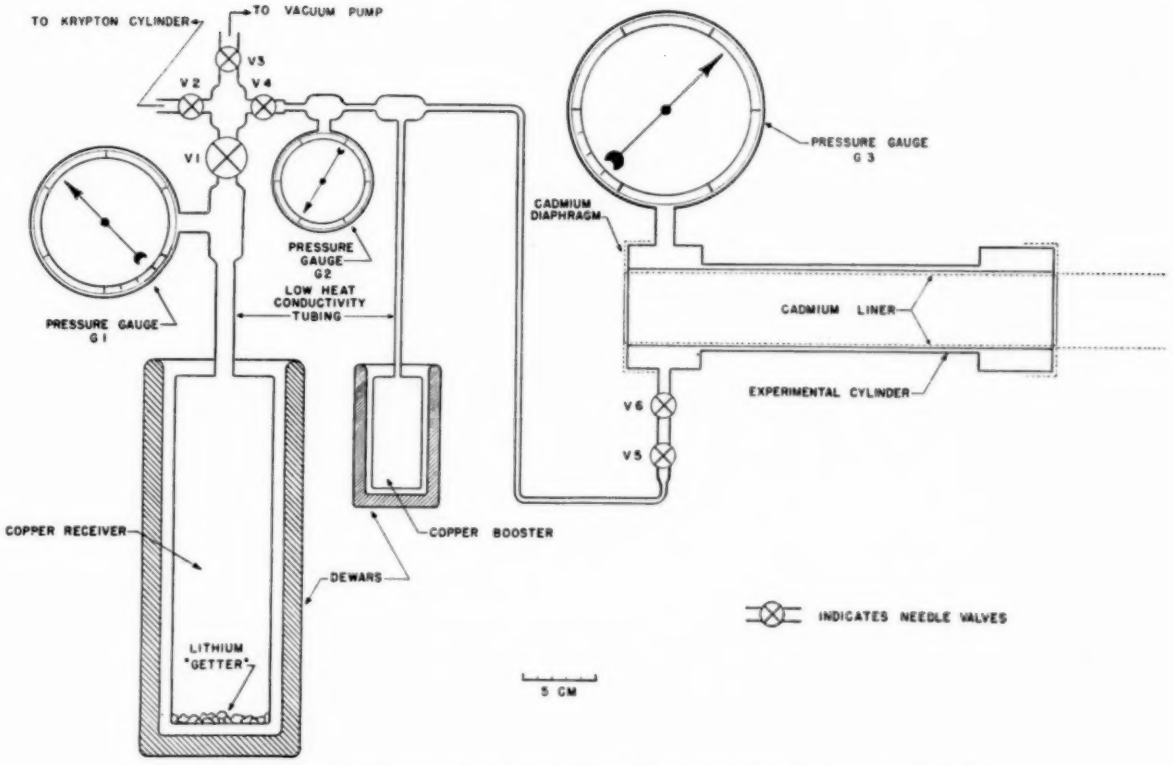

FIG. 4. Schematic arrangement of receiver and booster for high pressure gas transfer.

necessary to interpose the two cylinders alternately in the beam. To insure accurate register of each cylinder axis with the axis of the system, a double cradle and slide was designed consisting of two brass plates with double V notches in which the cylinders were supported. The slide plates moved in lubricated tracks provided with stops on either side. All gas connections were made with copper tubing to provide necessary flexibility, to withstand high pressure and to eliminate excessive absorption of hydrocarbons observed in rubber tubing and waxes.

In order to minimize scattering of neutrons from the room and adjacent apparatus, the entire assembly of Fig. 1, with the exception of the ionization chamber, was mounted in the center of the room on an open pipe-work frame, rigidly braced.

C. Cell design

The cross section measurements of the proton in water and paraffin necessitated the use of accurately constructed cells of uniform bottom thickness. The cell design is shown in Fig. 3. The bottoms were hollow dural disks and the caps were selected Eastman thin slide cover glasses of low boron content. The tolerance on the thickness of both cell bottoms, cover glasses, and a "dummy" plate was held to less than 0.001 cm. Several cells were made to hold suitable thicknesses of absorber, which gave neutron transmissions ranging from 35 percent to 65 percent.

The paraffin results were obtained from hollow dural cells similar to the above, without the cover glasses. The paraffin plaques were cast in these cells by melting the paraffin in a water bath just above the melting point. To investigate the possibility of air trapped during cooling in any way vitiating the results, some of the plaques were cast and allowed to cool under a bell jar at a pressure of about 5 or 6 mm of mercury. No transmission difference was discernible in these casts over paraffin plaques subjected to normal air cooling.

D. High pressure transfer systems

Since many of the gases had small cross sections, it was necessary to use filling pressures which in some cases exceeded 2500 lb./in.^{2}. None

of the gases was supplied at this pressure, which made it necessary to design a system for raising the original pressure to the appropriate value. Actually, two "booster" systems were used, one exclusively for krypton, in order to minimize loss of this valuable gas, and the other for oxygen, helium, etc. The krypton transfer system is shown schematically in Fig. 4. The method of transfer was to condense the krypton, by means of liquid nitrogen, into an intermediate evacuated cylinder of small volume and allow the system to warm up to room temperature. Transfer back to the main reservoir was accomplished in the same manner.

TABLE I. *Neutron-proton measurements for gaseous hydrogen*

P	$\log_{10} P^{-1}$	Pressure lb./sq. in. gage	g/cm²	Cross Section per Proton $\times 10^{24}$ cm^{-2}
0.726	0.86094	77.0	0.01512	31.9
0.668	0.82478	114.0	0.0211	31.5
0.656	0.81690	119.5	0.0240	31.1
0.502	0.70070	205.0	0.0363	31.4
0.413	0.61595	277.0	0.0484	31.1
0.319	0.50379	375.0	0.0645	30.8

In order to maintain high purity of the krypton, a glass capsule, packed with metallic lithium particles, was shattered inside the receiver and used as a "getter" to clean up any residual contaminating gases. When the krypton was transferred to the "booster," the receiver could be heated and pumped to remove any gases absorbed by the lithium.

A similar procedure was employed with other gases.

Measurements

The cross sections were calculated from the relation

$$P = e^{-n\sigma x},$$

where n = number of nuclei per cubic centimeter of the scatterer, σ = the total cross section of the scatterer, x = thickness of scatterer, P = percent of neutrons transmitted by the scatterer.

In order to calculate the percent transmission, P, four measurements were made in equal time intervals.

1. N_1, the number of neutrons transmitted through the scatterer.

2. N_2, the number of neutrons transmitted through both scatterer and a sheet of cadmium of 0.8 g/cm² placed near the source.

3. N_3, the total number of neutrons traversing the open beam, i.e., with the dummy cell in place.

4. N_4, the number of neutrons transmitted through the sheet of cadmium and the dummy cell.

Then, the percent transmission is given by

$$P = (N_1 - N_2)/(N_3 - N_4).$$

Cyclic runs were taken in all cases. The statistical precision given for the results is based on $1/\sqrt{N}$, where N is the number of neutrons counted. During any experiment, not less than 40,000 neutrons were counted for N_1 and N_3. All absolute cross sections may be considered reliable to 3 percent after allowing for other sources of variation, but the relative values are more precise.

Table I shows the measurements made for a number of hydrogen gas pressures. These served as a check on the cross section value and also as a test of the exponential transmission of the system.

The cross section measurements of the proton in the hydrocarbon series are given in Table II. Included in the table for comparison is the cross section for liquid hydrogen[18] (normal).

TABLE II. *Interaction of slow neutrons with bound protons.*

Substance	State	g/cm²	Percent Transmission	Cross Section per Proton $\times 10^{24}$ cm^{-2}
Hydrogen (H_2) Normal	Liquid*			24.0
Water (H_2O)	Liquid	0.1778	57.2	44.6 ±0.5
Hydrogen (H_2)	Gas	0.0363	50.2	31.8 ±0.5
Methane (CH_4)	Gas	0.0683	61.8	45.4 ±0.3
Ethane (C_2H_6)	Gas	0.1059	54.6	46.4 ±0.5
Propane (C_3H_8)	Gas	0.1177	53.3	46.9 ±0.6
Butane (C_4H_{10})	Gas	0.1242	51.2	48.7 ±0.6
Paraffin ($\sim C_{22}H_{46}$)	Solid	0.1304	54.8	49.8 ±0.2
Dotriacontane ($nC_{32}H_{66}$)	Solid	0.1368	52.8	50.2 ±0.2

* Reference 18 in text.

TABLE III. *Interaction of slow neutrons with the nuclei of gases.*

Substance	State	Pressure lb./sq. in.	g/cm²	Percent Transmission	Cross Section per Nucleus $\times 10^{24}$ cm^{-2}
D_2O	Liquid		0.737	70.3	5.73 ±0.14
Helium	Gas	1980	0.758	83.8	1.51 ±0.09
Neon	Gas	1600	2.620	80.4	2.79 ±0.14
Argon	Gas	1600	5.220	92.1	2.53 ±0.10
Krypton	Gas	465	3.145	53.6	27.3 ±0.5
Nitrogen	Gas	495	1.173	54.4	12.2 ±0.2
Nitrogen*	Liquid				12.8
Oxygen	Gas	1500	3.94	54.0	4.12 ±0.10
Oxygen*	Liquid				4.05

* Reference 18 in text.

[18] Brickwedde, Dunning, Hoge and Manley, Phys. Rev. **54**, 266 (1938).

The value listed for each substance represents the average of several sets of measurements.

Listed in Table III are the cross sections for deuterium, the rare gases, and nitrogen and oxygen in gaseous form.

The cross sections of nitrogen and oxygen in the liquid state[18] are also included. A comparison of the cross sections of the gaseous and liquid forms shows that the cross section did not change appreciably in going from the gaseous to the liquid state.

Discussion of Results

A. Hydrogen and the hydrocarbon series

The experimental value (31.8×10^{-24} cm^2), Fig. 5, for the proton cross section as obtained from hydrogen gas will be decreased when correction is made for the thermal motion of the molecules. (See below, Section C.) The influence of chemical binding on the cross section may be noted from the increase in cross section per proton for increasing mass of the molecule of the scattering system as shown in Table II. In this series, the cross section of carbon was taken[7,12] to be 4.80×10^{-24} cm^2. The proton cross section was calculated after subtracting the carbon cross section from the cross section of the whole molecule.

The increase of the proton cross section for C neutrons with increase in the square of the reduced mass is more clearly evident in the lower curve of Fig. 6. Arley's treatment of this scattering problem predicts that for zero energy neutrons the proton cross section should vary linearly as the square of the reduced mass. This is shown by the upper curve of Fig. 6, which includes the value for the free proton cross section obtained experimentally by Cohen, Goldsmith and Schwinger[19] using rhodium filtered neutrons and a rhodium detector with a G-M counter and also as determined more precisely by Hanstein[20] for indium and iodine resonance neutrons. Hanstein's value is 21 ± 1 $\times10^{-24}$ cm^2.

From the upper curve, the bound proton cross section would be 84×10^{-24} cm^2 since the squares of the reduced masses of the free and bound proton are in the ratio of one to four. The experimental value for the bound proton cross section (for paraffin) is actually 50×10^{-24} cm^2 for thermal neutrons at 300°K. It can be seen from the graph that while the proton cross section for hydrogen gas shows only a small departure from linearity, which would be slightly larger if corrected (see below, Section C), the departure becomes progressively larger for the heavier molecules. Previous experiments (unpublished) with neutrons emerging from paraffin at ~115°K show that from 300°K the proton cross section increases by a factor of 1.3 to an absolute value of 65×10^{-24} cm^2 which approaches the limiting value for zero energy neutrons.

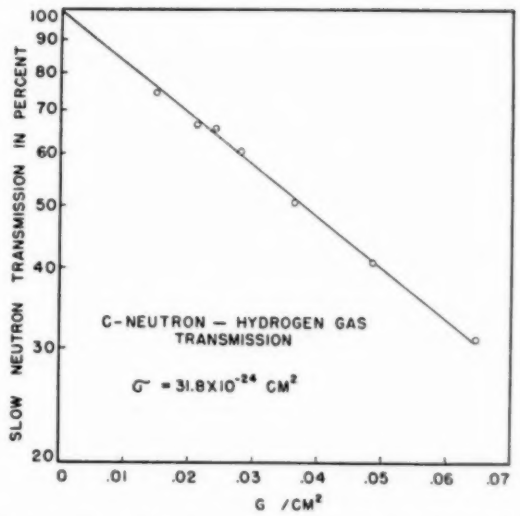

FIG. 5. Above is shown a semi-logarithmic graph of the percent neutron transmission plotted against the grams per square centimeter for a series of hydrogen pressures. As can be seen from the linearity of the plot, the transmission follows quite well an exponential law. The average cross section is $31.8\pm0.5\times10^{-24}$ cm^2.

Results of subsequent measurements on liquid and solid cetane show that the variation of the cross section may in part be due to interference effects. The existence of these effects cannot be disregarded in a critical survey of the relative change in the measured cross sections.

Owing to its complexity, the general problem of neutron-proton scattering has not been solved theoretically. Attempts have been made based on certain simplifying assumptions[4] and their modifications.

1. The original assumption of interaction

[19] V. W. Cohen, H. H. Goldsmith and J. Schwinger, Phys. Rev. **55**, 106 (1939).
[20] H. B. Hanstein, Phys. Rev. **59**, 489 (1941).

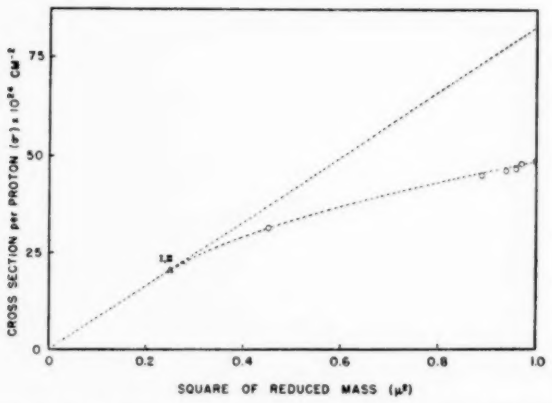

FIG. 6. C neutron cross section per proton for hydrocarbon series. *I*—Cohen, Goldsmith and Schwinger, Phys. Rev. **55**, 106 (1939); *II*—Hanstein, Phys. Rev. **59**, 489 (1941).

between a neutron and bound proton was modified[4] to that of interaction between a neutron and a system of proton "molecules," this system being chosen to have a mass of fourteen times the neutron mass. The system was admittedly artificial in that interference effects were neglected and interactions were assumed to take place by energy transfer to six vibrations of the group composing the molecules with neglect of the rotations of the group.

The actual interaction which takes place between neutron and the paraffin will depend upon the binding between the molecules and it is difficult to determine the aggregate.

2. The original assumption made was that a beam of zero energy neutrons was used.[1] This was modified by Arley to a beam of neutrons whose energy distribution was strictly Maxwellian. While it has been shown by the method of a mechanical velocity selector[5] that the maximum of the energy distribution of C neutrons at room temperature corresponds to an energy of the order of kT, the actual distribution is probably only approximately Maxwellian.

For the various molecules studied in the gaseous state, the theoretical neutron-proton cross section would have to be studied in more detailed fashion as a function of the energy distribution of the neutrons and energy levels effective in the interaction before more accurate agreement between theory and experiment could reasonably be expected.

From the graph, the value of the "chemical factor" for paraffin can be calculated from the ratio of the free and bound proton cross sections. The ratio for C neutrons is 2.4. Arley has calculated this ratio for his paraffin model and found the value to be 2.7.

B. Deuteron cross section

A theoretical calculation of the deuteron cross section has been made by Motz and Schwinger.[10] Their results arrived at by numerical integration of the wave equation for two choices of potential give cross sections of 4.57×10^{-24} cm² and 6.91×10^{-24} cm² as against the value given in Table III of 5.7×10^{-24} cm². In their calculations polarization effects were neglected because of the great difficulties introduced into the calculation.

C. Rare gas series

The small experimental cross section (1.51×10^{-24} cm²) for helium (see Table III) is consistent with the assumption that the α-particle is a saturated system. In calculating this value, the thermal motion of the gas molecules was neglected. Due to their motion, the cross section is increased and a correction should be applied which will give the "effective" cross section for stationary molecules. Schwinger[21] has calculated this effective cross section by using the relative velocity of neutron and scattering molecule, and the molecular velocity distribution function which represents the Maxwellian distribution appropriate to the temperature of the gas, and arrives at the value of 1.25×10^{-24} cm². This correction should become less important as the mass of the molecule increases as was the case for the hydrocarbon series.

Argon[2] and neon[2] have three isotopes each and krypton[2] has six. While no definite inference can be drawn from the experimental cross section of these gases, it is quite possible that in the case of krypton the contribution to the cross section may well be due to one of those which has a large capture cross section for neutrons of the energy used.

D. Nitrogen and oxygen

The cross sections for these gases agree well with the measurements made in the liquid[18]

[21] J. Schwinger, Phys. Rev. **58**, 1004 (1940).

state. However, the measured value of 4.1×10^{-24} cm^2 for gaseous oxygen is significantly higher than the value of 3.3×10^{-24} cm^2 as obtained[7,11] from SiO_2, assuming additivity of cross sections. Effects similar to this have been previously observed[7] and interpreted in terms of interference phenomena.

Dependence of Neutron Scattering on Structure

The results of the measurements on highly purified cetane are given in Table IV.

The melting point of pure cetane is 16.1°C. As this is very close to room temperature, a slight lowering of the temperature of a cell of liquid cetane caused the cetane to solidify. An ice water bath enabled alternate measurements to be made of the slow neutron transmission in both liquid and solid states.

The 10 percent difference in the measured values of the proton cross section can be explained in terms of interference effects since the solid was more transparent than the liquid. A corresponding effect was not observed in the case of lead and bismuth.[22] In certain respects the conditions were more favorable in the case of cetane since (a) the spacing of the interference centers is about 1.5A whereas for bismuth and lead, it is about 5.5A. For the neutron distribution, the most probable wave-length is about 1.7A and only very small interference effects could be expected from bismuth and lead; (b) on solidification, large well-defined crystals of cetane were formed.

The amount of coherent scattering which must be present to account for the observed difference in cross section between solid and liquid cetane in terms of interference effects is fairly large. As pointed out by Schwinger, some discrepancies still exist between the experimental results[18,23] and the theory[21,24] of the scattering of neutrons by ortho- and parahydrogen. Furthermore the theory[25] must be considerably extended if it is to take into account all of the possible contributions to interference effects such as the net effect of the ortho- and para-states in the case of an aggregate of paraffin molecules in a crystalline structure.

The cetane results clearly suggest, however, that the cancellation of the scattering by the singlet and triplet states is not complete so that some coherent scattering results. A further contribution to the coherent scattering is also possible from the carbon atoms. It appears, therefore, that although the inelastic scattering is comparatively large in paraffin, the experiments show that a considerable amount of coherent scattering still exists and that structure does play an important role in neutron scattering even in organic molecules.

Table IV. *Slow neutron-cetane cross section.*

Substance	State	g/cm^2	Percent Transmission	Cross Section per Proton $\times10^{24}$ cm^{-2}
Cetane ($nC_{16}H_{34}$)	Solid	0.1721	47.7	44.9 ±0.4
Cetane ($nC_{16}H_{34}$)	Liquid	0.1573	47.1	50.1 ±0.4

It is a pleasure to acknowledge my indebtedness to Professor J. R. Dunning both for suggesting this problem and also for many helpful suggestions and encouragement during the course of this research. Thanks are also due to Dr. F. J. Metzger and Dr. F. R. Balcar for their cooperation in supplying some of the rare gases.

[22] F. Rasetti, Phys. Rev. **58**, 321 (1940).

[23] L. W. Alvarez and K. S. Pitzer, Phys. Rev. **58**, 1003 (1940).

[24] J. Schwinger and E. Teller, Phys. Rev. **52**, 286 (1937). M. Hammermesh and J. Schwinger, Phys. Rev. **55**, 697 (1939). R. G. Sachs and E. Teller, Phys. Rev. **57**, 1076 (1940). W. Rarita and J. Schwinger, Phys. Rev. **59**, 556 (1941).

[25] G. C. Wick, Physik. Zeits. **38**, 403 (1937); **38**, 689 (1937). O. Halpern and M. H. Johnson, Phys. Rev. **55**, 898 (1939). J. H. Van Vleck, Phys. Rev. **55**, 924 (1939).

The Mass Differences of the Fundamental Doublets Used in the Determination of the Isotopic Weights C^{12} and N^{14}

E. B. JORDAN
University of Illinois, Urbana, Illinois
(Received September 26, 1941)

The values of the mass of C^{12} as determined by different observers, show a discrepancy well outside the corresponding probable errors. This mass is important since it is used in the determination of so many of the other isotopic weights. Fundamental to its determination is the mass difference $C^{12}H_4-O^{16}$. With the large spectrograph completed last year, a new determination of this mass difference has been made. In addition, the $C^{12}H_2-N^{14}$ mass difference has been checked by means of the doublets $C^{12}H_3-N^{14}H$ and $C^{12}H_4-N^{14}H_2$. These values together with the associated experiments are reported in the present paper.

I. INTRODUCTION

THE importance of the isotopic weight of C^{12} and consequently the mass difference of the fundamental doublet $C^{12}H_4-O^{16}$ which is used in its determination, has been discussed in a series of letters to *Nature* by Dr. Aston.[1] Since C^{12} is the most important substandard used in the determination of isotopic weights, and since there is a discrepancy between the value obtained by Dr. Aston[2] and that obtained by Bainbridge and Jordan, and later by others,[3,4] a careful study of the $C^{12}H_4-O^{16}$ doublet has been made on the new mass spectrograph.[5] A complete discussion of this discrepancy is included in Dr. Aston's papers as well as in a recent paper by Mattauch.[6]

Last year, shortly after the mass spectrograph was completed, a number of $C^{12}H_4-O^{16}$ doublets were obtained on one plate which gave a value for this mass difference approximately that of the average of the values reported to date, i.e., of the first four values listed in Table I.

Since this value differed appreciably from any of the others, and since at that time, all of the preliminary runs on the spectrograph had not been completed, a report of this mass difference was delayed until additional plates could be obtained. Although, since then, a large number of $C^{12}H_4-O^{16}$ doublets have been photographed on six different plates, some of these plates having been exposed only after radical variations were made, the resulting mass difference is essentially the same as that obtained from the first plate. For convenience in discussing the details of these separate experiments a schematic diagram of the mass spectrograph is shown in Fig. 1.

TABLE I. *The $C^{12}H_4-O^{16}$ mass differences in terms of 10^{-4} mass unit.*

Aston	360.1 ±1.6
Bainbridge and Jordan	364.9 ±0.8
Mattauch and Bonisch	364.06±0.40
Asada, Okuda, Ogata and Yoshimoto	364.2 ±0.9
Jordan	363.2 ±0.35*

* This error is three times the probable error computed from internal consistency of data.

II. EXPERIMENTAL DETAILS

A. Source

The discharge tube used was the usual cylindrical type in which a low pressure discharge was maintained by a unidirectional pulsating potential difference of fifteen to twenty kilovolts. An aluminum cathode of the Thomson type was mounted on the iron base which supports the discharge tube. The gas, in this case a mixture of methane, nitrogen and oxygen, was admitted into the tube within the cathode opening.

The discharge was collimated by means of a large water-cooled solenoid mounted on the front end of the analyzer magnet and carefully aligned so that its axis was parallel to the axis of the collimating slits S_1 and S_2 (Fig. 1).

[1] F. W. Aston, Nature **137**, 357 (1936); **137**, 613 (1936); **138**, 1094 (1936); **139**, 922 (1937); **141**, 1096 (1938); **143**, 797 (1939).
[2] F. W. Aston, Proc. Roy. Soc. **A163**, 391 (1937).
[3] J. Mattauch, Zeits. f. tech. Physik **19**, 578 (1938); Physik. Zeits. **39**, 892 (1938).
[4] T. Asada, T. Okuda, K. Ogata and S. Yoshimoto, Nature **143**, 797 (1939). Proc. Phys. Math. Soc. Japan **22**, 23 (1940).
[5] E. B. Jordan, Phys. Rev. **57**, 1072A (1940).
[6] J. Mattauch, Phys. Rev. **57**, 1155 (1940).

By means of this solenoid, field strengths of the order of 1000 gauss were maintained within the source region when a run was made. This field together with the opening in the aluminum cathode serves to align the narrow pencil-shaped beam of electrons passing from cathode to anode, and thus a maximum positive ion beam intensity is obtained at all times.

The most important feature of this arrangement is that it ensures uniform illumination of the image slit by all types of positive ions present. That this is an important factor was demonstrated in one experiment in which the solenoid and cathode were adjusted so that the core of the discharge made a slight angle with the axis of the collimating slits. After development, the photographic plate showed lines corresponding to the $N^{14}H^{1+}_2$ and O^{16+} ions, but no line corresponding to the $C^{12}H^{1+}_4$ ion, although a large portion of the gas in the discharge tube was methane. It is thus not hard to conceive of cases in which there would be a uniform illumination of the image slit by one ion corresponding to a given doublet pair, and only partial illumination by the other ion. One could even obtain matched doublets under such conditions, but the resulting error in the completed mass difference would be large. In addition to obviating these difficulties, the magnetic field tends to steady the discharge at all times.

B. Disperser magnetic field

Initially the pole pieces of the disperser magnet (indicated by the letter H_2 in Fig. 1) were first surface ground and then polished by hand. After assembly, the gap width (5 mm) was checked by means of a steel wedge and was found to be accurate to $\pm 0.0005''$. This gap width is 66 percent greater than that used in other instruments, and thus the percentage error due to small surface variations is correspondingly less. The angles which the end faces make with the top surface were estimated to be accurate to ± 20 seconds of arc.

In spite of the many precautions taken in the original construction of this unit, it was later taken apart and thoroughly rechecked and resurfaced when it was found that the $C^{12}H^{1}_4-O^{16}$ mass difference differed slightly from previously reported values. Spectra taken before and after this change yielded values for the $C^{12}H^{1}_4-O^{16}$ mass difference which are in agreement within the small probable error computed from the internal consistency of the data.

C. Stray field

The integrated effect of the stray magnetic fields on each side of the pole pieces H_2 (Fig. 1), was initially calculated[7] and taken into account by cutting back the pole edges. Since the line breadth depends upon the accuracy of this correction, several runs were also made in order to find its value experimentally and at the same time to determine if there was any effect on the calculated mass differences due to these stray

[7] I am indebted to Dr. Nye of this department for many helpful suggestions concerning this correction.

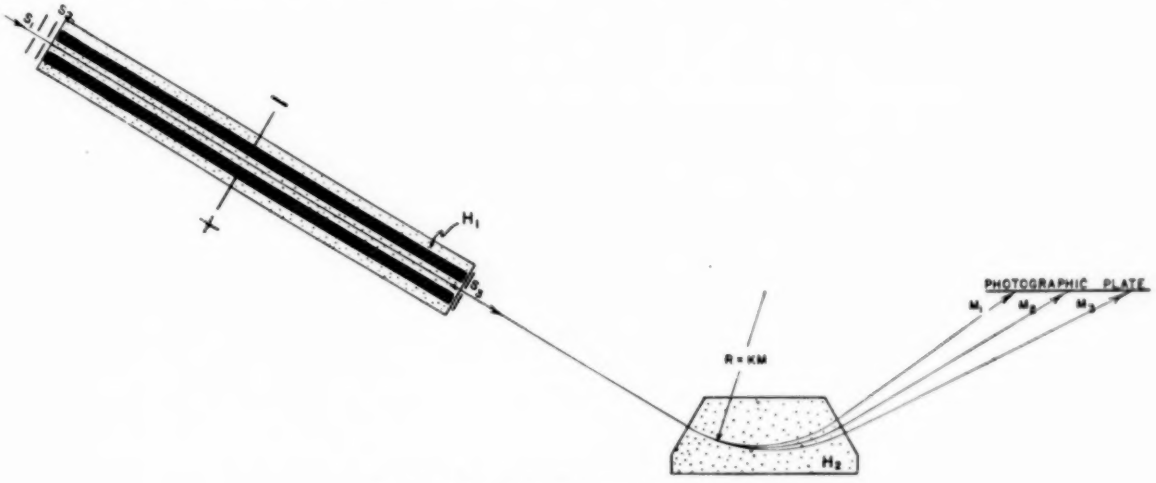

FIG. 1. Schematic diagram of apparatus.

FIG. 2. $C^{12}H^1_4-N^{14}H^1_2-O^{16}$ matched triplet, natural size. $S_1=0.1$ mm, $S_2=0.04$ mm, $S_3=2$ mm.

fields. The allowed stray field correction and thus the effective dispersion of this magnet was altered by raising or lowering the disperser pole pieces relative to the rest of the spectrograph. After each change the apparatus was accurately realigned, the position of the photographic plate being kept the same throughout.

$C^{12}H^1_4-O^{16}$ doublets have been photographed for these pole pieces in two different positions. In one position the correction allowed for the effect of the stray field was 1.25 gap widths, and in the other 1.50 gap widths. The resulting mass differences for both cases were consistent and once again showed close agreement. These data also indicated that the best value for this stray field correction should be 1.65 gap widths, a value which is utilized in the present alignment.

D. Spectra

Local disturbances in the field of the instrument, if any, were minimized by photographing spectra at several different positions on each plate. When all six plates are considered, the range in distance over which useful doublets were obtained was 10 cm.

The dispersion lines used in the determination of the $C^{12}H_4-O^{16}$ mass differences were those corresponding to the $C^{12}H^{1+}_3$ ion at mass position fifteen and the $N^{14}H^{1+}_3$ ion at mass position seventeen. In some spectra a strong line corresponding to the $O^{16}H^{1+}$ ion was also present and, in such cases, was used in the determination as an additional check. These lines were identified not only by position, but also by taking exposures when only one gas was present in the discharge tube. Since deuterium has not yet been used in the spectrograph no lines due to its compounds were expected.

Another source of error, especially in the case of low resolving power instruments, is the presence of the $C^{13}H^1_3$ line. Unless it is completely resolved, this line although faint, is of sufficient density to distort seriously the shape of the $C^{12}H^1_4$ line and thus cause the resulting mass difference to be considerably lower than its true value. In the present instrument, it is separated from the $C^{12}H_4$ line by a distance of 0.4 mm.

In order to test the effect of slit S_3 (Fig. 1), doublets have been photographed for values of this opening from one to three millimeters. Although there was a slight broadening of the lines when the larger opening was used, the computed mass differences were in agreement in all three cases.

III. RESULTS

Figure 2 is a contact print of one of the mass sixteen triplets $C^{12}H^1_4-N^{14}H^1_2-O^{16}$.

In all, twenty-one doublets, obtained under the various conditions noted above, yielded a value for the $C^{12}H_4-O^{16}$ mass difference equal to 0.03632 mass unit. This value, together with those of the other observers previously referred to, is given in Table I.

It is interesting to note that Mattauch, whose value is closest to that reported in this paper, states in his last paper[6] that he has found a small systematic error which tends to lower the value he has reported for this doublet. He did not state the magnitude of this error, however, and up to the present time has not reported his later measurements. The combination check

FIG. 3. $C^{13}H_3-N^{14}H$ doublets, enlarged 5 times. $S_1=0.10$ mm, $S_2=0.05$ mm, $S_3=2$ mm.

doublets which he has reported[6] also yield values lower than that obtained by direct measurement. From the $C^{12}H^1_2-N^{14}$; $N^{14}H^1_2-O^{16}$ doublet combination he obtains a value for the $C^{12}H_4-O^{16}$ mass difference equal to 0.036361 $\pm$0.00004, and from the $C^{12}H_2-N^{14}$; $N^{14}_2-C^{12}O^{16}$ combination a value 0.036384$\pm$0.000061. Both of these values are in agreement with the value reported above by myself.

IV. The $C^{12}H^1_2-N^{14}$ Mass Difference and Check Doublets

In a recent letter to *The Physical Review*,[8] the mass difference $C^{12}H^1_2-N^{14}$ was reported and compared to the values obtained by other investigators. Since then a few check doublets at mass positions fifteen (the $C^{12}H_3-N^{14}H$ doublet) and sixteen (the $C^{12}H_4-N^{14}H_2$ doublet) have been photographed. These repeat the same mass difference respectively, one and two units higher. The value of the mass difference $C^{12}H_3-N^{14}H^1$ as obtained from five matched doublets is 0.012563. The agreement with the value 0.012560 previously obtained from measurements on doublets at mass position fourteen and already reported is very good. Enlarged spectra of this doublet are shown in Fig. 3, and a densitometer trace of one of them in Fig. 4.

Ten matched check doublets ($C^{12}H_4-N^{14}H_2$) at mass position sixteen were obtained on four different plates while attempting to obtain matched $C^{12}H_4-O^{16}$ doublets. These plates were exposed under different conditions as regards slit sizes, line focus, and plate position. A contact print of some of these spectra is shown in Fig. 2.

Table II. *Mass differences in terms of 10^{-4} mass unit.*

Doublet	$C^{12}H_2-N^{14}$	$C^{12}H_3-N^{14}H$	$C^{12}H_4-N^{14}H_2$
Mattauch and Bonisch	125.81 $\pm$0.23	125.63 $\pm$0.27	126.26 $\pm$0 51
Jordan	125.60 $\pm$0.15	125.63 $\pm$0.13	125.50 $\pm$0.13

[8] E. B. Jordan, Phys. Rev. **58**, 1009 (1940).

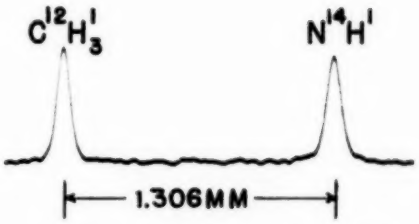

Fig. 4. Densitometer curve of one of the $C^{12}H_3-N^{14}H$ doublets.

These doublets yielded a value for the $C^{12}H_4-N^{14}H_2$ mass difference equal to 0.012550 $\pm$0.000013.[9] Here again the agreement with the other two values as listed above is very good.

It is interesting to compare in Table II these values with those obtained by Mattauch and Bonisch[6] for the same doublets. The agreement is most excellent except in the case of the $C^{12}H_4-N^{14}H_2$ check doublet, for which Mattauch and Bonisch obtain a value somewhat higher than they do for the other two doublets.

Additional measurements on the $C^{12}H_4-O^{16}$ mass difference and check doublets used in its determination as well as other light element doublets are in progress.

The construction of the mass spectrograph was made possible by a grant to Professor Loomis and the author from the Graduate School Research Fund.

It is a pleasure to acknowledge the suggestions and aid received from Mr. Ernest Englund who was responsible for the construction of the instrument and who has aided in making the many mechanical changes discussed in this paper. I am also indebted to Professors Bartlett, Mott-Smith, Serber and Goldhaber for valuable suggestions. Valuable aid has also been received from Professor H. E. White of the University of California and Professor F. G. Dunnington of Rutgers University.

[9] This error is three times the probable error computed from internal consistency of data.

Pulses in Negative Point-to-Plane Corona

L. B. Loeb, A. F. Kip, and G. G. Hudson
University of California, Berkeley, California

and

W. H. Bennett
Electronic Research Corporation, Newark, Ohio

(Received September 22, 1941)

The failure of W. H. Bennett working with very fine negative points and of G. G. Hudson working with larger carefully polished negative Pt points in clean dry dust-free air to observe the regular relaxation oscillator-like pulses reported by Trichel for negative points in room air led to a further study of the Trichel pulses. Certain results obtained by A. F. Kip in an earlier study of the Trichel pulses in room air have been added to the findings of Bennett and Hudson and are here reported. It was found by Kip and Bennett independently that the onset potentials and the current voltage characteristics of the corona showing Trichel pulses are independent of the metal and thus of the work function of the point. Bennett's studies indicate that the mechanism of the pulses depends entirely on the nature of the field about the point in air and that the pulses occur only in gases attaching electrons to form a space charge cloud of slowly moving negative ions whose time of movement across a critical region in the gap determines the frequency of the pulses. The absence of Trichel pulses in gases where electrons do not attach to form negative ions has independently been confirmed by G. L. Weissler in pure N_2, H_2 and A in studies to be published separately. It is further independently shown by Bennett and by Hudson that the regular Trichel pulses originating as they do in the gas require the presence of a source of triggering electrons. These can be furnished from fine points or by roughness on larger points through field emission, by very fine dust specks through the Paetow effect and probably by adequate photoelectric or thermionic emission from the point. Thus room air, yielding negative ions and providing ample numbers of fine dust specks for triggering, yields the regular Trichel pulses while clean, dry dust-free air, giving but rare dust specks, yields random bursts of pulses of irregular form. Observations of pre-onset phenomena by Kip and of the nature of the "active spots" and their action on the Pt point by Hudson are also reported. The theory of the phenomenon is reconsidered in the light of the findings and it is shown that the theory proposed by Trichel is applicable except as modified by the influence of the negative ion space charge and the necessity of triggering electrons. The appearance of what seems to be an incipient retrograde streamer process of the type pictured by Loeb and Meek in their study of long sparks is reported in the observations by Kip and Hudson of negative coronas from larger points well above onset.

Introduction

THE initial study of negative point-to-plane corona by G. W. Trichel[1] revealed the presence of regular relaxation oscillator-like pulses in room air. These pulses appeared at or near corona onset with moderately small points at frequencies of a few thousand per second. They rapidly increased in frequency as the current increased with increasing potential and were distinguishable as separate pulses up to frequencies of a hundred thousand per second. The physical processes leading to the phenomena were explained in a tentative fashion by Trichel in his paper and appear in general to be substantiated. As will be seen below, the mechanism postulated, however, requires modification in some of its details. Trichel worked in room air with points of a limited range in size which were roughly polished.

At about the same time the above studies were being made, W. H. Bennett was independently making studies on extremely sharp points and extended them to include measurements in clean dust-free air. It was found that in these latter cases, the regular pulses did not occur at all times and this fact was communicated to Loeb early in 1940. Hudson working with larger points in dust-free air under Loeb's direction had also encountered this difficulty and was engaged in a study of the cause. Bennett suggested that the regular pulses probably required some kind of small surface imperfection on the duller points, and that the sharper points gave currents triggered by cold emission, a suggestion which proved fruitful as will be seen. Bennett's data on extremely sharp points follows.

[1] G. W. Trichel, Phys. Rev. **54**, 1078 (1938).

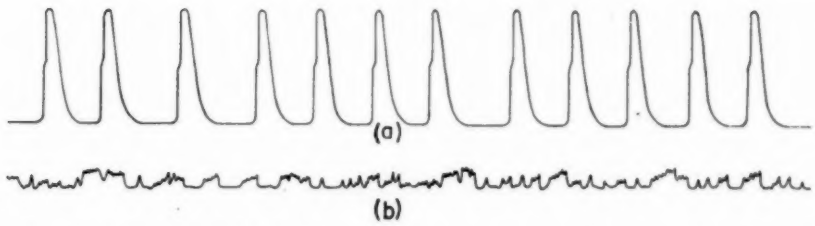

FIG. 1(a). Regular Trichel pulsations obtained with points having radius of curvature greater than about 0.002 centimeter. (The break shown in the steep wave front is probably instrumental in character. Pulses observed by Kip and by Hudson did not show this break, but were of the same form as photographed by Trichel, reference 1; (b) irregular forms of pulses obtained with points having radius of curvature of about 0.0004 centimeter. The jagged form is very similar to the irregularities in current obtained in cold emission from unconditioned points during "breakdown."

SHARP POINTS

Points were polished to form hyperboloids of revolution, and measured under a microscope. The radius of curvature R at the tip was used in calculating the field intensity, E_p, at the tip, in terms of the radius, the distance to the plane, x, and the potential between electrodes, V, by the same method used before in investigations of cold emission:[2]

$$E_p=\frac{2V}{R\log(4x/R)}.$$

Measurements were made with the point at various distances from the plane to test for consistency of data in order to insure that the support for the point was slim enough and that the disk used for the plane was large enough.

The regular forms of pulsation occurred at onset for all points with radii of curvature down to about 0.0025 cm, but a smaller and much more jagged form appeared for points with radii smaller than this. The pulsation forms are shown in Figs. 1(a) and 1(b).

The observed values of field intensity at the tip at onset are given in Tables I and II for various sharpnesses of point and various distances from point-to-plane. Tungsten and steel points were used: Table I is for point negative, and Table II is for point positive. Onset on positive could not be observed for points finer than $R=0.001$ cm because the current increased smoothly from less than 10^{-10} ampere, so the observations for the finer points on positive are for current equal to 10^{-8} ampere to correspond approximately to the average current at onset for the duller points. At distances of 0.1 cm, the finer points arced over without an onset, and were destroyed. Data on such points are missing. The finest points on positive could not be measured on negative because the shape of the tip changed too rapidly during the measurements.[3]

COLD EMISSION

These field intensities for the sharpest points are higher than those observed by Bennett for

TABLE I. *Negative onset field intensity in 10^5 volts per centimeter at tip of point for various plate distances x and radii R.*

x IN CM	R IN CM 0.00058	0.0012	0.0025	0.0050	0.0115	0.047
8	8.0	3.7	2.22	1.73	0.64	0.62
4	8.0	3.8	2.21	1.73	0.68	0.62
2	—	3.9	2.21	—	0.73	—
1	7.7	3.8	2.19	1.75	0.74	0.63
0.5	7.6	3.7	2.22	1.78	0.70	0.72
0.1	—	—	—	(1.86)	—	(0.79)
Av.	7.8	3.8	2.21	1.75	0.70	0.65

TABLE II. *Positive onset field intensity in 10^5 volts per centimeter at tip of point for plate distance x and radii R.*

x IN CM	R IN CM 0.00027	0.00058	0.0012	0.0025	0.005	0.0115	0.047
8	22.2	11.1	4.9	3.00	2.00	0.79	0.62
4	20.8	11.0	5.0	3.4	2.07	0.84	0.62
2	—	—	5.1	2.92	—	0.89	—
1	21.5	10.9	5.0	2.87	2.04	0.94	0.66
0.5	—	10.7	4.9	2.91	2.19	0.98	0.69
0.1	—	(10.6)	—	—	(2.18)	—	(0.89)
Av.	21.5	10.9	5.0	2.07	2.07	0.88	0.65

[2] C. F. Eyring, S. S. Mackeown and R. A. Millikan, Phys. Rev. **31**, 900 (1928).

[3] W. H. Otto and W. H. Bennett, J. Chem. Phys. **8**, 899 (1940).

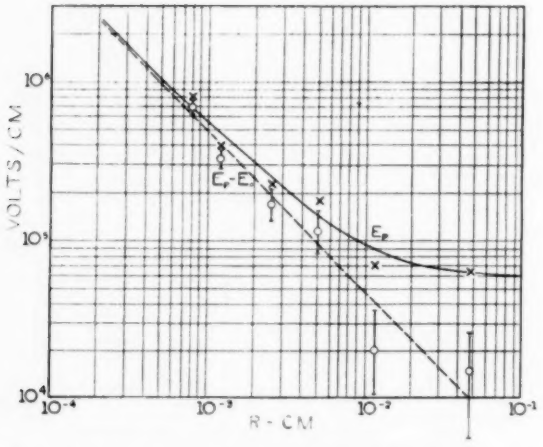

FIG. 2. Point negative, onset field intensity at tip of point. Full line with crosses represents the logarithm of onset field in volts per centimeter as a function of logarithm of radius of curvature of point at tip in centimeters. Dashed line with circles represents $\log(E_p-E_0)$ as function of $\log R$.

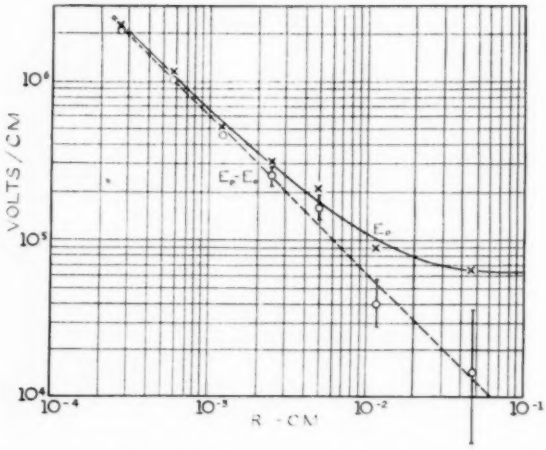

FIG. 3. Point positive, onset field intensity at tip of point. Full line with crosses represents the logarithm of onset field in volts per centimeter as a function of logarithm of radius of curvature of point at tip in centimeters. Dashed line with circles represents $\log(E_p-E_0)$ as a function of $\log R$.

equal currents in cold emission in vacuum from unconditioned copper spheres $\frac{3}{4}''$ in diameter,[4] and are about the same order as those published by Millikan and Lauritsen[5] for current-conditioned wires with more nearly the same radius. Mechanisms similar to those postulated by Bennett in his theory of magnetically self-focusing streams[6] probably occur to result in pitting a cathode point but not an anode point. The irregular pulse forms shown in Fig. 1(b) for the sharpest points on negative are thus seen to be due to the rapidly fluctuating cold emission currents during rapid successive breakdowns and fatigues amplified by ionization.

Since the onset field intensities are approximately constant for the duller points, but increase to a higher order of magnitude through the range to the sharpest points, it was supposed that the condition for onset on negative might be that the field must exceed some minimum field E_0 throughout an "ionization sheath" thickness x_0. If this be the case, then since the field near a hyperboloid of revolution of radius R varies with distance x according to

$$E=\frac{R}{R+x}E_p$$

the field will exceed E_0, throughout x_0, if

$$E_p-E_0=(x_0E_0/R).$$

The data were plotted in Figs. 2 and 3 by assuming a value of E_0 (50 kv/cm) which would give a negative slope of one to a plot of $\log(E_p-E_0)$ *versus* $\log R$. The data fit this assumption as closely as may be expected from the spread of the data.

This result, together with the observation that for the sharpest points on negative the pulse forms become those characteristic for cold emission, shows that Trichel pulses are caused by some mechanism in the air near the point rather than at the surface of the point, provided that sufficient trigger electrons are available. As discussed later, this mechanism is an electron attachment to form negative ions. The question of sufficiency of triggers is treated by Hudson's observations which follow.

THE ACTIVE SPOTS

The appearance of the regular Trichel pulses is found always to be associated with the concentration of the discharge at a single localized active spot which covers a small area as indicated by Trichel.[1] See Figs. 4(b) and 6(b). The size of such spots is never *more* than 0.2 mm in diameter. Larger areas of glow occur but are seen to be composed of multiple spots with the discharge

[4] W. H. Bennett, Phys. Rev. **37**, 582 (1931).
[5] Millikan and Lauritsen, Proc. Nat. Acad. Sci. **13**, 45 (1928).
[6] W. H. Bennett, Phys. Rev. **45**, 890 (1934).

often jumping from one spot to the other. The oscillograph patterns in such cases indicate the presence of groups or bursts of pulses which are independent in phase and are often superposed. Smaller areas of 0.2 mm diameter or less are single active spots in room air. If the high field region of the tip is of 0.2 mm diameter or less, the production of *multiple* spots is hindered and in room air the appearance of single active spots is facilitated. Larger points give high field regions sufficiently extensive so that active spots can, but do not necessarily form at several points. If they do form, the discharge jumps from one spot to the next at low currents. With larger currents one or more spots may be active simultaneously on large electrodes. The currents for the same potential are, according to Kip, usually larger with regular Trichel pulses than when the discharge is interrupted as with multiple spots. Macroscopic sharp points, foreign material, finger prints, or moisture must be avoided. Kip found that points of brass, copper, aluminum, iron, and platinum all give Trichel pulses in room air, and Bennett found the same for tungsten, rhodium, and various alloys containing nickel, copper, zinc, tin and antimony. No *measurable differences in onset potential or current attributable to such differences in material were observed*, provided the points were properly "conditioned." The character of the "conditioning" process was never clearly understood but points run for some time in room air usually became "conditioned" unless subjected to the disturbing factors above mentioned.

The Effect of Clean Dry Air and the Associated Phenomena

When the studies were made in a clean container with carefully filtered air dried over liquid air or CO_2 snow, the regular Trichel pulses could not be obtained. Instead, at onset bursts of up to a dozen or more irregular pulses similar in shape to those recorded by Trichel were seen. Above onset the pulses were quite irregular in amplitude and frequency. The amplitude of these irregular pulses was greater than in the regular Trichel pulses and they were randomly spaced in time.

In the work of Hudson, unlike the earlier work of Trichel and Kip, the platinum point electrodes (of 0.5 mm diameter) were carefully polished at first with rouge, later with tin oxide. They were carefully inspected under 100-fold magnification and were found to show only a few very fine scratches.

Hudson found that by the time a smooth point had become "conditioned," it had also collected *several very small dust specks*. Accordingly a newly polished point was dusted with MgO powder whose particles were of the order of 0.01 mm in diameter, which was the size of the collected particles on a "conditioned" point. In room air this dusted point at once gave Trichel pulses that were constant in amplitude and frequency. As the discharge continued and the dust particles were broken up or thrown off, fluctuations appeared and irregularities were again observed. Observations were next repeated in air of varying humidity with smooth and rough points, both clean and dusted with MgO. In these tests the evacuated chamber was filled with different amounts of saturated water vapor from a side chamber containing distilled water. Dry air was then admitted from a high pressure cylinder. Values of 0, 45, and 100 percent relative humidity at about 22°C were used.

Dusted points always started by giving Trichel pulses but in dry air these rapidly gave way to the irregular type. In the presence of moisture the rough, dusted point continued to produce periodic pulses for 35 minutes or more, which was two or three times as long as with the smooth dusted point. When the irregularities began to appear it was found that the particles had largely been removed from the tip of the point. This observation, taken together with the fact that dusted points always started to give good pulses

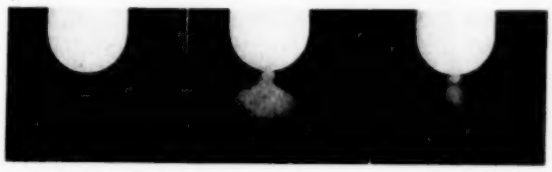

Fig. 4. Photographs of the negative point discharge. (a) A 6-min. exposure of the pre-onset glow at 4.07 kv. (b) Glow from main spot and also from a large dust speck near tip at 7.0 kv and 7 μa current. (The outline of the point was made by means of a mask over the print, the size and location of which were checked photographically.) (c) Appearance of active spot when regular pulses occur. With a shorter exposure than for (b) the dark space between the two parts of the glow can be seen.

FIG. 5. (a) Photomicrograph of the tip of a 0.45 mm diameter Pt point after a 2¼-hr. negative run in partially saturated room air at 6.5 kv and 3 μa. A dark reflection is seen in the central smooth spot (1), which is surrounded by a heavy oxide ring (2). The narrow clear zone (3) and the thin outer dark ring (4) are also evident; (b) Negative point after a 3-hr. run in dry air at 10 kv and 17.8 μa. Several small, bright pits appear instead of a large bright spot as in (a).

in dry air, seems to indicate that the moisture in the air tends to hold the MgO specks on the point surface. It is interesting to note that the triggering dust specks usually occur at the side of the active spots. These enter as near as possible to the strong field region adjoining the spot. One can conclude that the presence of fine particles on the tip of the point is a necessary condition for the appearance of Trichel pulses. This explains why unconfined room air with plenty of fine dust and particles gave the pulses whereas in clean filtered air one had to wait a long time to capture such a speck. Larger dust particles such as lint, etc., as observed by Kip, of course spoiled the regularity by producing a fine point corona of its own. Kip with his telemicroscope of low resolving power did not observe the fine specks while Hudson using a hundredfold magnification found them. The function of the fine specks is obviously of the same sort as that observed by Paetow[7] in spark discharge. Here the specks of oxide became highly charged by ultraviolet light and by positive ions. These lead to bursts of electrons either produced by field emission, small sparks through the specks or by some short wave-length ionizing photon emission. These mechanisms obviously furnished the needed triggering electrons for the regular Trichel pulses. Why these electrons are needed and why the work function of the metal is of no influence will become clear in a discussion of the mechanism occurring. The effect of the triggering electrons is still further shown by the fact that when a clean point became "conditioned" by collecting dust the offset potential was lowered by as much as 10 percent.

[7] H. Paetow, Zeits. f. Physik **111**, 770 (1939). See also L. B. Loeb, *Fundamental Processes of Electrical Discharge in Gases* (John Wiley & Sons, New York, 1939), p. 498.

PRE-ONSET PHENOMENA

Trichel[1] had observed that below a certain voltage pulses cease to be of constant frequency (the low limit was about 1000 per second) and became random, and spaced far apart in time (order of 1 second). This was confirmed by Kip. Kip used a preamplifier to look for evidence of small discharges before onset of the larger pulses. With a 0.318-cm diameter brass point and a gap of 4.2 cm in room air the following sequence was observed. At 11.7-kv current irregularities were first visible. There was, however, no detectable sudden onset at this voltage at which one could definitely say that irregularities appeared. It was later observed that this "pre-onset" current had associated with it a faint glow at a distance from the point as shown in Figs. 4(a) and 6(a). There was, however, no active spot next to the point surface. Increasing the potential to 13.89 kv increased the size of the oscillograph irregularities and increased the current from less than 10^{-9} amp. at 11.7 kv to 10^{-8} amp. at 13.89 kv. Above

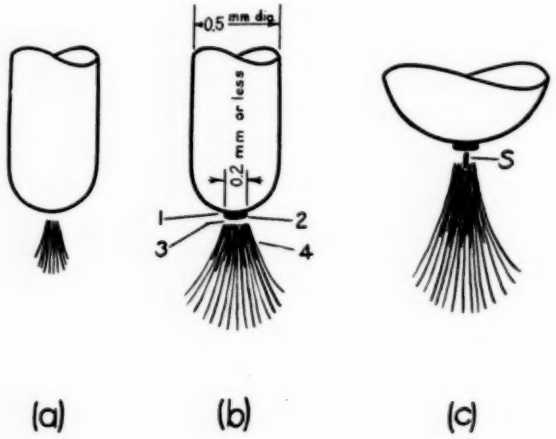

FIG. 6. Drawings of typical preonset and active spot negative corona phenomena. (a) Shows pre-onset glow also seen in Fig. 4(a), and after onset in Fig. 4(b), (b) shows the structure of the typical active spot accompanying Trichel pulses with Crookes dark space (1), negative glow (2), Faraday dark space (3) and positive column 4. (c) shows the incipient retrograde streamers with large points and high current densities.

this the first single, random pulses began, and with a further increase in voltage the pulses became periodic as shown in Fig. 1(a) and the corona took the form of Figs. 4(c) and 6(b). The same weak glow discharge giving fluctuations that were not detectable without a preamplifier were observed by Hudson. Sometimes more than one such discharge would occur. With the microscope these discharges were clearly attributable to the presence of fairly large dust specks, Fig. 4(a).

Effect of the Discharge on the Point

After a short run with regular pulses the negative point begins to show the formation of a smooth bright spot where the glow is centered. This is surrounded by a dark ring. As the discharge continues in air the ring becomes thicker and wider. In dry air a run of about an hour produces another ring of larger diameter, brown or yellow in color and which may be separated from the heavier inner deposit by a narrow zone of clean platinum surface. Typical photomicrographs are shown in Fig. 5 and typical dimensions on a 0.45-mm diameter point are as follows: central bright spot 0.05-mm diameter; first dark brown or black ring 0.03 mm wide; clean zone less than 0.01 mm wide; outer dark ring 0.01 mm wide with outer diameter of 0.14 mm. The cathode glow diameter corresponds closely to the diameter of the central bright spot.

During one run of 4 hours in dry air with irregular bursts and a current of about 1.6×10^{-5} amp. a large amount of black material was formed on the tip in a spot 0.09 mm across. In this there were a dozen small pits each about 0.01 mm in diameter. This leads to an estimate of the removal of about 7×10^{14} atoms of metal for an equivalent charge transfer of 15×10^{17} electrons or ions.

The nature of these deposits was ascertained as follows. Heating the wire changed the color of parts of the deposit to black. Heating further to red heat caused the black material to disappear. Organic solvents did not affect the dark material, while chemical reactions of the deposit showed that it was not carbon or Pt black but apparently an *unstable* oxide of Pt. The formation of such oxides of Pt in an electrical discharge was reported by J. Piazza.[8] It is believed that the nitric oxides react with the Pt and that the molecules of oxide are blasted off the surface by the positive ions in the active spots. Where the discharge is irregular several active spots of limited size form and pitting results. The pitting may be about triggering points and may be caused by the mechanism of self-focusing beams.[6] When the regular pulses occur, aided by triggering electrons, the discharge spreads over a larger area and the localized pitting is not observed.

The Effect of Ultraviolet Light on Negative Point Discharge

Ultraviolet light was obtained from a quartz Hg arc placed up to 6 inches distant from the discharge. The ultraviolet light appears to produce two effects working in opposite directions: It tends to increase the current at a given voltage by insuring a supply of triggering electrons at the point surface, and it tends to decrease the current by the production of low mobility ions in air. Either effect may predominate, depending on the size and surface conditions of the point, the maximum increase comes when the point is active at several spots. In this case the ultraviolet light tends to produce a single active spot working at a constant frequency, which in general increases the current apparently by furnishing the essential triggering electrons. More work is undoubtedly needed to clarify the question, but enough results were obtained to indicate some of the effects involved.

Effect of Heating the Point

The sharp bend in a V-shaped piece of wire heated electrically was used as a negative point. When cold it gave fairly good Trichel pulses but as it was warmed they became very irregular. When, however, the hot wire began to emit light visible in a darkened room the pulses again became regular. As the temperature became higher the frequency increased. This latter effect may be ascribed to decreased air density about the hot point; for, as Trichel showed, the frequency increases with decreasing gas pressure. On cooling the phenomena reversed in order

[8] J. Piazza, Anal. Soc. Cient. Santa Fe **6**, 23 (1934).

except that the cold point no longer showed regular pulses as the point had been burned. This series of phenomena appears to confirm the conclusion that triggering electrons are needed for the appearance of Trichel pulses. Further work is needed on this question owing to the complicating effects of change in density which produced changes in the wave form of the pulses with fine points in some of Bennett's studies but not in the case of Hudson's studies.

Theoretical Conclusions

The mechanism postulated by Trichel[1,9] for these pulses was as follows. When the field about the point becomes sufficiently great that the integral $\int_0^{x_0}\alpha dx$ has an appreciable value electron avalanches containing $\exp[\int_0^{x_0}\alpha dx]$ electrons and positive ions are formed by an initial electron moving out a distance x_0 from the point surface. The distance x_0 is such that beyond it with the diminishing field strength Townsend's first coefficient α for ionization by electron impact takes on negligible values (less than 1).[10] The mobile electrons formed continue to move outward beyond x_0, decreasing their drift velocity towards the anode as they recede. The relatively immobile positive ions (mobilities about 10^{-2} times those of the electrons) then remain behind as a space charge cloud moving slowly toward the point. The cloud has a density of ions depending on $\alpha\exp[\int_0^{x}\alpha dx]$ and therefore rises nearly exponentially at first to a maximum and then declines rapidly as α decreases and before x_0 is reached. If the density of the ionization in the avalanche reaches a sufficient magnitude two effects occur. The number of photons produced in the avalanche of electrons becomes large enough to produce effective photo-ionization in the surrounding gas. Simultaneously the density of the $\alpha\exp[\int_0^{x}\alpha dx]$ positive ions produced and left behind by the avalanche electrons increases and gives a strong space charge between the tip and the electron avalanche. This cloud of ions is being slowly (in comparison to electron velocities) drawn into the point where each ion has the probability γ of producing a secondary electron on impact with the point. This chance γ is none other than Townsend's coefficient for electron liberation by positive ion impact on the cathode. If the combination of the photoelectrically produced electrons in the gas and from the point together with the $\gamma\exp[\int_0^{x_0}\alpha dx]$ electrons furnished by ion impact exceeds unity then the discharge at the point could become self-sustaining, for these new electrons can themselves start avalanches which in their turn will furnish more positive ions. Under such conditions positive ions can proceed to accumulate in the gap and augment the positive space charge mentioned above. This charge *increases* the field close to the point, and increases α over very short distances next to the point. It reduces the field strength beyond the positive space charge, thus bringing x_0 closer to the point. The ionization beyond the space charge is thus reduced and ionizations by the electron avalanche are retarded. The photo-ionization effectively spreads the later avalanches laterally over the point surface by starting new avalanches at points about the initial avalanche.

This original picture of Trichel[1] is, however, not entirely satisfactory as the results here given show. First as pointed out by W. H. Bennett[11] the Trichel pulses require the presence of slow negative ions in order effectively to choke off the discharge. This is borne out by the fact that the pulses occur only in gases where electron attachment occurs. They are not observed in pure H_2 as reported by Bennett,[10] nor in H_2, N_2, or A as found by Weissler. Furthermore, the low frequency limit of the Trichel pulses is that to be expected from the time of movement of *negative* ions in the existing fields from point-to-plane. Such times have actually been measured for the transit of positive ions with a positive point-to-plane arrangement by Kip.[12]

In the second place if the triggering of the new discharge were caused primarily by the liberation of electrons by positive ion impact as postulated by Trichel, the Trichel pulses would depend very critically on the nature of the point surface and on γ. Doubtless this secondary emission does constitute *one* of the means of liberation. How-

[9] L. B. Loeb, *Fundamental Processes of Electrical Discharge in Gases* (John Wiley & Sons, New York, 1939), p. 515 ff.

[10] L. B. Loeb and J. M. Meek, *Mechanism of the Electrical Spark* (Stanford Press, 1941), p. 127.

[11] W. H. Bennett, Phys. Rev. **58**, 992 (1940).

[12] A. F. Kip, Phys. Rev. **55**, 549 (1939).

ever, since the positive ions are largely drawn into the point before the negative ion cloud has time to become ineffective* the low value of γ and the resulting statistical fluctuations in secondary emission are such as to be inadequate regularly to set off the corona pulses. Thus the pulses observed will be irregularly spaced in time, and frequently interrupted. Set off by chance secondary electrons after intervals in which the negative charge has sufficiently dissipated, the resulting pulses will vary in amplitude, larger pulses coming from longer intervals of dissipation. Were adequate numbers of electrons always on hand, the amplitude and frequency of the pulses would only be determined by the minimum time of clearing for re-ignition, the pulses thus being small and close together as observed by Trichel on increasing the potential. An adequate supply of triggering electrons for the regular Trichel pulses must then be furnished by outside agencies such as field emission from small rough points, ultraviolet light of adequate strength or by the Paetow effect[7] produced by minute specks of oxide. This explains clearly the observations by Kip, Hudson, and Bennett showing independence of γ, the effects of dust, etc., and the short irregular bursts of pulses when clean dry air is used with smooth points. The currents obtained by the regular Trichel pulses which are of uniformly smaller amplitude are, however, larger than those with the larger irregular bursts of discharge as the latter are interrupted frequently as Kip observed.

Even in the case of extremely sharp points where cold emission provides far greater electron currents from the point than required for triggering, the principal effect is that the irregular form of the cold emission current produces a correspondingly irregular pulse form instead of the regular Trichel pulses. The negative ion space charge still acts to control the number of ionizations per initial electron: $N=\exp[\int_0^{x_0}\alpha dx]$ in the distance x_0. This distance x_0 is not decreased much by a large increase of the priming cold emission current, because the exponential form of the expression requires a small change in x_0 to compensate a large change in the initiating electron current to sustain any given *average* negative ion space charge density.

In other words, the very disruptive nature of cold emission during breakdown is ballasted by the strongly controlling effect of the negative ion space charge.

The lateral spread of the discharge out to 0.1 mm in the high field region near the triggering dust speck can be explained as due to photoionization in the gas and the concentration of the discharge in a layer close to the point by the nature of the field and space charges. Its size is determined by the rate of propagation of the photoelectric ionization laterally and the duration of the discharge before it is interrupted by negative ion space charge.

The purple glow occasionally observed outward of the larger points below onset with no active spot by Kip and by Hudson is now to be ascribed to specks of dust or fine points as shown by Hudson. These points emit a stream of electrons that become visible by cumulative ionization and space charge formation well out in the wider high field regions beyond the point. The glows occur at potentials sufficient to cause the fine points to become emitters before pulses can normally originate at the large point surface.

At larger points there are visible in the negative point corona before onset accompanying the Trichel pulses what appear to be active spots showing negative glow, Faraday dark space and positive column as observed by Trichel, with, however, a bright radial blue streak in the center starting from the edge of the column towards the point. The streak extends back toward the cathode into the Faraday dark space.† While it could be associated with the triggering dust speck in the Trichel discharge, the position of the speck at the side as well as the conditions of its occurrence indicate a more interesting explanation. It is illustrated in Fig. 6(c). It occurs well above onset with larger points having a larger high field region. It is thus to be ascribed to the

* The negative space charge cloud need not cross to the plane to be ineffective. In fact Trichel found the frequency independent of gap length. The cloud must move sufficiently far away from the point in a weak field to exert no more influence on the positive ion cloud. This may be a matter of one or two mm with the points used here.

† It must be noted that visual and photographic observations record as superimposed many repetitions a *sequence* of events in a pulse cycle. Care must be used in interpreting such composite pictures as they record phenomena separated in time and space as if simultaneous.

attempts of the electron avalanches to initiate the retrograde streamers which are the forerunners of negative point breakdown with larger points.[13] They result from avalanches which would cause breakdown by positive streamers in a larger uniform gap. The streamers cannot advance all the way to the point cathode owing to the positive space charge which accumulates before the whole discharge is choked off. For still larger points the retrograde streamers reach the point and may cause breakdown.

The authors wish to express their appreciation to Makio Murayama, of the University of California Institute of Experimental Biology, for his valuable assistance in obtaining the photomicrographs.

[13] L. B. Loeb and J. M. Meek, *Mechanism of the Electrical Spark* (Stanford Press, 1941), pp. 82, 87, 99, 170.

NOVEMBER 15, 1941 PHYSICAL REVIEW VOLUME 60

Zeeman Effect Data and Preliminary Classification of the Spark Spectrum of Praseodymium—Pr II

NATHAN ROSEN,* GEORGE R. HARRISON, AND J. RAND MCNALLY, JR.
George Eastman Research Laboratories of Physics, Massachusetts Institute of Technology, Cambridge, Massachusetts

(Received August 29, 1941)

The Zeeman effect of praseodymium has been studied at fields up to 95,000 oersteds over the range 2400 to 7100A. g and J values have been determined for 74 Pr II levels from resolved Zeeman patterns of 141 lines. With these data, together with new wave-length data from the M.I.T.-W.P.A. Wavelength Project which have been applied to the spectroscopic interval sorter and interval recorder, a quadratic term array has been set up which accounts for 312 lines. This array is consistent with King's temperature classification of the lines and with all previous hyperfine structure observations. It is self-consistent in g values to an average deviation of 0.005 unit, and in wave numbers to an average deviation of 0.08 cm^{-1}. Previously published hyperfine structure measurements were found insufficiently precise to aid the classification, but were of value in its verification. The lowest term of Pr II is found to be $f^3(^4I^\circ)\cdot s-{}^5I^\circ_4$. Most of the strong lines showing hyperfine structure arise from the f^3s configuration.

THE spectra of praseodymium have long defied classification, both because of the complexity of this rare-earth atom, and because many of its lines show hyperfine structure difficult to measure. White[1] has published extensive and valuable data on the hyperfine structure of Pr II, but these prove to be not quite precise enough to establish a classification.

The *M.I.T. Wavelength Tables*[2] list 2708 strong lines of praseodymium, and the unpublished W.P.A. card catalog at M.I.T. contains 3454 lines of all intensities assigned to the element. Actually the spectrum is so rich that the number of observable lines is limited only by the difficulty of distinguishing true lines from bands. The available description of the spectrum between 8000 and 2400A is fairly good, though limited in wave-length precision by the difficulties of measurement introduced by partially resolved hyperfine structure patterns (h.f.s.). Unless wave-length values accurate to ±0.003A can be obtained, it is impossible in so complex a spectrum to determine which is the correct quadratic array of the many obtained from the combination

TABLE I. *Fields for various spectrograms.*

SET NO.	FIELD	SET NO.	FIELD
Z 41 H	95,000 oersteds	Z 47	89,900 oersteds
Z 41 L	72,340	Z 48	87,400
Z 42	90,860	Z 63	89,290
Z 44	91,500	Z 73	87,540
Z 45	91,500	Z 75−p	85,510
Z 46	86,400	Z 75−n	87,970

* Now at University of North Carolina, Chapel Hill, North Carolina.

[1] H. E. White, Phys. Rev. **34**, 1397 (1929).

[2] (John Wiley and Sons, New York, 1939.)

principle with the interval sorter[3] and recorder.[4] In the absence of data of suitable precision regarding wave-length and h.f.s., Zeeman effect measurements appeared to give the most powerful method of attacking the classification of the Pr spectra.

No Zeeman effect measurements on Pr lines appear to have been made hitherto, probably because of the high magnetic and spectrographic resolution needed for lines showing h.f.s. The availability of fields approaching 100,000 oersteds,[5] combined with spectrographs of high dispersion capable of giving Zeeman exposures in a few minutes, has now made possible the resolution of many patterns. The data thus obtained gave the desired start on the classification, which was then verified and extended by wave-length, h.f.s., and temperature class data.

The three concave gratings and other apparatus used have been described in previous papers dealing with the spectra of other elements.[6, 7] An arc carrying 4 amp. was run between electrodes of silver containing 20 percent of powdered praseodymium chloride. The arc so obtained was the brightest and steadiest we have yet produced in a strong magnetic field with any element, but most of the lines emitted were found to belong to Pr II and Pr III. Eleven sets of spectrograms were obtained, at fields listed in Table I. Each set contained *p*, *n*, and no-field exposures on each of from 12 to 24 plates 20 inches long, distributed throughout the spectrum.

All spectrograms were measured in both directions with an automatic comparator,[8] and were reduced by W.P.A. clerical workers, who have been of great assistance in reading, recording, and averaging the measurements used in calculating the data which follow. The field intensities given in Table I were calculated from measurements on the *raies ultimes* of silver, copper, and calcium, and are believed to be correct to within ±0.3 percent.

[3] G. R. Harrison, Rev. Sci. Inst. **4**, 581 (1933).
[4] G. R. Harrison, J. Opt. Soc. Am. **28**, 290 (1938).
[5] G. R. Harrison and F. Bitter, Phys. Rev. **57**, 15 (1940).
[6] G. R. Harrison and J. Rand McNally, Jr., Phys. Rev. **58**, 703 (1940).
[7] J. P. Molnar and W. J. Hitchcock, J. Opt. Soc. Am. **11**, 523 (1940).
[8] G. R. Harrison, J. Opt. Soc. Am. **25**, 169 (1935); Rev. Sci. Inst. **9**, 15 (1938); G. R. Harrison and J. P. Molnar, J. Opt. Soc. Am. **30**, 343 (1940).

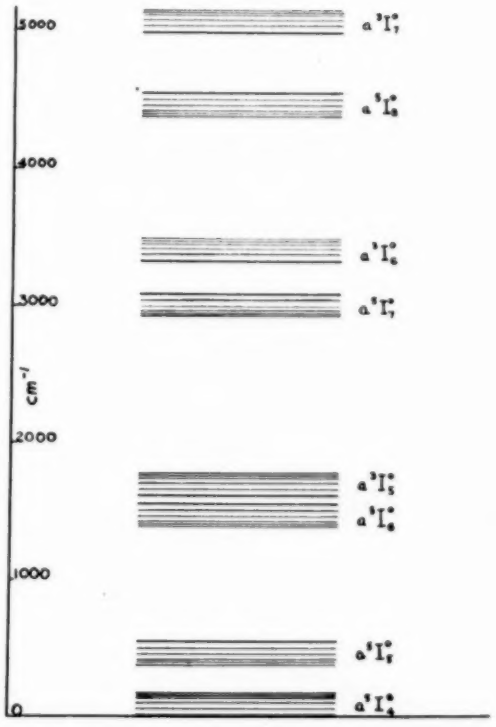

FIG. 1. Lowest terms of Pr II, showing alternate inverted and normal hyperfine-structure multiple terms in pairs.

RESULTS

Table II contains the lines of Pr II which we have classified thus far with reasonable assurance. The wave-lengths in angstroms given in the first column have been taken from the *M.I.T. Wavelength Catalogs*, as have the arc intensities in the second column. The third column gives the temperature class, while the fourth gives the h.f.s. of the line according to White,[1] or in cases marked *a*, from King.[9] *v* and *r* in this column indicate shaded toward short and long wave-lengths, respectively. The next column contains the observed wave number, while the column headed *o*−*c* gives the difference, in 0.01 cm^{-1} units, between the observed wave nunber and that calculated from the difference between the finally assigned wave numbers of the parent levels. The column headed "Comb." gives the lower and upper terms which appear to produce the line. This is followed by two columns giving the *g* values for these lower and upper levels as deduced from the observed patterns of the line where these could be interpreted.

[9] A. S. King, Astrophys. J. **68**, 194 (1928).

TABLE II. Pr II *Lines*.

λ	*I*	CLASS H.F.S.		σ OBS.	σ−*c*	COMB.	g_1	g_2
7099.54	2	—	—	14081.54	+ 8	$b^3I^\circ_5 - 3_5$	—	—
7021.54	6	—	—	14237.97	−13	$a^3H^\circ_5 - 8_5$	—	—
6850.55	4	—	—	14593.35	−12	$b^3I^\circ_4 - 2_4$	—	—
6564.632	10	V	—	15228.95	+ 6	$b^3I^\circ_4 - z^5K_5$	0.622	0.818
6475.287	3	—	—	15439.07	+ 2	$b^3I^\circ_4 - 5_5$	—	—
6454.865	3	—	—	15487.75	−11	$b^3I^\circ_5 - 11_6$	—	—
6397.996	12	V	—	15625.58	+13	$b^3I^\circ_5 - z^5K_6$	0.926	(0.959)
6305.262	9	V	—	15885.39	+ 1	$b^3I^\circ_7 - z^5I_7$	—	—
6278.675	9	V	—	15922.52	+ 2	$b^3I^\circ_6 - z^5K_7$	(1.073)	1.056
6262.539	9	V	—	15963.56	+10	$b^3I^\circ_6 - 17_6$	(1.073)	1.120
6244.344	10	V	—	16010.08	+ 6	$b^3I^\circ_6 - z^5I_6$	—	—
6200.79	5	—	—	16131.40	− 3	$b^3I^\circ_7 - z^5K_8$	1.145	(1.143)
6182.343	12	V	—	16170.64	− 9	$b^3I^\circ_5 - 30_5$	1.233	1.073
6165.945	50	V	—	16213.64	− 3	$b^3I^\circ_4 - z^5I_4$	0.620	(0.684)
6161.194	50	V	—	16226.15	+ 5	$b^3I^\circ_5 - z^5I_5$	0.92	0.89
6159.093	3	—	—	16231.67	+18	$a^3H^\circ_5 - 17_5$	1.04	1.04
6141.508	6	V	5?*a*	16278.15	+10	$a^3H^\circ_5 - z^5I_6$	—	—
6025.723	25	V	—	16590.93	− 2	$b^1I^\circ_6 - z^3I_6$	—	—
5967.837	15	V	—	16751.86	+ 1	$b^3I^\circ_6 - 22_6$	1.075	0.991
5892.231	10	V	—	16966.81	+ 1	$b^3I^\circ_6 - z^5I_7$	1.235	(1.187)
5879.253	10	V	—	17004.26	0	$b^3I^\circ_7 - z^5K_7$	1.149	(1.106)
5823.723	60	V	2	17166.40	−30	$b^3I^\circ_5 - z^5I_5$	—	—
5813.593	3	—	—	17196.31	−11	$b^3I^\circ_7 - z^5I_8$	1.153	(1.154)
5810.622	10	—	—	17205.10	− 2	$b^3I^\circ_8 - z^5K_9$	1.227	(1.217)
5807.55	2	—	—	17214.21	− 2	$b^3I^\circ_6 - z^5I_7$	—	—
5791.382	8	V	—	17262.26	+ 1	$a^3H^\circ_5 - 25_5$	1.043	1.063
5775.920	4*h*	—	—	17308.47	+ 5	$b^3I^\circ_4 - 12_4$	—	—
5719.090	10	V	—	17480.46	− 4	$a^3L^\circ_6 - 9_7$	1.08	(1.107)
5717.785	2*h*	—	—	17484.45	− 1	$a^3K^\circ_7 - 9_7$	—	—
5715.37	4	—	—	17491.84	0	$a^3K^\circ_6 - 4_6$	—	—
5711.65	8	—	—	17503.23	0	$b^3I^\circ_7 - z^3H_6$	1.147	(1.103)
5695.93	8	—	—	17551.54	− 1	$b^3I^\circ_6 - 26_7$	1.078	(1.067)
5689.185	1	—	—	17572.35	+ 8	$b^3I^\circ_7 - z^3I_7$	—	—
5687.19	4*h*	—	—	17578.51	−20	$a^3K^\circ_5 - 1_5$	—	—
5685.61	3	—	—	17583.40	+ 5	$a^3H^\circ_5 - z^3H_5$	—	—
5681.896	7	V	—	17594.89	− 8	$a^3H^\circ_5 - z^3H_5$	1.035	(1.101)
5677.04	3	—	—	17609.94	− 1	$a^3L^\circ_7 - 4_6$	—	—
5662.19	2	—	—	17656.12	+ 7	$b^3I^\circ_5 - 19_5$	—	—
5647.64	2	—	—	17701.61	− 1	$a^3K^\circ_7 - z^5K_6$	—	—
5637.36	2	—	—	17733 64	−14	$b^3I^\circ_6 - 27_6$	—	—
5634.93	2	—	—	17741.54	− 7	$b^3I^\circ_6 - 28_5$	—	—
5621.854	15	V	—	17782.80	−10	$a^3L^\circ_6 - 1_6$	—	—
5610.219	6	V	—	17819.68	+10	$a^3H^\circ_5 - 26_5$	1.043	1.073
5582.39	3	—	—	17908.51	+ 2	$b^3I^\circ_5 - 22_6$	—	—
5582.11	2	—	—	17909.41	− 9	$a^5K^\circ_8 - z^5K_7$	—	—
5580.39	2	—	—	17914.93	+ 3	$a^3K^\circ_6 - 6_6$	—	—
5571.841	10	V	—	17942.42	+ 1	$a^3K^\circ_5 - 2_5$	0.684	0.998
5560.21	1	—	—	17979.95	+ 4	$a^3K^\circ_7 - z^5K_6$	—	—
5551.08	2	—	—	18009.52	−12	$a^3H^\circ_5 - 28_5$	—	—
5543 87	2	—	—	18032.95	− 6	$a^3L^\circ_7 - 6_6$	—	—
5519.39	2	—	—	18112.93	+ 2	$b^3I^\circ_5 - z^3K_5$	—	—
5509.146	50	V	—	18146.61	+ 1	$a^3L^\circ_6 - 2_5$	0.723	0.998
5502.20	2	—	—	18169.51	+13	$a^5K^\circ_9 - z^5K_8$	—	—
5431.135	3	—	—	18407.25	+ 8	$b^3I^\circ_6 - z^3H_7$	—	—
5411.555	25	IV	—	18473.85	+ 4	$a^5K^\circ_5 - 3_5$	0.660	1.141
5381.262	60	V	—	18577.85	+ 2	$a^5K^\circ_6 - z^5K_5$	0.685	0.822
5368.830	5*d*	—	—	18620.87	+13	$a^5K^\circ_6 - 4_6$	—	—
5352.403	80	V	3?*a*	18678.02	+ 2	$a^5L^\circ_6 - 3_5$	0.712	1.155
5331.483	6	V	—	18751.31	0	$a^5K^\circ_6 - 11_6$	0.914	1.157
5322.778	30	V	—	18781.97	− 5	$a^5L^\circ_6 - z^5K_5$	0.718	0.820
5321.82	4	—	—	18785.35	−11	$a^5K^\circ_5 - 23_7$	—	—
5321.086	8	V	—	18787.94	− 5	$a^5K^\circ_6 - 5_5$	—	—
5312.327	5	V	6*ra*	18818.92	− 2	$a^3I^\circ_5 - 9_7$	—	—
5311.119	10	V	—	18823.20	−10	$a^5K^\circ_9 - 30_8$	1.217	1.073
5308.96	3	—	—	18830.86	+ 9	$a^5L^\circ_8 - 15_7$	—	—
5300.145	2	—	—	18862.18	+10	$b^3I^\circ_6 - z^3H_6$	—	—
5300.145	2	—	—	18862.18	+14	$a^5L^\circ_7 - 10_8$	—	—
5298.106	25	V	—	18869.44	+ 2	$a^5L^\circ_7 - 11_6$	0.928	1.160
5292.630	50	IV	—	18888.95	+ 1	$a^5K^\circ_6 - z^5K_6$	0.914	(0.959)
5292.10	60	V	6*ra*	18890 85	−24	$a^3I^\circ_7 - 10_8$	(1.143)	1.138
5289.937	6	—	—	18898.57	+10	$a^3I^\circ_7 - 11_8$	1.142	(1.156)
5263.878	25	IV	—	18992.13	− 5	$a^5L^\circ_6 - 5_5$	0.724	0.996
5259.743	125	V	—	19007.07	+ 2	$a^5L^\circ_7 - z^5K_6$	0.925	(0.959)
5258.20	2	—	—	19012.64	0	$b^3I^\circ_7 - z^3H_7$	—	—
5251.738	10	V	5?*a*	19036.03	− 7	$a^3I^\circ_7 - z^5K_6$	1.138	(0.959)
5220.113	80	IV	—	19151.35	0	$a^5L^\circ_8 - z^5K_7$	1.03	(1.062)
5219.053	50	IV	—	19155.24	− 7	$a^5K^\circ_7 - z^5K_7$	1.040	1.064
5216.761	8	—	—	19163.66	− 7	$a^5K^\circ_5 - 7_5$	—	—
5208.460	0	—	—	19194.20	−11	$b^3I^\circ_4 - 25_5$	—	—
5207.905	15	V	—	19196.27	0	$a^5K^\circ_7 - 17_6$	—	—
5206.562	30	V	—	19201.20	− 3	$a^5K^\circ_8 - z^5I_7$	—	—
5195.307	20	V	—	19242.79	− 4	$a^5K^\circ_7 - z^5I_6$	—	—
5195.110	10	V	—	19243.52	0	$a^5K^\circ_9 - z^5I_8$	—	—
5183.848	5	V	—	19285.33	− 1	$a^5L^\circ_7 - z^3K_6$	—	—
5175.833	10	—	—	19315.20	+ 1	$a^3I^\circ_6 - 4_6$	—	—
5173.898	100	IV	—	19322.41	+ 3	$a^5L^\circ_8 - z^5K_8$	1.116	(1.143)
5161.743	40	V	2?*a*	19367.92	0	$a^5L^\circ_6 - 7_5$	0.720	(0.896)
5135.125	50	V	—	19468.31	+ 3	$a^5K^\circ_8 - z^5K_8$	1.160	1.141
5129.520	100	IV	—	19489.58	− 1	$a^5K^\circ_6 - z^5I_5$	0.91	0.91
5121.7	2	—	—	19519.34	+24	$a^5K^\circ_5 - 8_5$	—	—
5118.021	4	—	—	19533.37	+ 6	$a^5I^\circ_8 - 10_8$	—	—
5110.768	80	V	—	19561.10	0	$a^5L^\circ_{10} - z^5K_9$	1.19	(1.217)
5110.382	80	V	—	19562.58	− 3	$a^5K^\circ_5 - z^5I_4$	0.686	0.686
5064.84	2*h*	—	—	19738.47	+22	$a^3I^\circ_6 - 6_6$	—	—
5061.50	1	—	—	19751.50	−14	$b^3I^\circ_4 - 26_5$	—	—
5060.40	2	—	—	19755.79	+ 5	$a^3I^\circ_5 - z^3I_6$	—	—
5034.415	30	V	—	19857.76	+ 7	$a^5K^\circ_9 - z^5K_8$	1.219	1.219
5015.543	4	—	—	19932.48	−15	$a^3I^\circ_5 - 1_5$	—	—
5013.20	2	—	—	19941.79	+ 9	$b^3I^\circ_4 - 28_5$	—	—
5004.584	5	—	—	19976.14	− 1	$a^5L^\circ_9 - 30_8$	—	—
5002.454	8	V	—	19984.63	− 3	$a^5K^\circ_7 - 22_6$	—	—
4991.774	3	—	—	20027.39	+12	$a^5I^\circ_6 - 1_5$	—	—
4991.774	3	—	—	20027.39	+ 8	$a^5L^\circ_8 - 23_7$	—	—
4977.578	2*h*	—	—	20084.50	+10	$a^5L^\circ_6 - 11_6$	—	—
4971.18	4	—	—	20110.35	+18	$a^5K^\circ_7 - 24_6$	—	—
4968.35	1	—	—	20122.22	+17	$a^5K^\circ_8 - 30_8$	—	—
4956.645	40	V	6?*a*	20169.33	+12	$a^3I^\circ_7 - 15_7$	(1.143)	1.057
4943.735	3	—	—	20221.99	− 4	$a^5L^\circ_8 - z^5K_6$	—	—
4931.28	1	—	—	20273.07	+ 4	$a^5K^\circ_6 - 16_5$	—	—
4925.630	10	V	5?*a*	20296.32	− 1	$a^3I^\circ_5 - 2_5$	—	—
4914.418	3	—	—	20342.63	0	$a^5K^\circ_8 - z^5K_7$	—	—
4912.629	10	V	—	20350.04	− 7	$a^5K^\circ_8 - z^3K_7$	1.13	(1.106)
4901.483	5	—	—	20396.31	− 6	$a^5L^\circ_9 - z^3I_8$	—	—
4886.045	20	V	—	20460.75	+ 1	$a^5L^\circ_7 - z^5K_7$	—	—
4879.121	30	—	6*r*	20489.79	0	$a^3I^\circ_7 - z^5K_7$	—	—
4877.81	40	V	6*r*	20495.30	+17	$a^3I^\circ_6 - 9_7$	1.046	1.108
4876.257	20	—	—	20501.46	−24	$a^5L^\circ_7 - 17_6$	—	—
4865.237	40	V	—	20548.26	+13	$a^5K^\circ_7 - z^3H_6$	1.057	(1.073)
4859.038	40	V	6*r*	20574.48	−18	$a^3I^\circ_6 - 11_6$	—	—
4839.540	25	—	—	20657.37	+ 1	$a^5K^\circ_5 - 12_4$	—	—
4826.649	40	—	6*r*	20712.54	+25	$a^3I^\circ_6 - z^5K_6$	—	—
4826.310	9	—	—	20713.99	−10	$a^5K^\circ_7 - z^5K_8$	—	—
4824.655	5	—	—	20721.09	− 2	$a^5K^\circ_5 - 13_5$	—	—
4814.344	30	V	—	20765.48	0	$a^5K^\circ_9 - z^5K_8$	1.20	(1.145)
4801.150	40	V	—	20822.54	−14	$a^5L^\circ_8 - z^5I_5$	0.73	0.92
4799.94	2	—	—	20827.79	+ 6	$a^3I^\circ_5 - 3_5$	—	—
4794.903	7	—	—	20849.67	+ 2	$a^5K^\circ_6 - 14_5$	—	—
4783.354	125	V	6*v*	20900.00	+ 6	$a^5I^\circ_7 - 9_7$	1.170	1.105
4779.196	15	—	—	20918.19	+ 7	$a^5K^\circ_8 - z^5I_7$	—	—
4778.303	35	—	6*v*	20922.10	−27	$a^5I^\circ_6 - 3_5$	—	—
4766.906	35	V	—	20972.13	+ 4	$a^5I^\circ_7 - 10_8$	—	—
4766.322	20	—	6*r*	20974.69	+ 3	$a^3I^\circ_5 - 4_6$	—	—
4765.222	80	V	6*v*	20979.53	+ 6	$a^5I^\circ_7 - 11_6$	1.179	(1.156)
4762.727	60	V	6*r*	20990.52	− 6	$a^3I^\circ_6 - z^5K_6$	1.038	(0.992)
4758.910	3	—	—	21007.36	−18	$a^5L^\circ_8 - 29_7$	—	—
4757.937	100	—	—	21011.66	+16	$a^5K^\circ_7 - 29_7$	—	—
4754.635	15	—	6*v*	21026.25	−14	$a^5I^\circ_6 - z^5K_5$	—	—
4746.635	15	—	6*v*	21026.25	−14	$a^5I^\circ_6 - z^5K_5$	—	—
4746.93	100	V	6*r*	21060.38	− 1	$a^5K^\circ_6 - 21_5$	(0.915)	0.886
4744.925	100	V	6*v*	21069.28	− 2	$a^5I^\circ_6 - 4_6$	(1.064)	1.10
4738.622	8*d*	—	—	21097.30	+10	$a^3I^\circ_7 - 20_6$	—	—
4734.177	100	V	6*v*	21117.09	− 1	$a^5I^\circ_7 - z^5K_6$	1.176	0.961
4728.630	40	V	6*r*	21141.88	− 3	$a^5I^\circ_5 - 5_5$	(0.860)	0.98
4721.910	3	—	—	21171.97	− 1	$a^5K^\circ_6 - 22_6$	—	—
4707.939	50	IV	6*v*	21234.79	+45	$a^5I^\circ_5 - 1_5$	0.858	0.986
4707.541	80	V	6*v*	21236.58	+ 3	$a^5I^\circ_6 - 5_5$	1.064	(0.994)
4689.341	4	—	—	21319.01	−13	$a^5I^\circ_7 - 22_6$	—	—
4685.447	5	—	—	21336.73	+ 3	$a^5L^\circ_7 - 23_7$	—	—
4679.498	2	—	—	21363.94	+ 4	$a^5L^\circ_8 - 30_8$	—	—
4679.112	8	—	6*r*	21365.61	−14	$a^3I^\circ_7 - 23_7$	—	—
4678.168	12	—	—	21369.93	0	$a^5K^\circ_5 - z^5H_4$	—	—
4672.595	3	—	—	21395.41	+ 2	$a^5I^\circ_7 - z^3K_6$	—	—
4672.081	100	IV	6*r*	21397.76	+ 4	$a^3I^\circ_5 - 6_6$	0.868	1.070
4663.454	6	—	—	21414.39	+ 4	$a^5K^\circ_6 - 25_5$	—	—
4668.230	10	—	6*r*	21415.42	−14	$a^3I^\circ_6 - 13_6$	—	—
4664.647	100	V	6*r*	21431.87	− 6	$a^3I^\circ_6 - z^3I_6$	1.037	(1.009)
4651.517	125	V	6*v*	21492.35	− 1	$a^5I^\circ_6 - 6_6$	1.05	1.07
4646.059	50	V	6*r*	21517.61	− 4	$a^3I^\circ_5 - 7_5$	0.863	0.893
4628.751	200	III	6*v*	21598.06	+ 2	$a^5I^\circ_5 - 2_5$	0.873	0.994
4627.05	15	—	—	21606.01	−11	$a^5L^\circ_6 - 16_5$	—	—
4612.072	60	IV	6?*a*	21676.19	− 9	$a^3I^\circ_4 - 1_5$	0.601	0.995
4603.478	4	—	—	21716.64	− 4	$a^5L^\circ_5 - 17_6$	—	—
4595.87	6	—	—	21752.59	+12	$a^5L^\circ_7 - z^5I_7$	—	—
4589.76	5*d*	—	—	21781.55	+ 3	$a^3I^\circ_7 - z^5I_7$	—	—
4581.584	10	V	6?*a*	21820.42	+ 5	$a^5I^\circ_7 - 13_7$	—	—
4578.139	40	V	6*r*	21836.84	+10	$a^5I^\circ_7 - z^3I_6$	(1.177)	1.010
4576.320	50	V	6*ra*	21845.51	+11	$a^3I^\circ_6 - 15_7$	(1.037)	1.066
4574.636	4	—	—	21853.56	0	$a^5L^\circ_7 - z^3H_6$	—	—
4570.565	40	V	6*r*	21873.02	0	$a^3I^\circ_5 - 8_5$	0.856	1 064
4568.545	30	—	—	21882.69	+ 8	$a^3I^\circ_7 - z^3H_6$	—	—
4561.461	6	—	—	21916.68	+15	$a^3I^\circ_5 - z^5I_4$	—	—
4561.10	3	—	—	21918.41	+ 8	$a^5L^\circ_9 - z^3K_8$	—	—
4554.790	4	—	—	21948.78	−13	$a^5L^\circ_5 - 18_5$	—	—
4550.882	10	V	6*v*	21967.63	− 3	$a^5I^\circ_6 - 8_5$	1.07	1.07
4550.06	15	—	—	21971.59	− 9	$a^5K^\circ_6 - 26_5$	—	—
4540.151	5	—	—	22019.54	+ 2	$a^3L^\circ_7 - z^5K_8$	—	—
4535.921	125	III	6*r*	22040.08	+10	$a^5I^\circ_4 - 2_5$	0.605	0.998
4534.154	150	IV	6*r*	22048.67	+10	$a^3I^\circ_7 - z^3K_8$	(1.143)	1.146
4524.695	5	—	—	22094.76	−13	$a^5K^\circ_7 - z^5H_6$	—	—
4524.365	10	—	—	22096.37	− 1	$a^3I^\circ_6 - 16_5$	—	—
4517.595	40	IV	6*v*	22129.48	− 1	$a^3I^\circ_5 - 3_5$	0.880	1.165
4510.160	200	III	6*r*	22165.97	− 1	$a^3I^\circ_6 - z^5K_7$	1.029	(1.062,
4501.828	20	—	—	22206.99	+ 5	$a^3I^\circ_6 - 17_6$	—	—
4496.429	200	III	6*r*	22233.65	−16	$a^3I^\circ_5 - 11_6$	0.861	1.153
4496.429	200	III	6*v*	22233.65	+19	$a^5I^\circ_6 - z^5K_5$	0.875	(0.821)
4493.119	25	—	6*v*	22250.03	−21	$a^5I^\circ_6 - 9_7$	—	—

TABLE II.—*Continued.*

λ	I	CLASS	H.F.S.	σ OBS.	o−c	COMB.	g_1	g_2
4493.119	25	—	6r	22250.03	−18	$a^5I^o_7 - 15_7$	—	—
4492.427	25	V	6r	22253.45	− 5	$a^3I^o_6 - z^3I_6$	—	—
4487.821	40	V	6r	22276 29	− 8	$a^3I^o_5 - 4_6$	—	—
4479.618	35	—	—	22317.09	+16	$a^5L^o_7 - 29_7$	—	—
4477.259	125	IV	6v	22328.85	+ 8	$a^5I^o_6 - 11_6$	1.054	1.150
4473.835	30	—	—	22345.93	− 5	$a^3I^o_7 - 29_7$	—	—
4468.712	125	III	6r	22371.56	−20	$a^3I^o_5 - z^5K_6$	0.864	0.963
4458.336	90	V	6v	22423.62	−12	$a^5I^o_6 - z^3I_7$	(1.250)	1.125
4454.382	60	IV	6v	22443.52	−10	$a^5I^o_5 - 5_6$	—	—
4449.867	125	III	6r	22466.30	−10	$a^5I^o_6 - z^5K_6$	1.075	0.961
4429.238	60	III	6r	22570.93	−45	$a^5I^o_4 - 3_5$	0.608	1.165
4429.238	100	III	6v	22570.93	+14	$a^5I^o_7 - z^5K_7$	(1.177)	1.061
4421.231	100	IV	6v	22611.80	+ 5	$a^5I^o_7 - 17_6$	1.175	1.110
4413.765	90	III	6ra	22650.05	0	$a^3I^o_6 - z^3K_6$	0.860	0.992
4412.155	50	IV	6v	22658.31	0	$a^5I^o_7 - z^5I_8$	(1.177)	1.046
4408.844	125	III	6r	22675.34	− 6	$a^3I^o_4 - z^5K_5$	0.605	0.823
4405.849	100	IV	6r	22690.75	− 4	$a^3I^o_5 - z^5K_6$	(1.250)	1.146
4403.605	100	V	6r	22702.31	− 3	$a^3I^o_7 - 30_8$	—	—
4395.788	30	V	—	22742.68	−17	$a^3I^o_6 - 19_7$	1.052	(1.025)
4372.385	10	—	—	22864.41	+ 6	$a^5K^o_5 - z^3H_6$	—	—
4368.327	125	III	6r	22885.65	+ 9	$a^5I^o_4 - 5_5$	0.605	0.994
4365.328	6	—	—	22901.37	+ 2	$a^5L^o_7 - z^3K_7$	—	—
4359.795	100	IV	6r	22930.43	+ 3	$a^3I^o_7 - z^3K_7$	(1.143)	1.102
4352.752	4	—	—	22967.54	+ 9	$a^5L^o_6 - z^5I_7$	—	—
4351.849	80	III	6r	22972.30	−11	$a^3I^o_5 - z^5I_5$	(0.860)	0.904
4347.490	100	IV	6r	22995.33	0	$a^3I^o_5 - 22_6$	1.047	(0.990)
4338.694	100	IV	6r	23041.98	+ 4	$a^3I^o_6 - 23_7$	(1.037)	1.075
4333.913	150	IV	6r	23067.37	+32	$a^5I^o_6 - z^5I_5$	1.062	0.910
4332.487	30	—	—	23074.97	− 6	$a^3I^o_5 - 13_6$	—	—
4331.472	5	—	—	23080.37	+21	$a^5L^o_6 - z^5H_5$	—	—
4329.415	50	IV	6?r?a	23091.34	− 6	$a^3I^o_5 - z^5I_6$	(0.860)	1.009
4327.698	3	—	—	23100.50	− 8	$a^5K^o_5 - 26_6$	—	—
4323.922	35	—	6r	23120.67	−17	$a^3I^o_6 - 24_6$	—	—
4323.551	100	IV	6r	23122.65	+ 9	$a^3I^o_7 - z^5I_8$	(1.143)	1.167
4314.74	2	—	—	23169.87	+20	$a^5I^o_6 - 13_6$	—	—
4313.843	4	—	—	23174.69	− 4	$a^3I^o_5 - 8_6$	—	—
4308.457	20	—	—	23203.66	+ 9	$a^3I^o_4 - 14_5$	—	—
4305.763	150	III	6ra	23218.18	− 6	$a^5I^o_5 - z^5I_4$	0.877	0.683
4302.100	60	—	—	23237.95	+25	$a^3I^o_6 - 25_6$	(1.037)	1.065
4297.764	50	III	6r	23261.40	+10	$a^5I^o_4 - 7_5$	0.601	0.895
4292.351	4	—	—	23290.72	+ 8	$a^5K^o_5 - 28_6$	—	—
4290.99	5	—	—	23298.11	−10	$a^5I^o_5 - 14_5$	—	—
4288.830	8	—	—	23309.85	−19	$a^5K^o_7 - z^5K_6$	—	—
4282.440	75	IV	6v	23344.63	+ 7	$a^5I^o_6 - 30_8$	1.245	1.071
4272.271	50	III	6r	23400.18	+ 4	$a^5I^o_7 - 22_6$	1.177	0.991
4263.805	50	IV	6r	23446.65	−10	$a^3I^o_7 - 23_7$	—	—
4261.796	15	IV	6ra	23457.71	0	$a^3I^o_6 - z^5I_7$	—	—
4259.64	5d	—	—	23469.58	+22	$a^5L^o_7 - z^5I_7$	—	—
4254.420	35	IV	6r	23498.38	− 3	$a^3I^o_7 - z^5I_7$	(1.143)	1.191
4249.484	20	V	6ra	23525.67	+ 2	$a^5I^o_7 - 24_6$	(1.177)	0.98
4247.662	60	III	6r	23535.75	− 9	$a^5I^o_5 - 11_6$	0.878	1.156
4243.528	20	III	6r	23558.69	−11	$a^5I^o_6 - z^5H_6$	1.022	(1.073)
4241.019	50	IV	6v	23572.62	0	$a^5I^o_8 - z^3K_7$	(1.250)	1.108
4236.210	20	III	6r	23599.38	−13	$a^5I^o_6 - 15_7$	(1.064)	1.085
4225.327	50	III	6r	23660.17	− 1	$a^5I^o_4 - z^5I_4$	0.604	0.685
4222.98	125	III	6v	23673.31	−16	$a^5I^o_5 - z^5K_6$	0.877	0.961
4213.96	12	—	—	23723.99	+14	$a^3I^o_5 - z^5H_4$	—	—
4208.305	18	III	6ra	23755 87	+ 2	$a^3I^o_5 - 16_5$	(0.860)	0.980
4206.739	50	III	6v	23767.71	− 7	$a^5I^o_5 - z^5I_6$	1.256	1.160
4191.615	40	III	6r	23850.45	− 4	$a^5I^o_6 - 16_6$	(1.064)	0.985
4189.518	100	III	6v	23862.39	−13	$a^5I^o_7 - z^5I_7$	1.175	1.121
4180.68	8	—	—	23812.84	−13	$a^3I^o_5 - z^5I_6$	—	—
4179.422	200	III	6v	23920.04	− 5	$a^5I^o_6 - z^5K_7$	1.061	(1.062)
4172.273	75	III	6r	23961.02	− 3	$a^5I^o_6 - 17_6$	(1.064)	1.14
4171.824	75	III	6r	23963.60	− 1	$a^5I^o_7 - z^3H_6$	(1.177)	1.074
4169.459	15	V	6r	23977.19	− 7	$a^3I^o_6 - 27_6$	—	—
4168.08	20	—	—	23985.12	+ 3	$a^3I^o_6 - 28_6$	—	—
4164.192	200	III	6v	24007.52	− 9	$a^3I^o_6 - z^3I_6$	—	—
4161.65	8	—	—	24022.18	+ 1	$a^3I^o_6 - 29_7$	—	—
4148.457	15	III	5?a	24098.58	+ 2	$a^3I^o_5 - 18_6$	0.863	1.011
4143.136	200	III	6v	24129.52	− 5	$a^5I^o_7 - z^5K_6$	(1.177)	1.141
4141.257	150	III	6v	24140.47	−16	$a^5I^o_8 - z^3I_7$	1.242	1.172
4132.230	15	IV	6va	24193.21	+ 1	$a^3I^o_6 - 18_5$	—	—
4118.481	250	III	6v	24273.97	−15	$a^5I^o_5 - z^5I_5$	(0.875)	0.920
4111.871	30	IV	5a	24312.99	0	$a^5I^o_5 - 12_4$	0.878	0.914
4100.746	200	III	6v	24378.94	− 1	$a^5I^o_6 - z^5K_6$	1.256	1.221
4100.22	15	—	—	24382.08	+ 1	$a^5I^o_7 - 27_6$	—	—
4096.822	30	III	6?r?a	24402.30	− 2	$a^3I^o_5 - 19_5$	0.858	1.024
4091.686	50	—	—	24432.93	+ 7	$a^3I^o_5 - 20_6$	—	—
4081.018	50	III	6v	24496.80	−16	$a^5I^o_6 - 19_7$	(1.064)	1.035
4075.917	15d	—	—	24527.46	− 4	$a^5I^o_6 - 20_6$	—	—
4073.305	9	—	—	24543.18	− 3	$a^3I^o_5 - 21_5$	—	—
4062.817	150	III	6r	24606.54	− 5	$a^3I^o_6 - z^3K_7$	1.035	1.106
4061.336	4	—	—	24615.51	+ 4	$a^5L^o_7 - z^3K_6$	—	—
4056.543	100	III	6r	24644.60	+ 8	$a^3I^o_7 - z^3K_6$	(1.143)	1.149
4054.845	50	III	6r	24654.92	+12	$a^3I^o_5 - 22_6$	0.862	0.991
4044.818	50	III	6ra	24716.03	− 3	$a^3I^o_4 - z^5I_5$	0.605	0.910
4039 357	50	III	6v	24749.45	+ 1	$a^5I^o_5 - 22_5$	1.08	0.98
4038.467	15	III	6?ra	24754.91	− 2	$a^5I^o_4 - 12_4$	0.613	0.918
4034.30	20	—	6r	24780.47	+16	$a^3I^o_6 - 24_6$?	—	—
4033.857	50	III	6v	24783.19	−15	$a^5I^o_7 - 30_8$	(1.177)	1.077
4031.755	50	III	6v	24796.11	+ 6	$a^5I^o_6 - 23_7$	(1.064)	1.089
4015.389	50	III	6?ra	24897.18	+ 1	$a^3I^o_5 - 25_5$	0.858	1.073
4008.714	150	III	6r	24938.64	−14	$a^3I^o_7 - z^5H_7$	(1.143)	1.209
4000.190	50	III	6v	24991.77	− 4	$a^5I^o_6 - 25_6$	(1.064)	1.080
3997.054	100	III	6v	25011.38	− 2	$a^5I^o_7 - z^3K_7$	(1.177)	1.101
3994.834	300	III	6v	25025.28	−28	$a^5I^o_5 - z^5H_4$	0.89	0.89
3989.718	200	III	6v	25057 29	−27	$a^5I^o_4 - 16_5$	0.873	0.982
3982.063	125	III	6r	25105.53	− 3	$a^3I^o_6 - z^5H_6$	(1.037)	1.106
3972.164	125	III	6v	25168.11	− 1	$a^5I^o_5 - 17_6$	0.877	1.118
3971.164	100	III	6r	25174.44	−16	$a^3I^o_6 - z^3I_7$	(1.037)	1.187
3966.573	100	III	6v	25203.57	+ 1	$a^5I^o_7 - z^5I_8$	(1.177)	1.154
3965.263	100	III	6v	25211.90	+ 8	$a^3I^o_6 - z^3I_7$	(1.064)	1.128
3964.825	125	III	6v	25214.68	0	$a^5I^o_5 - z^5I_6$	(0.875)	1.039
3964.261	60	III	6r	25218.27	0	$a^3I^o_5 - z^3H_6$	0.858	1.071
3962.445	60	III	6?a	25229.83	− 6	$a^3I^o_5 - z^5H_5$	0.869	1.108
3953.516	150	III	6v	25286.81	+ 7	$a^5I^o_6 - z^3K_6$	(1.250)	1.145
3949.438	150	III	6v	25312.92	+ 1	$a^5I^o_6 - z^3H_6$	1.08	1.08
3947.633	125	III	6v	25324.49	− 4	$a^5I^o_6 - z^5H_5$	(1.064)	1.125
3935.823	125	III	6?va	25400.48	+21	$a^5I^o_5 - 18_5$	(0.875)	0.990
3927.454	80	III	6?ra	25454.60	+10	$a^3I^o_5 - 26_5$	0.859	1.066
3925.456	125	III	3a	25467.56	+ 6	$a^5I^o_4 - z^5H_4$	0.603	0.903
3920.524	30d	III	2a	25499.60	+10	$a^5I^o_4 - 16_5$	(0.605)	0.985
3918.856	100	III	4a	25510.45	+ 8	$a^5I^o_7 - z^5H_6$	(1.177)	1.094
3912.898	150	III	4a	25549.29	+15	$a^5I^o_6 - 26_6$	(1.064)	1.097
3908.033	100	IV	5?a	25581.10	+10	$a^5I^o_4 - z^5H_7$	(1.250)	1.220
3899.555	10	—	—	25636.71	− 2	$a^5I^o_5 - 27_6$	—	—
3889.330	150	IV	5a	25704.11	+13	$a^5I^o_5 - 19_5$	(0.875)	1.025
3885.190	100	IV	4a	25731.51	+14	$a^5I^o_4 - 27_5$	1.058	1.068
3884.741	4	—	—	25734.48	− 9	$a^5I^o_5 - 20_6$	—	—
3884.039	5	—	—	25739.13	− 7	$a^5I^o_6 - 28_6$	—	—
3878.307	—	—	—	25777.17	−11	$a^5I^o_6 - 29_7$	—	—
3868.578	15	—	—	25841.99	−22	$a^5I^o_4 - 18_5$	—	—
3868.125	4	—	—	25845.02	+10	$a^5I^o_5 - 21_5$	—	—
3826.708	—	—	—	26124.74	+ 3	$a^5L^o_6 - z^3H_7$	—	—
3823.571	10	—	—	26146.17	+20	$a^5I^o_4 - 19_5$	—	—
3803.110	50d	—	—	26286.83	− 3	$a^5I^o_4 - 21_5$	—	—
3792.435	4	—	—	26360.82	+12	$a^5I^o_6 - z^5K_7$	—	—
3769.695	20d	V	2a	26519.84	−14	$a^5I^o_5 - z^3H_6$	—	—
3711.099	8d	V	—	26938.56	+12	$a^5I^o_4 - 27_5$	—	—
3710.012	6	—	—	26946.45	+18	$a^5I^o_5 - 28_6$	—	—
3699.952	12	—	—	27019.72	− 6	$a^5I^o_7 - z^5H_7$	—	—
3650.176	30	—	—	27388.16	− 5	$a^5I^o_4 - 28_5$	0 607	0.888

The complexity introduced by h.f.s., coupled with the natural richness of the spectrum, has made the disentangling of overlapping patterns difficult, and less precision can be expected in the g values than is obtained with a spectrum consisting mostly of sharp lines.[10] Where a g value is in parenthesis the pattern of the line was incomplete, overlapped, or unresolved, so this g value was assumed from the average for the level, and the other g value was calculated from this and the experimental data. In other cases unresolved n patterns were used, a procedure which introduces small errors.

On account of the complexity of the patterns and the necessity of using exposures at various field strengths to interpret them, any table of actual measurements would be unduly extensive even if reported in abbreviated notation.[10] For this reason only final g values are given, their use being to substantiate the quantum numbers assigned, and detailed results are held for a later report.

[10] G. R. Harrison, W. E. Albertson, and N. Hosford, J. Opt. Soc. Am. **31**, 439 (1941).

TABLE III. Pr II *terms*.

TERM	WAVE NUMBER	h.f.p.	No. COMB.	g LS (THEOR.)	g (MEAS.)	No. PATTERNS RESOLVED
$a^5I^\circ_4$	0.00	$6i$	15	0.600	0.605	12
$a^5I^\circ_5$	441.94	$6n$	23	0.900	0.875	12
$a^5I^\circ_6$	1649.01	$6n$	32	1.071	1.064	3
$a^5I^\circ_5$	1743.65	$6i$	30	0.833	0.860	16
$a^5I^\circ_7$	2998.31	$6n$	24	1.179	1.177	12
$a^5I^\circ_6$	3403.12	$6i$	26	1.024	1.037	3
$a^5L^\circ_6$	3893.38	—	14	0.714	0.721	5
$a^5K^\circ_5$	4097.57	—	16	0.667	0.683	3
$a^5I^\circ_8$	4437.09	$6n$	10	1.250	1.250	7
$a^5I^\circ_7$	5079.31	$6i$	20	1.143	1.143	1
$a^5L^\circ_7$	5108.36	—	16	0.911	0.926	1
$a^5K^\circ_6$	5226.47	—	12	0.905	0.915	1
$a^5K^\circ_7$	6413.79	—	14	1.054	1.042	0
$a^5L^\circ_8$	6417.75	—	6	1.042	1.06	0
$b^5I^\circ_4$	7446.51	—	9	0.600	0.622	1
$a^5K^\circ_8$	7659.60	—	7	1.153	1.161	0
$a^5L^\circ_9$	7805.50	—	4	1.133	1.115	0
$b^5I^\circ_5$	8489.94	—	7	0.900	0.93	0
$a^5K^\circ_9$	8958.35	—	5	1.222	1.219	1
$a^5L^\circ_{10}$	9254.94	—	1	1.200	1.19	0
$a^5H^\circ_3$?	9378.57	—	8	1.033	1.044	0
$b^5I^\circ_6$	9646.60	—	11	1.071	1.073	1
$b^5I^\circ_7$	11005.45	—	7	1.179	1.153	1
$b^5I^\circ_8$	11610.92	—	6	1.250	1.231	2
1_5	21676.28	—	6	—	1.001	2
2_5	22039.98	—	7	—	0.997	4
3_5	22571.38	—	7	—	1.163	4
z^5K_5	22675.40	—	6	0.667	0.821	4
4_6	22718.31	—	7	—	1.10	0
5_5	22885.56	—	7	—	0.994	2
6_6	23141.37	—	5	—	1.062	1
7_5	23261.30	—	4	—	0.896	3
8_5	23616.67	—	5	—	1.068	1
z^5I_4	23660.18	—	5	0.600	0.684	2
9_7	23898.25	—	6	—	1.107	2
10_8	23970.40	—	4	—	1.14	0
11_6	23977.78	—	10	—	1.156	5
z^5K_6	24115.41	—	10	0.905	0.959	5
z^5K_6	24393.70	—	6	0.857	0.992	1
z^5I_5	24716.06	—	8	0.900	0.911	2
12_4	24754.93	—	4	—	0.911	2
13_6	24818.68	—	5	—	—	0
z^5I_6	24835.05	—	4	1.024	1.009	2
14_5	24947.22	—	4	—	—	0
15_7	25248.52	—	5	—	1.07	0
z^5H_4	25467.50	—	4	0.900	0.905	1
16_5	25499.50	—	7	—	0.984	3
z^5K_7	25569.10	—	10	1.054	1.062	1
17_6	25610.06	—	9	—	1.116	2
z^5I_6	25656.62	—	9	1.071	1.042	2
18_5	25842.21	—	4	—	0.999	2
19_5	26145.97	—	6	—	1.025	2
20_6	26176.51	—	4	—	—	0
21_5	26286.86	—	4	—	0.89	0
22_6	26398.45	—	9	—	0.990	3
23_7	26445.06	—	8	—	1.08	0
24_6	26523.96	—	4	—	1.02	1
25_5	26640.82	—	6	—	1.075	1
z^5I_7	26860.83	—	10	1.179	1.123	3
z^5H_6	26961.92	—	9	1.167	1.073	2
z^5H_5	26973.54	—	5	1.100	1.101	1
z^5K_8	27127.88	—	9	1.153	1.143	1
26_5	27198.15	—	7	—	1.067	1
27_6	27380.38	—	6	—	1.06	0
28_5	27388.21	—	8	—	0.886	1
29_7	27425.29	—	6	—	—	0
30_8	27781.65	—	8	—	1.075	4
z^5K_7	28009.71	—	8	1.018	1.106	3
z^5I_8	28201.87	—	8	1.250	1.154	1
z^5H_6	28508.68	—	6	1.214	1.103	1
z^5I_7	28577.72	—	7	1.143	1.187	3
z^5K_9	28816.04	—	4	1.222	1.217	0
z^5K_8	29723.83	—	7	—	1.145	1
z^5H_7	30018.09	—	7	1.286	1.215	0

That so many values of $o-c$ are less than 10 (i.e., less than 0.1 cm^{-1}) is gratifying, as it is difficult to make exact wave-length measurements on lines with partially resolved h.f.s. 132 lines are found to agree with the wave number calculated from the combination principle to within ± 0.05 cm^{-1}, and 78 more to within ± 0.10, leaving only 108 with deviations greater than 0.10 cm^{-1}.

In the first column of Table III are listed the term assignments, followed by the wave number of each and the hyperfine structure deduced from all lines considered as arising from the term, where i indicates wider separations at lower wave numbers, and n at higher. The fourth column gives the number of combinations with the term in the present array. The fifth column contains the theoretical g value of a term of the designation given, calculated from Landé's formula for LS coupling. The next column contains the measured g value of the term, averaged from measurements on the number of resolved patterns given, or on unresolved patterns reduced from several plates. The observed g values are in most cases believed to be correct to within ± 0.005 unit.

LOW CONFIGURATIONS OF Pr II

In accordance with the Bohr-Stoner theory the normal praseodymium atom ($Z=59$) can be expected to have three electrons outside a closed shell. Pr II, with two such electrons, would have a simpler spectrum than Pr I, but in both cases two $6s$ electrons are present which are very loosely bound, and it is necessary in Pr II to take four electrons into account when predicting terms. Among the odd configurations to be expected are fds^2, fd^2s, f^3s and f^3d. Even configurations which should be important are f^2ds, f^2s^2, f^3p, and f^4.

Many of the strongest lines of Pr II, which presumably arise from low levels, show wide h.f.s. patterns. These usually arise when a single s electron occurs in a configuration, making

TABLE IV. *Expected important terms of* Pr II.

$4f^36s$	$^{5,3}(IGFDS)^\circ$, $^{3,1}(LKIH_2G_2F_2D_2P)^\circ$
$4f^35d$	$^{5,3}(LKIHG, IHGFD, HGFDP, GFDPS, D)^\circ$ $^{3,1}(NML_2K_4I_6H_7G_9F_9D_7P_5S_3)^\circ$
$4f^36p$	$^{5,3}(KIH, HGF, GFD, FDP, P)$ $^{3,1}(ML_2K_3I_4H_5G_6F_6D_5P_3S)$

TABLE V. *Principal supermultiplet of* Pr II.*

	$a^5I^\circ_8$	$a^5I^\circ_7$	$a^5I^\circ_6$	$a^5I^\circ_5$	$a^5I^\circ_4$	$a^3I^\circ_7$	$a^3I^\circ_6$	$a^3I^\circ_5$
z^5K_9	200 III 6v	X	X	X	X	X	X	X
8	100 IV 6v	200 III 6v	X	X	X	150 IV 6r	X	X
7	—	100 III 6v	200 III 6v	X	X	30 — 6r	200 III 6r	X
6	X	100 V 6v	125 III 6v	125 III 6v	X	10 V 5?a	40 — 6r	125 III 6r
5	X	X	15 — 6v	200l III 6v	125 III 6r	X	—	—
z^5K_8	150 III 6v	—	X	X	X	100 III 6r	X	X
7	50 IV 6v	100 III 6v	4 — —	X	X	100 IV 6r	150 III 6r	X
6	X	3 — —	—	—	X	—	60 V 6r	90 III 6ra
z^5I_8	50 III 6v	100 III 6v	X	X	X	100 IV 6r	X	X
7	90 V 6v	100 III 6v	100 III 6v	X	X	5d — —	15 IV 6ra	X
6	X	50 IV 6v	200 III 6v	125 III 6v	X	—	25 V 6r	8 — —
5	X	X	150 IV 6v	250 III 6v	50 III 6ra	X	—	80 III 6r
4	X	X	X	150 III 6va	50 III 6r	X	X	6 — —
z^5I_7	150 III 6v	—	—	X	X	35 IV 6r	100 III 6r	X
6	X	40 V 6v	—	—	X	2 — —	100 V 6r	50 IV 6?r?a
5	X	X				X		
z^5H_7	100 IV 5?a	12 — —	—	X	X	150 III 6r	—	X
6	X	100 III 4a	—	—	X	—	125 III 6r	—
5	X	X	125 IV 6v	—	—	X	—	60 III 6?a
4	X	X	X	300 III 6v	125 III 3a	X	X	12 — —
3	X	X	X	X		X	X	X
z^5H_6	X	75 III 6v	150 III 6v	20d V 2a	X	30 — —	20 III 6r	60 III 6r
5	X	X				X		
4	X	X	X			X	X	

* X—indicates line forbidden by selection principle for ΔJ. ——indicates line not found.

plausible the assumption that the lowest terms of Pr II arise from such a configuration. Three likely configurations are then fd^2s, f^2ds and f^3s. Resulting terms of the latter are given in Table IV. When Hund's theory and Meggers and Laporte's rule are used the lowest terms to be expected from these three configurations are $^5I^\circ_4$, $^5K_5$, and $^5I^\circ_4$, respectively.

Our analysis indicates that the level $f^3(^4I^\circ)\cdot s^5I^\circ_4$ is the lowest. As will be seen from Fig. 1, all eight levels of the low $^5I^\circ$ and $^3I^\circ$ terms arising from the addition of an s electron to the parent $^4I^\circ$ term of Pr III have been found. Combinations of these terms with the even triads ^5KIII and ^3KIII which arise from the f^3p configuration give rise to the strongest lines of the spectrum. The *raies ultimes* of praseodymium are usually given[11] as 4179.422 and 4062.817A. These lines we have classified as $a^5I^\circ_6-z^5K_7$ and $a^3I^\circ_6-z^3K_7$. From the usual multiplet intensity rules one would expect the leading line of the supermultiplet to be strongest, with a prediction of $a^5I^\circ_8-z^5K_9$ as the *raie ultime*. This line, at 4100.746, is of intensity 200, but other lines are stronger. The estimated intensities of the lines of the basic supermultiplet are given in Table V, where an irregularity in intensities is to be noted. A similar irregularity is found in the homologous supermultiplet of Nd II.[12] The intensities need more careful study before the cause of this anomaly can be explained.

[11] *M. I. T. Wavelength Tables.*

HYPERFINE STRUCTURE

The eight levels of the terms $f^3(^4I^\circ)\cdot s^5I^\circ$ and $^3I^\circ$ have marked hyperfine structure which appears to be due mainly to the interaction of the 6s electron with the moment of the nucleus. It is of interest to apply to this case the equations given by Goudsmit and Bacher.[13] The change in atomic energy due to the interactions between electronic and nuclear moments (h.f.s.) is given by

$$\Gamma_F=\tfrac{1}{2}A[F(F+1)-I(I+1)-J(J+1)], \quad (1)$$

where J represents the mechanical moment of the electrons, I that of the nucleus ($=5/2$ for Pr), F the total moment, and A is a number independent of F.

If we assume that the hyperfine structure is due to the s electron and that there is JJ coupling between the latter and the ion, then, as shown by Goudsmit and Bacher,

$$A=a\frac{J(J+1)+s(s+1)-J'(J'+1)}{2J(J+1)}, \quad (2)$$

[12] McNally, Harrison, and Albertson, to be published shortly.

[13] S. Goudsmit and R. F. Bacher, Phys. Rev. **34**, 1501 (1929).

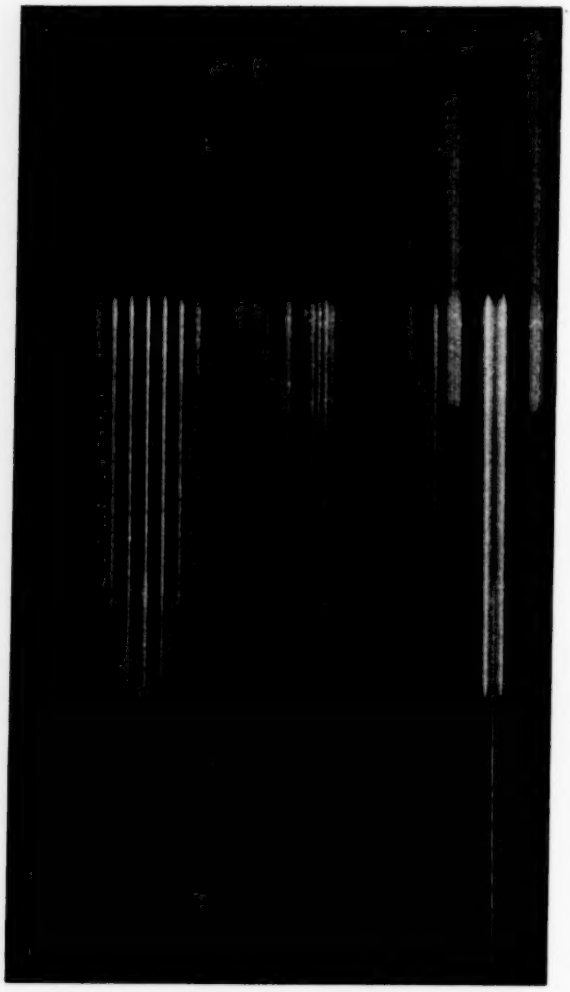

FIG. 2. Zeeman patterns of Pr II line showing hyperfine structure. Below, no-field pattern; middle, n components; above, p components. The strong line at the left is λ4368.327A.

where s is the spin of the electron ($=\frac{1}{2}$), J' the moment of the ion, and a a constant which measures the strength of the interaction between the s electron and the nuclear moment.

There are two cases to be considered. For the levels $^5I^\circ_{5,6,7,8}$

$$J'=J-\tfrac{1}{2}$$

and (2) gives

$$A=a/2J. \tag{3}$$

For the levels $^5I^\circ_4$ and $^3I^\circ_{5,6,7}$

$$J'=J+\tfrac{1}{2}$$

and

$$A=-a/[2(J+1)]. \tag{4}$$

The difference in signs of (3) and (4) is in agreement with the observed difference in the shading of the h.f.s. for lines involving the two groups of levels.

For $J>1$, the total width of the hyperfine structure $\Delta\sigma$ is found from (1) to be given by

$$\Delta\sigma=\Gamma_{J+I}-\Gamma_{J-I}=AI(2J+1). \tag{5}$$

In attempting to make a quantitative comparison of theory and observation, one is confronted with the difficulty that there is a great deal of variation in the measured h.f.s. data[1] for lines going to a common level that is responsible for the observable h.f.s. One can take an average over these lines to get information about the level in question, but it is to be expected that some uncertainty will remain.

Table VI gives the $\Delta\sigma$ values for the eight levels as determined from White's h.f.s. data for those lines the classification of which we have confirmed with Zeeman measurements. A minus sign indicates that the h.f.s. is inverted. From the $\Delta\sigma$ in each case the corresponding value of a was calculated by means of (5) and (3) or (4). The various calculated values differ somewhat.

TABLE VI. *Values of $\Delta\sigma$ from White's h.f.s. data.*

LEVEL	$\Delta\sigma$(OBS.)	a(CALC.)	$\Delta\sigma$(CALC.)
$^5I^\circ_4$	−0.80	+0.36	−0.90
$^3I^\circ_5$	−0.74	0.32	−0.92
$^3I^\circ_6$	−0.84	0.36	−0.93
$^3I^\circ_7$	−0.91	0.39	−0.94
$^5I^\circ_5$	+1.13	0.41	+1.10
$^5I^\circ_6$	+1.10	0.41	+1.08
$^5I^\circ_7$	+1.05	0.39	+1.07
$^5I^\circ_8$	+1.11	0.42	+1.06

TABLE VII. *g sums for $f^3(^4I^\circ)\cdot s$ levels of* Pr II.

TERM	g(MEAS.)	$g(LS)$	$g(J_i)$	J_i	SUM g(MEAS.)	SUM g(THEOR.)
$a^5I^\circ_4$	0.605	0.600	0.600	$(4\frac{1}{2}, \frac{1}{2})$		
					0.605	0.600
$a^5I^\circ_5$	0.875	0.900	0.855	$(4\frac{1}{2}, \frac{1}{2})$		
$a^3I^\circ_5$	0.860	0.833	0.878	$(5\frac{1}{2}, \frac{1}{2})$		
					1.735	1.733
$a^5I^\circ_6$	1.064	1.071	1.051	$(5\frac{1}{2}, \frac{1}{2})$		
$a^3I^\circ_6$	1.037	1.024	1.044	$(6\frac{1}{2}, \frac{1}{2})$		
					2.101	2.095
$a^5I^\circ_7$	1.177	1.179	1.171	$(6\frac{1}{2}, \frac{1}{2})$		
$a^3I^\circ_7$	1.143	1.143	1.151	$(7\frac{1}{2}, \frac{1}{2})$		
					2.320	2.322
$a^5I^\circ_8$	1.250	1.250	1.250	$(7\frac{1}{2}, \frac{1}{2})$		
					1.250	1.250

TABLE VIII. *g sums for even levels of* Pr II.

	9		8		7		6		5		4	
	ΣM	ΣT	ΣM	ΣT	ΣM	ΣT	ΣM	ΣT	ΣM	ΣT	ΣM	ΣT
z^5K_5									0.821	0.667		
z^5I_4											0.684	0.600
z^5K_6							0.959	0.905				
z^3K_6							0.992	0.857				
z^5I_5									0.911	0.900		
z^3I_6							1.009	1.024				
z^5H_4											0.905	0.900
z^5K_7					1.062	1.054						
z^5I_6							1.042	1.071				
z^5I_7					1.123	1.179						
z^3H_6							1.073	1.167				
z^5H_5									1.101	1.100		
z^5K_8			1.143	1.153								
z^3K_7					1.106	1.018						
z^5I_8			1.154	1.250								
z^5H_6							1.103	1.214				
z^3I_7					1.187	1.143						
z^5K_9	1.217	1.222										
z^5H_7					1.215	1.286						
Sums	1.217	1.222	2.297	2.403*	5.693	5.680	6.178	6.238	2.833	2.667*	1.589	1.500*

* Indicates that all terms of that particular j value derivable from parent term ^4I+p have not been found and g sum rule is not applicable. This assumes that ^4I is perfect LS coupling.

partly because of errors in the values of $\Delta\sigma$ and partly, probably, because of incomplete JJ coupling, etc. By taking

$$a=0.40\ \text{cm}^{-1},$$

the value of $\Delta\sigma$ was calculated in each case on the basis of the above equations. It is evident that the agreement is quite satisfactory.

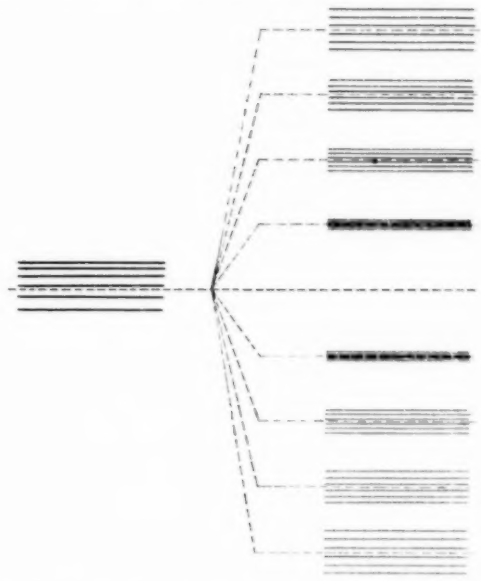

FIG. 3. Effect of a strong magnetic field in breaking a normal hyperfine-multiple level, $a^5I^\circ_4$, containing six levels, up into 54 levels.

In the presence of the magnetic field which is used to produce the Zeeman effects, the character of the h.f.s. changes completely. The magnetic field used in practice is a strong field from the standpoint of the h.f.s. and hence it destroys the coupling between I and J, so that the component of each in the direction of the field is quantized nearly independently (Back-Goudsmit effect).[14]

In this case the change in atomic energy due to the external magnetic field and the magnetic moment of the nucleus is given by

$$\Delta E=(-g_I M_I+gM)\frac{He}{4\pi mc^2}+A M_I M, \qquad (6)$$

where M and M_I are the components along the field of J and I, respectively, A is the same constant as in (1), g is the usual g factor for the extra-nuclear electrons, and g_I is the nuclear g factor. Since g_I is usually small compared to g, one can take

$$\Delta E=gM\frac{He}{4\pi mc^2}+A M_I M. \qquad (7)$$

The first term in the right-hand member corresponds to the ordinary Zeeman effect, the

[14] E. Back and S. Goudsmit, Zeits. f. Physik **47**, 174 (1928).

second gives the h.f.s. In this case, the width of the h.f.s. is given by

$$\Delta\sigma = (\Delta E)_{M_I=+I} - (\Delta E)_{M_I=-I}. \quad (8)$$

Hence in a Zeeman pattern, the sharpest lines should be found near the center of the p and of each s branch, for which cases $|M|$ is a minimum. An example of this is to be seen in Fig. 2, which shows the no-field line 4368.327A and its Zeeman pattern. A diagram of the h.f.s. for the lower parent level of this line, $a^5I^\circ_4$ without and with a magnetic field, according to Eqs. (1) and (7), is given in Fig. 3, where the h.f.s. spacing has been exaggerated in comparison with the separations of the Zeeman components.

Calculation of g Sums

In Table VII are given the g sums for Pr II levels arising from the configuration $f^3(^4I^\circ)\cdot s$. It will be noted that the agreement between the measured and theoretical sums is usually within a few tenths of a percent, though perturbations much greater than this cause deviations of the individual terms. In Table VIII, which gives the g sums for even levels, the agreement is not quite so satisfactory.

We desire to acknowledge the able assistance of workers on the M.I.T.-W.P.A. Wavelength Project, and of Mr. W. J. Hitchcock. A grant from the Rumford Committee of the American Academy of Arts and Sciences in support of the work is gratefully acknowledged.

NOVEMBER 15, 1941 PHYSICAL REVIEW VOLUME 60

On the $^2\Pi_u \rightarrow {}^2\Pi_g$ Bands of CO_2^+. Part I

S. MROZOWSKI
Ryerson Physical Laboratory, University of Chicago, Chicago, Illinois
(Received September 18, 1941)

The band spectrum appearing in emission in the region λ2900–4300 and believed to belong to the CO_2^+ or possibly CO_2 molecule has been studied and the excitation conditions found to be in substantial agreement with the former results of Duffendack and collaborators and of Smyth. The bands have been obtained with great intensity and photographs of most of them have been made in the second order of the 30-foot grating (actually obtained resolving power of 350,000). The rotational structure and the excitation conditions show that most of the bands belong to an extensive $^2\Pi \rightarrow {}^2\Pi$ system of bands of the molecule CO_2^+. The molecule is linear in both states; the lower $^2\Pi$ appears to be the ground state $^2\Pi_g$ and the upper $^2\Pi$ is the first excited state $^2\Pi_u$ of this molecule predicted by Mulliken. The complete rotational and vibrational analysis of this band system is still in progress; in this paper the analysis of 5 double bands of the $v''_1=v''_2=v''_3=0$ progression of the symmetrical vibration (v'_1 varying, $v'_2=v'_3=0$) is presented. The results of the analysis are: $\nu_0^{(0,0)}=28{,}532.60(^2\Pi_{3/2}\rightarrow{}^2\Pi_{3/2})$ and $\nu_0^{(0,0)}=28{,}468.48(^2\Pi_{\frac{1}{2}}\rightarrow{}^2\Pi_{\frac{1}{2}})$. The vibrational intervals (i.e., the distances between the origins of successive bands in the progression) are: $\Delta G'_1=1126.71$; $\Delta G'_2=1122.66$; $\Delta G'_3=1120.22$; $\Delta G'_4=1120.04$ (all $^2\Pi_{3/2u}$) and $\Delta G'_1=1125.97$; $\Delta G'_2=1120.79$; $\Delta G'_3=1116.09$; $\Delta G'_4=1111.76$ (all $^2\Pi_{\frac{1}{2}u}$). Further for $^2\Pi_{3/2g}B''_0=0.3796$; for $^2\Pi_{\frac{1}{2}g}B''_0=0.3812$; for $^2\Pi_{3/2u}B'_0=0.3485$; $B'_1=0.3475$; $B'_2=0.3465$; $B'_3=0.3457$; $B'_4=0.3453$; for $^2\Pi_{\frac{1}{2}u}B'_0=0.3501$; $B'_1=0.3492$; $B'_2=0.3483$; $B'_3=0.3475$; $B'_4=0.3466$. The Λ-doubling is observable only in the $^2\Pi_{\frac{1}{2}}\rightarrow{}^2\Pi_{\frac{1}{2}}$ sub-bands in this progression; in $^2\Pi_u$ it is bigger than in $^2\Pi_g$ ($p''_0=0.004$ for $v''_1=0$) and increases fast with the vibrational energy.

Introduction

WHEN a gas through which a discharge is passing contains carbon dioxide (or CO), in addition to the bands belonging to CO and CO^+ a great number of bands appear in the spectrum in the region λ2800–4500: the most prominent of these is the double band at λ2883–2896, which appears whenever the smallest traces of CO_2 (or CO) are present. All these bands have been observed by many investigators (some of them as far back as 1802), but there was considerable uncertainty about their emitter,

until Duffendack and collaborators[1–3] and later Smyth[4] showed rather definitely that they do belong to a triatomic molecule CO_2^+ or possibly CO_2. Their experiments were carried out with spectrographs of low dispersion; they tried to arrange the bands in progressions, and as we shall see from the results reported in this and in the following parts of this work, in several cases with considerable success. But several members of different progressions and consequently the level scheme suggested by Smyth[4] have not been confirmed.

The first photographs with high dispersion were made of the double band λ2883–2896 by Duncan,[5] but the resolution was insufficient to permit any conclusions concerning the type of the transition involved. A more extensive study of the spectrum with high dispersion was undertaken in this laboratory by Schmid. In the first part of his work Schmid[6] photographed the bands in the region λ3200–3900 in the third order of a 21-foot grating and showed that the stronger bands all possess two branches only, and fall into two classes: "non-staggering" and "staggering" bands. He measured the lines in 5 non-staggering (λ3247, 3370, 3503, 3545, 3674) and 5 staggering bands (λ3254, 3377, 3511, 3534, 3839) and determined that none of them shows an observable Zeeman effect (presumably in fields as high as 28,000 gauss). For the first three bands in each class, forming successive members of the two progressions *a* and *c* of Smyth, Schmid was able to find common combination differences. But a change of numbering by a half or one unit gave nearly as satisfactory combination differences so that it could not be decided which combination differences and which numbering (whole or half integral) is correct. Besides this, it was not certain whether the common combination differences belong to the upper or to the lower electronic state, and so the final numbering adopted by Schmid, and his *B* values, were to some extent arbitrary. But the simple structure of the bands showed conclusively that their triatomic emitter is linear in both upper and lower states. Schmid explained the staggering by a doubling of levels similar to Λ-doubling together with an absence of alternate levels due to the symmetry of the molecule. Mulliken[7] discussed the results of Schmid and pointed out various possible interpretations.

In the second part of his work Schmid[8] investigated the double band λ2883–2896, showed the presence of a Zeeman effect and suggested an interpretation as a $^2\Pi(a) \rightarrow {}^2\Pi(b)$ transition. But the resolution was unsatisfactory and the interpretation therefore doubtful. A little later Schmid[9] reported observations of the Zeeman effect in a group of bands near λ3600 which he believed to consist of four heads in two pairs forming a double band; the structure and the Zeeman effect of this band seemed to suggest a $^2\Sigma - {}^2\Pi$ transition. And finally Schmid[10] investigated a few bands using still higher resolving power (fourth and fifth orders of the 21-foot grating) and found a very slight staggering in the non-staggering bands λ3674 and λ3503. On the same pictures he found that the lines in the band λ3674 are very close doublets, and he discovered a similar doubling in high members of the non-staggering band λ3503 and of the staggering band λ3839. His conclusion was that probably all the bands show staggering and doublet structure of the lines if photographed with sufficiently great resolution.

In the same year 1933 Roy and Duffendack[11] studied the excitation potentials of the bands in question in a low voltage arc and showed that the double band λ2883–2896 has an excitation potential of 18.7 volts, slightly higher than that of all other bands (16.5 volt). Since the ionization potential of CO_2 was known to be $\sim$14.2 volts, these experiments gave evidence that the molecule of CO_2^+ is the emitter of the double band λ2883–2896 and possibly also of the other bands.

In one of a series of papers on the electronic structure of molecules Mulliken[12] discussed the

[1] G. W. Fox, O. S. Duffendack and E. F. Baker, Proc. Nat. Acad. **13**, 320 (1927).
[2] O. S. Duffendack and G. W. Fox, Astrophys. J. **65**, 234 (1927).
[3] O. S. Duffendack and H. L. Smith, Phys. Rev. **34**, 68 (1929).
[4] H. D. Smyth, Phys. Rev. **38**, 2000 (1931) and **39**, 380 (1932).
[5] J. F. Duncan, Phys. Rev. **34**, 1148 (1929).
[6] R. F. Schmid, Phys. Rev. **41**, 732 (1932).
[7] R. S. Mulliken, Phys. Rev. **42**, 364 (1932).
[8] R. Schmid, Zeits. f. Physik **83**, 711 (1933).
[9] R. Schmid, Zeits. f. Physik **84**, 732 (1933).
[10] R. Schmid, Zeits. f. Physik **85**, 384 (1933).
[11] A. S. Roy and O. S. Duffendack, Proc. Nat. Acad. **19**, 497 (1933).
[12] R. S. Mulliken, J. Chem. Phys. **3**, 720 (1935).

electronic configuration of the normal state of the molecule of CO_2 and the lowest states of CO_2^+ derived from it by removal of one electron from different outer shells. He showed that above the normal state $^2\Pi_g$ of CO_2^+ there has to be a $^2\Pi_u$ state and, probably a little higher, a $^2\Sigma^+_u$ state. On the basis of the excitation potential and the structure of the double band λ2883–2896 he identified the $^2\Sigma^+_u$ state with the upper state of this band, and the continuous absorption appearing in the spectrum of CO_2 above 18 volts as the absorption leading to the excitation of this level. This interpretation found a very good confirmation in the recent work of Price and Simpson[13] on the absorption spectrum of CO_2, and so this point seemed to be fairly well established. But there was no continuous absorption observed in CO_2, which could be correlated with the photoelectric excitation of the $^2\Pi_u$, and therefore Mulliken[12] could only suggest a tentative correlation: the double band λ3660 as a $(0,0)^2\Pi_u \rightarrow {}^2\Pi_g$ transition, and the remaining bands as transitions from still higher excited states to $^2\Sigma^+_u$ and possibly also to $^2\Pi_u$. But Mulliken was never satisfied with this correlation, the reasons being the following: (1) no other expected $^2\Pi_u \rightarrow {}^2\Pi_g$ bands besides the double band λ3600 were observed; (2) the excitation potential found by Roy and Duffendack[11] seems not to favor an interpretation involving higher levels than $^2\Sigma^+_u$; (3) the doublet structure of all lines in the staggering and non-staggering bands found by Schmid[10] cannot be reconciled with any attempted interpretation of the bands in question.

Since Dr. F. Bueso-Sanllehí already started a work on the $^2\Sigma^+_u \rightarrow {}^2\Pi_g$ double band, Professor Mulliken suggested to the author a year ago that he investigate the rest of the spectrum with the purpose of clearing up the mentioned difficulties. Some of the preliminary stages of this experimental work have been carried out in collaboration with Dr. F. Bueso-Sanllehí, who successfully concluded the analysis of the $^2\Sigma^+_u \rightarrow {}^2\Pi_g$ double band and reported it recently in this journal.[14] Subsequently the whole spectrum described by Duffendack and collaborators[1–3] and Smyth[4] has been obtained with very high intensity and all the stronger and many of the weaker bands have been photographed in the second order of the new 30-foot grating. The pictures showed that a great number of the bands belong to an extensive $^2\Pi \rightarrow {}^2\Pi$ system of bands; most of these correspond to transitions involving changes in the quantum number v_1 of the symmetrical vibration of the molecule CO_2^+, the quantum numbers of the antisymmetrical v_3 and bending vibrations v_2 remaining zero. The rotational analysis of this part of the system was first undertaken, and the results for the progression $v''_1=0$ are reported in this paper (the progression $v''_1=0$, $v'_1=0$, 1, 2, 3 and 4 is identical with progressions a_2-a_6 and c_3-c_7 of Smyth). The agreement of the combination differences with those from the rotational analysis of the $^2\Sigma^+_u \rightarrow {}^2\Pi_g$ double band,[14] and the direction of the staggering in the $^2\Pi_{1u} \rightarrow {}^2\Pi_{1g}$ sub-bands, give evidence that the lower $^2\Pi$ is the ground state $^2\Pi_g$ of the molecule CO_2^+ and the upper $^2\Pi$ is the $^2\Pi_u$ predicted by Mulliken[12] and mentioned above. The half-integral numbering of rotational lines which gave the best fit for the combination differences of the bands a_2-a_4 and c_3-c_5 in Schmid's[6] work but was considered by him as less probable than an integral numbering, has been shown to be correct; no staggering could be detected in the $^2\Pi_{3/2u} \rightarrow {}^2\Pi_{3/2g}$ sub-bands for $v''_1=0$ (for instance λ3503[10]). Also the doublet structure of the lines reported by Schmid[10] has not been confirmed, although the resolving power obtained is very much higher than that of the grating used by Schmid.

The analysis of all other bands belonging to the array (v'_1, v''_1) covering the range v'_1 from 0 to 7 and v''_1 from 0 to 3 is still in progress and the results will be reported as soon as the analysis is completed. Anticipating the publication of these results it may be mentioned that an interesting perturbation has been found in the state $^2\Pi_{3/2g} v''_1=1$, consisting in a vibrational perturbation, an anomalously big B'' value, and a Λ-doubling increasing approximately proportionally to the third power of the rotational number. Professor Mulliken suggests that the perturbation may be caused by interaction with levels having two quanta of bending vibration.

[13] W. C. Price and (Miss) D. M. Simpson, Proc. Roy. Soc. **169**, 501 (1939).
[14] F. Bueso-Sanllehí, Phys. Rev. **60**, 556 (1941).

A vibrational perturbation has been found to occur also in $^2\Pi_{3/2u}$ between $v'_1=4$ and 5, and a similar one for $^2\Pi_{1/2u}$ between $v'_1=6$ and 7. The slight staggering found by Schmid[10] in the band λ3674 has been confirmed (its existence is expected, since this band has been shown to be a $^2\Pi_{1/2u} \rightarrow {}^2\Pi_{1/2g}$ sub-band $v'_1=0 \rightarrow v''_1=1$), but not the doubling of the lines (see above). Until now no complete explanation of the double band λ3660 has been found, but it is certain that the real structure is quite different from what Schmid's lower resolution photographs seemed to indicate.

Besides all these $^2\Pi_u \rightarrow {}^2\Pi_g$ bands belonging to $v'_3=v''_3=0$ and $v'_2=v''_2=0$, there are weaker bands, one group of which having the same structure as the bands described above probably belongs to different $v'_1 \rightarrow v''_1$ transitions with $v'_3=v''_3=1$ and $v'_2=v''_2=0$. Another group of bands, which have a much more complicated structure (headless grouping of lines, several short branches) and seems to be associated with the $^2\Pi_u \rightarrow {}^2\Pi_g$ system, possibly belong to $v'_1 \rightarrow v''_1$ transitions with $v'_3=v''_3=0$ and $v'_2=v''_2=1$. A rotational analysis of all those bands is planned. If, as appears probable, not all observed bands will fit into the $^2\Pi_u \rightarrow {}^2\Pi_g$ system, the remaining bands (most of them are weak), according to their energy of excitation (smaller than 18 volts[11]), have probably as emitter the molecule CO_2, since there are no more low-lying levels in the CO_2^+ molecule.

Experimental

The excitation conditions were carefully studied in order to find a source which would give the band spectrum in question with high intensity and, in view of its complexity, as free as possible from other spectra (the bands of CO and CO^+ interfere especially in the long wave-length region). Hollow cathodes of different size and a discharge in a quartz tube with two outer ring electrodes excited by a 4-meter oscillator were tried, the spectrum being photographed on a medium size quartz spectrograph. Discharge in pure CO_2, in CO_2+O_2, in pure CO, and in $CO+O_2$ were studied and in every case all bands have been found, in the last two cases with a little lower intensity than in the first two. The CO was obtained by decomposition of $Ni(CO)_4$, O_2 by decomposition of $KClO_3$ in presence of MnO_2, and the CO_2 was twice resublimed commercial carbon dioxide. The results show that in the discharge an equilibrium between CO_2, CO and O_2 is obtained, the concentration of O_2 having no practical importance. Addition of helium, although it enhances the whole spectrum, was found not suitable because it favors the emission of the CO and CO^+ bands by slowing down the process of recombination of the CO and O into CO_2. The equilibrium is reached in the discharge in a very short time, since no observable enhancement of the spectrum in flowing gas was found. Only moderately high speed of flow has been tried; it seems therefore possible that in the case of the experiments of Schmid[6] extremely fast pumping could have a beneficial influence. It has been found that by far the most important factors are the current density and the pressure.

The bands can be divided according to their behavior into three groups, of which the two last are less clearly distinct: (1) the double band $^2\Sigma^+_u \rightarrow {}^2\Pi_g$; (2) the bands $^2\Pi_u \rightarrow {}^2\Pi_g$ in the region 2900–3300A; (3) all bands in longer wave-length region (>3300A). The intensity of all bands in pure CO_2, or with addition of helium, increases at first with current density, but after reaching a maximum drops quite fast. For the $^2\Sigma^+_u \rightarrow {}^2\Pi_g$ band the maximum lies at higher current densities than for the rest of the bands; at such high currents the lower pressures favor the emission of this double band, at higher pressures the bands of CO and CO^+ are more and more prominent. Increase of pressure in the case of low currents has an enhancing effect on the long wave-length bands (3). They seem to be emitted from molecular states which are not excited directly by electron impact but are brought down from higher states by collisions. The results show that the highest excitation potential belongs to the double band $^2\Sigma^+_u \rightarrow {}^2\Pi_g$, as was shown before by Roy and Duffendack.[11] Besides the $^2\Sigma^+_u$ state directly excited by electron impact are mostly higher vibrational levels of $^2\Pi_u$ $v'_1=2-5$ (corresponding to $^2\Pi_u \rightarrow {}^2\Pi_g$ bands in the region (2)); into the lower levels $v'_1=0,1$ (bands in the region (3)) the molecules are brought down by subsequent collisions. The

relative transition probabilities for electron excitation are to some extent similar to probabilities of absorption; since the B constant of the state $^2\Pi_g$ is about equal to that of the ground state of the CO_2 molecule, the excitation of the $^2\Pi_u$ state from the ground state of CO_2 in view of the large change in the B constant has to be connected with a corresponding change in vibrational energy. The complexity of the spectrum arising from the presence of several limits is probably the reason why the continuous absorption and the Rydberg series corresponding to a photo-ionization of CO_2 into the state $^2\Pi_u$ have not yet been detected in the far ultraviolet spectrum of CO_2.

Corresponding experiments carried out with excitation by short waves with different pressures and variable power of the oscillations failed to reveal any difference in excitation potential of the two groups of bands (2) and (3). It was hoped that, similarly to what is found in atomic spectra,[15] the maximum intensity of a group of bands with lower excitation potential would appear at a correspondingly higher pressure. The experiments revealed only a higher excitation potential for the $^2\Sigma^+{}_u \rightarrow {}^2\Pi_g$ double band than for the remaining groups (2) and (3); the reason being that with increase of pressure the number of molecules dissociating into CO and O quickly increases (the effect occurs at such low pressures ($\ll$1 mm Hg) that the excited CO_2 molecules dissociating during collisions seem to be in a metastable state). The spectrum of CO having the lowest excitation potential is so strongly excited at comparatively low pressures, that nothing definite can be said in this experiment about the difference of behavior of bands belonging to groups (2) and (3).

On the basis of the results of these preliminary experiments, a water-cooled hollow cathode with a rather large cross section was chosen (inside diameter of about 15 mm) for the final exposures on the big grating. The essential parts of the apparatus are described in the paper of Bueso-Sanllehí.[14] Most of the pictures were obtained with a current of 0.3–0.4 amp., under which conditions group (3) of bands has its maximum intensity and the spectra of CO and CO^+ do not interfere very seriously. Currents down to less than 0.1 amp. were tried, but the time of exposure increases so considerably (over 60 hours) that the relative weakening of the CO and CO^+ spectra is overbalanced by the loss in total intensity. The pressure of the flowing CO_2 gas was adjusted to give maximum intensity of the bands (3). Above a certain pressure the discharge in the cathode begins to be weaker, and since this limiting pressure is lower for lower currents, this is another reason why the bands (3) for low currents can be obtained only with relatively low intensity. The bands in the region 2950–4200A have been photographed in the second order, with a slit varying from 12 to 24 microns, on Eastman Process plates (all stronger bands) and Eastman 33 plates (the weaker bands). The exposure time varied from 6 to 48 hours. In the most favorable cases (as in the case of close doublets in the $(2,0)^2\Pi_{3/2} \rightarrow {}^2\Pi_{3/2}$ sub-band) a practical resolving power of 350,000 was obtained. As comparison spectrum the iron spectrum was used.

The wave-lengths were measured on a linear scale over a small region or regions (not exceeding 15 cm) on each plate by the automatic density comparator at M.I.T. (Cambridge, Massachusetts), through the kindness of Professor G. Harrison. Averages of mostly eight (sometimes six) M.I.T. readings from at least two different plates (backward and forward readings at two different heights, four readings for each plate) were taken. Independent measurements were made by the writer on a comparator in the case of three double bands (0,0), (1,0) and (2,0), and superior results were obtained in the case of closely spaced groups of lines (for instance doublets in (2,0)), the human eye being more sensitive for slight differences in density. But the time consumed in such measurements is considerable and therefore in the following such measurements were made only in exceptional cases of very complicated grouping of lines. Final wave-length values were obtained by addition of small corrections obtained from correction curves constructed with the help of the iron standards. Such correction curves should take care of the non-linearity of the dispersion of the grating and other possible sources of small errors. It was hoped at first that with a

[15] S. Mrozowski, Phys. Rev. **58**, 1086 (1940).

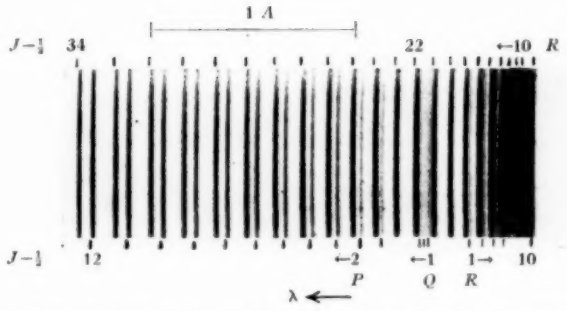

FIG. 1. (1,0) sub-band $^2\Pi_{3/2u} \rightarrow {}^2\Pi_{3/2g}$ of CO_2^+ at λ3370. Second order of the 30-foot grating. Exposure time 12 hours. Enlarged 12 times. Four lines are missing between the R and P branches; there is a very faint and diffuse line visible at $P(1\frac{1}{2})$, but probably it does not belong to the band.

dispersion of about 0.4A/mm an accuracy of about ±0.0005A could be obtained. But in the course of measurements it became clear that the experimental correction curve cannot be constructed with such a high degree of accuracy. The experimental correction curves deviate from the parabolic correction curves obtained from the grating formula so seriously (some of them differ in the maximum correction by as much as 100 percent; their shape is unsymmetrical) that no general interpolation formula can be found and the correction curves have to be obtained graphically. In view of the scarcity of iron standards such procedure involves much uncertainty. A careful study has shown that the deviations from the theoretical formula originate in the photographic plates themselves and in slight errors in the shape of the grating circle or plate-holder. The former are caused by waves on the surface of the glass and the emulsion, extending over considerable areas and detectable when three or more plates are available for comparison, and also by the distortions of the emulsion during the process of drying, which lead to smaller deviations of the readings from different plates (not exceeding ±0.001A) and varying over small areas of a few millimeters only. Although all these plate errors can be eliminated by taking averages of readings from many plates, selected as not having any waves, the irregularities in the grating circle remain uncorrected. Since these irregularities are very small and cannot be avoided (in the spectral region studied a deviation of 0.1 mm of the distance from the center of the circle in a region of 5 cm in the plate will cause a shift of the maximum of the wave-length correction curve in the maximum by about 0.04A, which corresponds to about 80 percent of the height of the maximum in the theoretical curve), the only way to increase the accuracy of the results would be to have at disposal more standard lines in the comparison spectrum. In view of the very high resolving power of the grating, greater sharpness of lines than that given by an arc in air is desirable. A hollow cathode discharge tube containing a substance rich in lines with interferometrically determined wave-lengths should be suitable for all investigations carried out with big gratings. Errors caused by the pole effect, pressure shift and so on would be not present for such a tube. It would be advisable to determine the wave-lengths of such standards with the interferometer in vacuum[16] and subsequently to drop the deeply rooted but very uncomfortable spectroscopic custom and use in the future vacuum wave-lengths only. This change would not affect in practice the low-dispersion investigations, but would be of great help in case of studies with high dispersion, since the calculation of reciprocals on calculating machines is faster and more reliable than the evaluation of wave numbers by interpolation from the tables of Kayser.

In the present work all wave-lengths were determined to four decimals, and correspondingly the wave numbers were evaluated to three decimals from the tables of Kayser, but in view of the magnitude of possible errors discussed above in all tables the last decimal has been omitted by rounding up to the nearest second decimal. The wave numbers for lines belonging to weaker bands, for instance for the bands (4,0) given below, are correspondingly less exact than for the stronger bands, since they are evaluated from more sensitive but coarser grained plates.

RESULTS

The $v''_1 = 0$ progression of bands

The five double bands belonging to the progression $v''_1 = 0$ are situated on the short

[16] A start in this direction has been made by W. E. Williams and A. Middleton, Proc. Roy. Soc. **172**, 159 (1939).

TABLE I. *Sub-bands* $^2\Pi_{3/2a} \rightarrow {}^2\Pi_{3/2g}$.

	(0,0) $\nu_0 = 28532.60$ Unres. Q branch edge $\nu = 28532.60$		(1,0) $\nu_0 = 29659.31$ Resolved Q branch $Q(1\frac{1}{2}) = 29659.28$, $Q(2\frac{1}{2}) = 29659.13$, $Q(3\frac{1}{2}) = 29658.92$		(2,0) $\nu_0 = 30781.97$ Unres. Q branch edge $\nu = 30781.92$		(3,0) $\nu_0 = 31902.19$ Q branch edge overlapped by $R(20\frac{1}{2})$		(4,0) $\nu_0 = 33022.15$ No Q branch observed		$^2\Pi_{3/2g}(v_1'' = 0)$	
$J - \frac{1}{2}$	R	P	R	P	R	P	R	P	R	P	$\Delta_2 F_0''$ Aver.	1st diff.
1	28534.23	missing	29661.00	missing	−Cu−	missing		missing				
2	34.76	28530.60	61.56	29657.33	30784.09*		31904.28				4.55	
3	35.27	29.68	62.06	56.46	84.56*	30779.01	04.75				6.07	1.52
4	35.68	28.73	62.46	55.50	84.97*	78.04		31898.26			7.60	1.53
5	36.06	27.67		54.43	85.31*	77.00		97.26*			9.11	1.51
6		26.59		53.32	85.57*	75.87		96.12			10.63	1.52
7		25.40		52.14	85.74*	74.69		94.88			12.15	1.52
8		24.20		50.90	h	73.43	06.05 h	93.58	33026.08 h		13.67	1.52
9	36.88 h	22.91	63.54 h	49.60	85.92 e	72.10	06.05 e	92.27	33026.08 e	33012.27	15.18	1.51
10	36.88 e	21.56	63.54 e	48.23	85.92 a	70.71	06.05 a	90.84	33026.08 a	10.88	16.70	1.52
11	36.88 a	20.16	63.54 a	46.79	d	69.26	06.05 d	89.33	d	09.35	18.22	1.52
12	d	18.67	63.43 d	45.30	85.74*	67.73		87.85		07.92	19.75	1.53
13		17.14	63.26	43.73	85.57*	66.17	05.58	86.23		06.25	21.26	1.51
14		15.54	63.02	42.11	85.31*	64.50	05.34	84.58	25.40	04.57	22.78	1.52
15	36.24	13.90	62.70	40.43	84.97*	62.78	04.97	82.86	25.00	02.87	24.31	1.53
16	35.89	12.16	62.32	38.67	84.56*	60.96	04.51	81.12	24.61	01.07	25.81	1.50
17	35.50	10.42	61.88	36.83	84.09*	59.13	04.04	79.22*	24.09	32999.18	27.33	1.52
18	35.04	08.55	61.38	34.96	−Cu−	57.21	03.48	77.20*	23.48	97.20	28.85	1.52
19	34.54	06.63	60.81	33.01	82.99	55.24	02.87	75.21*	22.86	95.22	30.37	1.52
20	33.96	04.68	60.20	31.01	82.30	53.19	02.16	73.12*	22.10	93.12	31.89	1.52
21	33.33	02.65	59.49	28.92	81.57	51.06	01.40	70.99*	21.42	90.98	33.40	1.51
22	32.61	00.58	58.75	26.79	80.76	48.89	00.58	68.80*	20.53	88.81	34.92	1.52
23	31.87	28498.41	57.93	24.59	79.90	46.63	31899.64	66.48	19.62*	86.51	36.43	1.51
24	31.04	96.18	57.05	22.32	78.99	44.34	98.71	64.19	18.71	84.11	37.94	1.51
25	30.17	93.92	56.11	20.00	77.98	41.96	97.67	61.73	17.63	81.77	38.46	1.52
26	29.22	91.60	55.11	17.59	76.95	39.52	96.59	59.27	16.50*	79.24	40.98	1.52
27	28.22	89.18	54.03	15.13	75.82	36.99	95.43	56.71	15.45	76.62	42.50	1.52
28	27.14	86.72	52.89	12.61	74.64	34.43	94.22	54.10*	14.20	74.08	44.01	1.51
29	26.02	84.20	51.70	10.03	73.37	31.79	92.93	51.44*	12.93	71.40	45.53	1.52
30	24.82	81.61	50.42	07.38	72.04	29.08	91.54	48.69*	11.48	68.69	47.04	1.51
31	23.58	78.95	49.10	04.67	70.67	26.28	90.13	45.89*	10.12	65.85	48.56	1.52
32	22.25	76.24	47.72	01.88	69.20	23.46	88.63*	43.00	08.73*	63.04	50.08	1.52
33	20.88	73.48	46.24	29599.03	67.67	20.59	87.08	40.03	07.08*	60.07	51.60	1.52
34	19.45	70.62	44.73	96.14*	66.09	17.59*	85.49	37.06	05.28	57.04	53.11	1.51
35	17.94	67.76	43.14	93.15	64.43	14.55	83.74		03.67*		54.62	1.51
36	16.37	64.82*	41.49	90.10	62.71	11.46	82.08*		02.00		56.14	1.52
37	14.75	61.79	39.77	87.00	60.92	08.28*	80.21*				57.65	1.51
38	13.05	58.70*	38.03	83.86	59.05	05.08*	78.22*				59.16	1.51
39	11.30	55.59	36.18	80.64*	57.12	01.79	76.36				60.67	1.51
40	09.51	52.42	34.32	77.40*	55.15	30698.43*					62.18	1.51
41	07.65	49.11	32.33	74.05*		94.98*					63.69	1.51
42	05.69	45.80	30.28	70.65		91.50					65.21	1.52
43	03.71	42.42	28.17	67.07		87.94					66.72	1.51
44	01.64	38.96*	26.00	63.56							68.25	1.53
45	28499.53	35.45	23.78								69.77	1.52
46	97.32	31.88	21.49								71.28	1.51
47	95.10	28.26*	19.11								72.79	1.51
48	92.81	24.54	16.65								74.30	1.51
49	90.45	20.83	14.20								75.81	1.51
50	87.96	17.02										
51	85.54											
52	82.93											

wave-length side of sequences of bands and since all bands in the spectrum are degraded toward the red, they are almost completely free from overlappings. An exception is the sub-band $^2\Pi_{3/2} \rightarrow {}^2\Pi_{3/2}(3,0)$, which is overlapped by a grouping of lines belonging probably to the bending vibration $v'_2 = v''_2 = 1$. Since the double band (4,0) is weak, very complete data have been obtained only for three $^2\Pi_{3/2} \rightarrow {}^2\Pi_{3/2}$ and four $^2\Pi_{\frac{1}{2}} \rightarrow {}^2\Pi_{\frac{1}{2}}$ sub-bands. In the $^2\Pi_{3/2} \rightarrow {}^2\Pi_{3/2}$ sub-bands ((0,0), (1,0) and (2,0)) weak Q branches (in one case resolved into separate lines) were observed, and in the case of two bands it was possible to establish definitely that four lines were missing near the origin, as expected. In Fig. 1 an enlargement of a photograph of the $^2\Pi_{3/2} \rightarrow {}^2\Pi_{3/2}$ sub-band of the (1,0) band is reproduced. For the (2,0) sub-band, where the P and R branches almost coincide, the high resolving power of the grating permitted resolving the lines into very narrow doublets, one P, one R, determining their wave numbers, and checking with high accuracy the absence of staggering. The complete resolution of all these three $^2\Pi_{3/2} \rightarrow {}^2\Pi_{3/2}$ sub-bands (except for a few lines at the head) permitted settling of the numbering of the lines in the P and R branches directly without use of the combination relations in each of these sub-bands independently. No Q branches have been observed in $^2\Pi_{\frac{1}{2}} \rightarrow {}^2\Pi_{\frac{1}{2}}$ sub-bands and therefore for all remaining sub-bands the numbering has been settled by finding

TABLE II. *Sub-bands* $^2\Pi_{\frac{1}{2}u} \rightarrow {}^2\Pi_{\frac{1}{2}g}$.

$J-\frac{1}{2}$	(0,0) $\nu_0=28468.48$ R	P	(1,0) $\nu_0=29594.41$ R	P	(2,0) $\nu_0=30715.20$ R	P	(3,0) $\nu_0=31831.29$ R	P	(4,0) $\nu_0=32943.05$ R	P	$^2\Pi_{1/2g}(v_1''=0)$ Δ_2F_0'' Aver.	1st diff.
0		missing	29595.56*	missing	30716.19	missing		missing		missing		
1			96.19*		16.86*	30714.05		31830.10			3.05	
2		28466.47	96.66*	29592.40	17.37	13.18		29.21			4.60	1.55
3		65.56	97.20*	91.48	17.91*	12.26		28.33			6.13	1.53
4	28471.63	64.60	97.52*	90.49	18.25	11.26		27.30			7.67	1.54
5		63.55	97.92*	89.43	18.61*	10.24		26.30			9.17	1.50
6		62.43	98.12*	88.34		09.09	31834.92*	25.14			10.70	1.53
7		61.29	98.47*	87.13	19.06*	07.92	31834.92*	23.96	32946.90		12.20	1.50
8	72.78* h	60.03	98.47* h	85.94	19.06* h	06.64	35.20 h	22.62	32946.90 h	32934.30*	13.73	1.53
9	72.88 e	58.78*	98.60 e	84.66	19.30 e	05.35	35.20 e	21.35	32946.90 e	33.13*	15.25	1.52
10	72.88 a	57.43	98.60 a	83.27	19.30 a	03.93	35.20 a	19.90	32946.90 a	31.56*	16.78	1.53
11	72.88 d	56.06	98.60 d	81.87	19.30 d	02.52	35.20 d	18.49	32946.90 d	30.22*	18.29	1.51
12	72.78*	54.56	98.47*	80.36	19.06*	00.98	34.92*	16.91		28.52*	19.82	1.53
13	72.78*	53.09	98.47*	78.84	19.06*	30699.44	34.92*	15.34	46.46	27.05*	21.34	1.52
14	72.55	51.43	98.12*	77.22	18.61*	97.74	34.45	13.60	46.03	25.16	22.87	1.53
15	72.35	49.86	97.92*	75.56	18.40	96.10	34.22	11.95	45.77	23.58	24.39	1.52
16	72.02	48.12	97.52*	73.78	17.91*	94.26	33.68	10.01	45.18	21.58	25.92	1.53
17	71.69	46.42	97.20*	72.04	17.59	92.48	33.35	08.25	44.80	19.83	27.44	1.52
18	71.20	44.54	96.66*	70.11	17.00	90.51	32.63	06.21	44.04	17.68	28.98	1.54
19	70.78	42.71	96.19*	68.24	16.50	88.63	32.14	04.30	43.54	15.80	30.49	1.51
20	70.18	40.72	95.56*	66.20	15.77	86.49	31.31	02.09	42.65	13.50	32.02	1.53
21	69.67	38.78	95.00	64.22	15.17	84.50	30.71	00.06	42.01	11.51	33.54	1.52
22	68.95	36.65	94.18	62.02	14.28	82.23	29.71	31797.75	40.95	09.08	35.08	1.54
23	68.31	34.59	93.49	59.94	13.59	80.12	28.96	95 59	40.17	06.95	36.60	1.52
24	67.43	32.32	92.54	57.59	12.54	77.70	27.87	93.09	39.01	04.33	38.13	1.53
25	66.65	30.15	91.76	55.37	11.70	75.44	27.01	90.83	38.12	02.07	39.64	1.51
26	65.66	27.81	90.66	52.92	10.52	72.93	25.74	88.19	36.83	32899.36	41.17	1.53
27	64.82*	25.47	89.76	50.59	09.56	70.55	24.74	85.79	35.77	96.95	42.68	1.51
28	63.69	22.96	88.52	48.01	08.28*	67.88	23.37	83.02	34.30*	94.06	44.22	1.54
29	62.71	20.55	87.49	45.55	07.16	65.37	22.25	80.50	33.13*	91.56	45.73	1.51
30	61.44	17.94	86.14	42.82	05.73	62.55	20.66	77.59	31.56*	88.54*	47.26	1.53
31	60.34	15.40	85.00	40.26	04.54	59.94	19.41*	74.93	30.22*	85.86	48.78	1.52
32	58.96	12.64	83.51	37.40	02.94	56.99	17.74*	71.83	28.52*	82.63	50.31	1.53
33	57.77	10.02	82.24	34.70	01.62	54.24	16.37	69.11	27.05*	79.93	51.82	1.51
34	56.26	07.15	80.64*	31.71	30699.88	51.16	14.48	65.86		76.59	53.35	1.53
35	54.94	04.40	79.26	28.90	98.43*	48.31	13.03	62.99		73.69	54.87	1.52
36	53.31	01.35	77.48*	25.78	96.57	45.05*	11.07	59.60		70.08	56.40	1.53
37	51.84	28398.47	76.00	22.85	94.98	42.07	09.48	56.59		67.21	57.92	1.52
38	50.10	95.34	74.11*	19.60	92.99	38.70	07.31	53.09		63.49	59.45	1.53
39	48.52	92.37	72.47	16.54	91.35	35.62	05.58	49.97		60.43	60.96	1.51
40	46.64	89.13	70.44*	13.16	89.16	32.08	03.25	46.31		56.60	62.48	1.52
41	44.97		68.70	10.01	87.35	28.87	01.41	43.03		53.30	64.00	1.52
42	42.97		66.54	06.45	85.05	25.19	31798.95	39.20		49.36	65.52	1.52
43	41.16		64.68	03.18	83.12	21.86	97.00	35.82		46.12	67.01	1.51
44	38.96*		62.39	29499.54	80.70	18.06	94.41	31.87		41.81	68.53	1.52
45	37.10		60.40	96.18	78.67	14.62*	92.34	28.38		38.39	70.04	1.51
46	34.81		57.99	92.39	76.08	10.66	89.60	24.28		34.05	71.57	1.53
47	32.81			88.84*	73.90	07.10	87.40	20.76			73.07	1.50
48	30.41			84.90*	71.19	03.00	84.50	16.44			74.59	1.52
49	28.26*			81.28*	68.92	30599.34	82.22	12.76			76.11	1.52
50	25.77			77.27	66.03	95.10		08.29			77.65	1.54
51	23.47			73.46	63.64	91.27		04.50				
52				69.30*	60.65							
53				65.41	58.15							
54				61.10	54.96							

common combination differences $\Delta_2F''_0$. Since the wave-lengths are much more precise than in Schmid's[6] measurements, the $\Delta_2F''_0$'s from different bands differ from the average values not more than ± 0.02 cm^{-1} and there can be found only one solution for the numbering. The wave numbers of the lines and the origins of the bands are presented in Tables I and II; the wave numbers marked by asterisks belong to lines which are blended. In the same tables are presented also $\Delta_2F''_0$ values, most of them being weighted averages of eight numbers (M.I.T. wave-length determination for five and direct measurements on measuring machine for three bands). The constants in the expression for the rotational energy terms of an inverted case **a** $^2\Pi$ state $T(J)=BJ(J+1)+DJ^2(J+1)^2\pm p(J+\frac{1}{2})+\cdots$ (p equal zero for $\Pi_{3/2}$) were obtained from the data of Table I and II by application of well-known graphical methods. For the vibrationless ground state of the molecule CO_2^+ we have:

$^2\Pi_{3/2g}$:

$$B''_0=0.3796\pm0.0003;$$
$$D''=-(1.3\pm0.3)10^{-7};$$

$^2\Pi_{\frac{1}{2}g}$:

$$B''_0=0.3812\pm0.0003;$$
$$D''_0=-(1.3\pm0.3)10^{-7};$$
$$p''_0=+0.004\pm0.0015.$$

Since the $^2\Pi_g$ state is inverted $A=-159.5$[14] the difference of the effective B values according to a formula of Hill and Van Vleck[17] for diatomic molecules should be equal to $2B^2/A=-0.0018$,

[17] Cf. R. S. Mulliken, Rev. Mod. Phys. **2**, 113 (1930).

which is in excellent agreement with the value -0.0016 found. In the second part of this work, where $\Delta G''$'s will be given, it will be shown that the obtained D''_0 value is exactly equal to the value expected on the basis of the elementary formula $D_e = -4B_e^3/\omega_e^2$. The decrease in the first differences of the $\Delta_2 F''_0$'s for high J values caused by the term with coefficient D''_0 is easily visible in Table I. High precision in the measurements is essential for the evaluation of the constant p''_0 of the Λ-doubling, since the first differences of the $\Delta_2 F''_0$'s in Table II are equal to $4B''_0 \pm 2p''_0$ and errors amounting to a few hundredths of a wave number would make the evaluation of p''_0 impossible (the second differences, which should be equal to $\pm 4p''_0$ amount to only ± 0.016 cm^{-1}!). The errors given for p''_0 represent the reliability of the result in the opinion of the author including all possible systematical errors. The results of Bueso-Sanllehí[14] show, however, that my $\Delta_2 F''_0$ values are in excellent agreement with his analysis of the $^2\Sigma^+_u \rightarrow {}^2\Pi_g$ double band as regards the reported p''_0 value; since his analysis is quite sensitive to a small change in p''_0, probably the value 0.004 is very close to the true value of p''_0. According to a formula of Van Vleck[18] the value $p''_0 = 0.004$ could be explained by the presence of a $^2\Sigma^+_g$ state at about 60,000 cm^{-1} above the $^2\Pi_g$ state (we assume a relation of "pure precession" between the two states, with $l=1$ for $^2\Pi_g$). The exact value of p''_0 is important for all data concerning the Λ-doubling, since the p's for all other vibrational states of $^2\Pi_{1/2u}$ and $^2\Pi_{1/2g}$ can be obtained from it using the differences $p''-p'$, which in turn can be easily evaluated from the study of the first differences in the P and R branches.

No tables of combination differences for the upper levels of the reported bands are given here, since after completion of the analysis of other bands much more exact $\Delta_2 F'$ values will be available (as weighted averages from several bands each). Therefore the B' and $\Delta G'$ values reported below should be considered as provisional only. The constants are:

$^2\Pi_{3/2u}$:	$B'_0 = 0.3485$		
	$B'_1 = 0.3475$		$\Delta G'_1 = 1126.71$
	$B'_2 = 0.3465$		$\Delta G'_2 = 1122.66$
	$B'_3 = 0.3457$		$\Delta G'_3 = 1120.22$
	$B'_4 = 0.3453$		$\Delta G'_4 = 1120.04$
$^2\Pi_{1/2u}$:	$B'_0 = 0.3501$	$p'_0 - p''_0 = \pm 0.0033$	
	$B'_1 = 0.3492$	$p'_1 - p''_0 = \pm 0.0040$	$\Delta G'_1 = 1125.97$
	$B'_2 = 0.3483$	$p'_2 - p''_0 = \pm 0.0050$	$\Delta G'_2 = 1120.79$
	$B'_3 = 0.3475$	$p'_3 - p''_0 = \pm 0.0062$	$\Delta G'_3 = 1116.09$
	$B'_4 = 0.3466$	$p'_4 - p''_0 = \pm 0.0094$	$\Delta G'_4 = 1111.76$

The errors are for B' ± 0.0004, for $p' - p''_0$ ± 0.0003, for $\Delta G'$ ± 0.08. The Λ-doubling may be attributed largely to the influence[18] of the upper state $^2\Sigma^+_u$ of the double band λ2883–2896, and all p's must then be positive, like p''_0. (It is practically certain that there can be no $^2\Sigma^+_u$ level below the $^2\Pi_u$. Besides for $p' - p''_0 < 0$ there would be a change in sign from p'_0 to p'_2. See also below about the symmetry of the levels.) The discussion of the p' values in relation to the distance of the perturbing $^2\Sigma^+_u$ state will be postponed; p'_0 appears to be considerably smaller than the value $+0.023$ calculated with the formula of Van Vleck assuming a relation of pure precession between the two states with $l=1$ for $^2\Pi_u$. The difference in B'_0 values for the two substates $^2\Pi_{3/2u}$ and $^2\Pi_{1/2u}$(0.0016) is somewhat smaller than the theoretical value 0.0025.

The direction of the staggering in all $^2\Pi_{1/2u} \rightarrow {}^2\Pi_{1/2g}$ sub-bands (the smaller distances appear in $P(J+1) - P(J)$ or $R(J+1) - R(J)$ for $J - \frac{1}{2}$ even) and the assumption $p' - p''_0 > 0$ are consistent with the requirement that only $-$ levels in $^2\Pi_u$ and $+$ levels in $^2\Pi_g$ are present.[19]

In conclusion the author wishes to express his sincere thanks to Professor R. S. Mulliken for his great kindness, continued interest and many important suggestions, and to Dr. F. Bueso-Sanllehí, Dr. A. Turkevich and Miss L. H. Woods for frequent and very valuable help given in the experimental part of this work.

[18] Cf. R. S. Mulliken and A. Christy, Phys. Rev. **38**, 87 (1931).

[19] See, for instance, Fig. 108, p. 262 in Herzberg's book on *Molecular Spectra and Molecular Structure*, Vol. I (New York, 1939).

Quenching and Depolarization of Mercury Resonance Radiation by the Rare Gases

LEONARD O. OLSEN
Case School of Applied Science, Cleveland, Ohio
(Received August 18, 1941)

The quenching and depolarization of mercury 2537A resonance radiation by helium, neon, argon, and krypton has been studied experimentally, the results being displayed in graphical and tabular form. Probable numbers of quenching and depolarizing collisions and cross sections for quenching and depolarization have been calculated and are presented in Table V.

INTRODUCTION

IN a recent paper[1] (referred to as I hereafter) a theory of quenching and depolarization of resonance radiation by foreign gases was presented. An experimental study of quenching and depolarization of mercury resonance radiation by several diatomic gases was also described.

In deriving formulae for polarization and rotation of the plane of maximum polarization as a function of foreign gas pressure and applied magnetic field, a quenching coefficient and two depolarizing coefficients were introduced. Two depolarizing coefficients were used because the experimental work indicated that a portion of the depolarizing collisions was adiabatic, leaving the excited atoms in states coherent with those which existed before the collisions.

In order to secure more information, especially concerning the depolarizing mechanism, it was decided to perform a series of experiments on the quenching and depolarization of mercury resonance radiation by some of the rare gases. The low quenching ability of these substances should make depolarization effects more discernible.

The formulae presented in paper I have been used to determine the quenching and depolarizing probabilities which are presented in this paper. The experimental procedure is unaltered except for the photometry of the photographic images secured in determining the match position. In this series of experiments the densities were measured with a Schulte photometer which is an ideal instrument for measuring the many images which must necessarily be secured when the Cornu method is used.

The experimental conditions were checked frequently by determining the polarization as a function of magnetic field with no foreign gas present. Good agreement with H. F. Olson's[2] data was always secured before experiments were performed with foreign gases present.

The helium, neon and argon used were spectroscopically pure. The krypton contained 5.4 percent xenon.

RESULTS

The observed values of polarization of the 2537A mercury line for various pressures of

TABLE I. *Polarization in helium and rotation of plane of polarization for various fields (measured in gauss) and pressures (measured in mm of Hg).*

	$p=0.15$						0.33	
H	P_{obs}	P_{calc} $\alpha''=0.35$	P_{calc} $\alpha''=0$	Tan 2ϕ obs.	Tan 2ϕ calc. $\alpha''=0.35$	Tan 2ϕ calc. $\alpha''=0$	P_{obs}	Tan 2ϕ obs.
0	0.66	0.66	0.66				0.55	
0.203	0.54	0.55	0.56				0.50	
0.406	0.37	0.37	0.39	*0.91*	*0.83*	*0.79*	0.38	*0.74*
0.812	0.18	0.17	0.19	*1.70*	*1.65*	*1.58*	0.19	*1.37*
1.218	0.11			*2.27*	*2.22*	*2.17*		*2.19*
1.624							0.06	

	$p=0.68$					
H	P_{obs}	P_{calc} $\alpha''=0.35$	P_{calc} $\alpha''=0$	Tan 2ϕ obs.	Tan 2ϕ calc. $\alpha''=0.35$	Tan 2ϕ calc. $\alpha''=0$
0	0.41	0.41	0.41			
0.203	0.38	0.38	0.39			
0.406	0.33	0.32	0.34	*0.53*	*0.50*	*0.44*
0.812	0.21	0.20	0.22	*0.97*	*1.00*	*0.88*
1.218	0.14	0.12	0.14	*1.46*	*1.50*	*1.33*

	$p=0.50$			1.07	1.97	3.2	5.5
H	P_{calc} $\alpha''=0.35$	P_{calc} $\alpha''=0$	Tan 2ϕ obs.	P_{obs}	P_{obs}	P_{obs}	P_{obs}
0	0.48	0.47	0.47		0.33	0.22	0.15	0.09
0.203	0.45	0.45	0.45					
0.406	0.36	0.35	0.37	*0.61*				
0.812	0.21	0.20	0.22	*1.06*				
1.218	0.14	0.12	0.14	*1.59*				

[1] A. Ellett, L. Olsen, and R. Petersen, Phys. Rev. **60**, 107 (1941).

[2] H. F. Olson, Phys. Rev. **32**, 443 (1928).

TABLE II. *Polarization in neon and rotation of plane of polarization for various fields (measured in gauss) and pressures (measured in mm of* Hg).

	$p=0.13$						0.145	
H	P_{obs}	P^{calc} $\alpha''=0.14$	P^{calc} $\alpha''=0$	Tan 2ϕ obs.	Tan 2ϕ calc. $\alpha''=0.14$	Tan 2ϕ calc. $\alpha''=0$	P_{obs}	Tan 2ϕ obs.
0	0.71	0.71	0.71				0.69	
0.203	0.56	0.57	0.57				0.54	
0.406	0.35	0.37	0.37	*1.02*	*0.91*	*0.89*	0.34	*1.08*
0.812	0.18	0.17	0.17	*1.83*	*1.79*	*1.76*	0.16	*1.86*
1.218	0.10			*2.78*		*2.32*	0.10	*3.08*

	$p=0.395$		0.62			0.76		
H	P_{obs}	Tan 2ϕ obs.	P_{obs}	P_{obs}	P^{calc} $\alpha''=0.14$	P^{calc} $\alpha''=0$	Tan 2ϕ obs.	Tan 2ϕ calc. $\alpha''=0.14$	Tan 2ϕ calc. $\alpha''=0$
0	0.59		0.54	0.52	0.51	0.51			
0.203	0.50		0.48	0.47	0.46	0.47			
0.406	0.34	*0.89*	0.36	0.36	0.36	0.37	*0.69*	*0.62*	*0.58*
0.812	0.17	*1.52*	0.20	0.20	0.20	0.21	*1.29*	*1.22*	*1.16*
1.218	0.11	*1.88*	0.13	0.13	0.12	0.13	*1.63*	*1.81*	*1.72*

	$p=1.08$		1.49	2.31	2.54	3.51	4.85	7.45
H	P_{obs}	Tan 2ϕ obs.	P_{obs}	P_{obs}	P_{obs}	P_{obs}	P_{obs}	P_{obs}
0	0.44		0.39	0.30	0.30	0.25	0.19	0.13
0.203	0.41			0.29				
0.406	0.34	*0.59*		0.25				
0.812	0.23	*1.01*		0.20				
1.218	0.14	*1.48*		0.14				

TABLE III. *Polarization in argon and rotation of plane of polarization for various fields (measured in gauss) and pressures (measured in mm of* Hg).

	$p=0.12$						0.15
H	P_{obs}	P^{calc} $\alpha''=0.13$	P^{calc} $\alpha''=0$	Tan 2ϕ obs.	Tan 2ϕ calc. $\alpha''=0.13$	Tan 2ϕ calc. $\alpha''=0$	P_{obs}
0.0	0.72	0.71	0.71				0.68
0.203	0.56	0.58	0.58				0.55
0.406	0.38	0.38	0.38	*1.01*	*0.89*	*0.88*	0.36
0.812	0.17	0.17	0.18	*1.68*	*1.76*	*1.74*	0.17
1.218	0.09			*2.20*		*2.34*	0.10

	$p=0.35$		1.51	2.30	3.60	5.00	8.25
H	P_{obs}	Tan 2ϕ obs.	P_{obs}	P_{obs}	P_{obs}	P_{obs}	P_{obs}
0.0	0.58		0.33	0.25	0.20	0.15	0.10
0.203	0.51						
0.406	0.35	*0.80*		0.26			
0.812	0.17	*1.41*		0.20			
1.218	0.11	*1.83*		0.14			

	$p=0.56$		0.67			1.12	
H	P_{obs}	P_{obs}	P^{calc} $\alpha''=0.13$	P^{calc} $\alpha''=0$	Tan 2ϕ obs.	P_{obs}	Tan 2ϕ obs.
0.0	0.52	0.50	0.50	0.50		0.41	
0.203	0.46	0.45	0.45	0.45		0.38	
0.406	0.35	0.36	0.35	0.36	*0.64*	0.33	*0.43*
0.812	0.19	0.21	0.20	0.21	*1.14*	0.21	*0.93*
1.218		0.13	0.12	0.13	*1.48*	0.16	*1.18*

TABLE IV. *Polarization in krypton and rotation of plane of polarization for various fields (measured in gauss) and pressures (measured in mm of* Hg).

	$p=0.17$				$p=0.43$			
H	P_{obs}	P^{calc} $\alpha''=0$	Tan 2ϕ obs.	Tan 2ϕ calc. $\alpha''=0$	P_{obs}	P^{calc} $\alpha''=0$	Tan 2ϕ obs.	Tan 2ϕ calc. $\alpha''=0$
0.0	0.68	0.68			0.56	0.57		
0.203	0.55	0.56			0.50	0.50		
0.406	0.38	0.38	*1.04*	*0.84*	0.38	0.38	*0.75*	*0.67*
0.812	0.19	0.18	*1.68*	*1.66*	0.22	0.20	*1.37*	*1.34*
1.218	0.12		*2.42*	*2.23*	0.13	0.12	*2.02*	*1.92*

	$p=0.75$				1.14			
H	P_{obs}	P^{calc} $\alpha''=0$	Tan 2ϕ obs.	Tan 2ϕ calc. $\alpha''=0$	P_{obs}	P^{calc} $\alpha''=0$	Tan 2ϕ obs.	Tan 2ϕ calc. $\alpha''=0$
0.0	0.49	0.48			0.40	0.40		
0.203	0.44	0.44			0.39	0.38		
0.406	0.37	0.37	*0.54*	*0.54*	0.34	0.33	*0.42*	*0.43*
0.812	0.23	0.22	*0.97*	*1.06*	0.23	0.22	*0.82*	*0.85*
1.218	0.18	0.14	*1.29*	*1.59*	0.17	0.15	*1.10*	*1.28*

H	$p=1.70$ P_{obs}	2.27 P_{obs}	3.25 P_{obs}	4.91 P_{obs}	7.30 P_{obs}
0.0	0.31	0.27	0.21	0.16	0.13

helium, neon, argon, and krypton and for various magnetic field intensities are given in Tables I to IV. In addition, the tangents of twice the angle of rotation of the plane of maximum polarization for various pressures and field intensities are listed in italics.

Quenching coefficients and depolarizing coefficients (α, α' and α'') have been chosen which give the best over-all agreement between the polarizations, etc., calculated from Eqs. (10) and (11) of paper I and those observed experimentally. Typical calculated results are also displayed in Tables I to IV.

In view of the rather small values of the adiabatic depolarizing coefficient α'', it was deemed desirable to determine the values of polarization calculated on the assumption that all the depolarizing collisions were non-adiabatic, that is, α'' equals zero and α' is the total depolarizing coefficient. Typical results have been included in the tables. The data are displayed graphically in Figs. 1 to 6, inclusive. The circles, squares, etc., locate the experimentally determined values and the solid curves are drawn through the points calculated from Eqs. (10) and (11) of paper I. The best values of α, α' and α'' have been used. In Fig. 6 only one plot of rotation of the plane of maximum polarization is shown for each gas in order to avoid confusion.

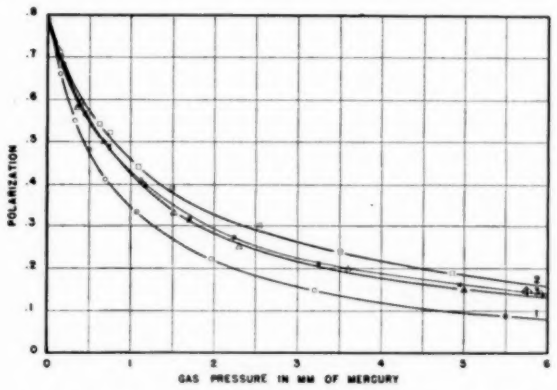

FIG. 1. Polarization of mercury resonance radiation as a function of gas pressure. The curves are drawn with the α's given in Table V. Curve 1 (○), helium; 2 (□), neon; 3(△), argon; 4 (×), krypton.

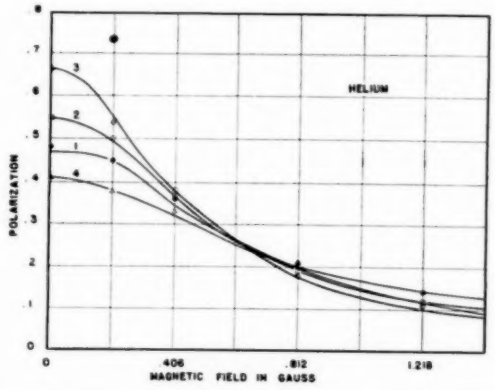

FIG. 2. Effect of magnetic fields on polarization of mercury resonance radiation at fixed helium pressures. The curves are drawn with $\alpha=0$, $\alpha'=1.4\times10^7$ and $\alpha''=0.35\times10^7$. Curve 1 (●), helium pressure = 0.50 mm of Hg; 2 (□), $p=0.33$ mm of Hg; 3 (○), $p=0.15$ mm of Hg; (△), $p=0.68$ mm of Hg.

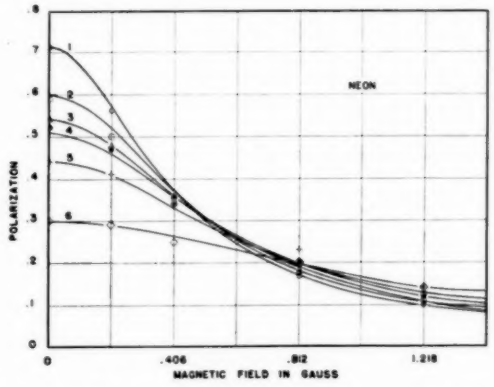

FIG. 3. Effects of magnetic fields on polarization of mercury resonance radiation at fixed neon pressures. The curves are drawn with $\alpha=0.02\times10^7$, $\alpha'=0.77\times10^7$ and $\alpha''=0.14\times10^7$. Curve 1 (○), neon pressure = 0.13 mm of Hg; 2 (□), $p=0.395$ mm of Hg; 3 (△), $p=0.62$ mm of Hg; 4 (●), $p=0.76$ mm of Hg; 5 (+), $p=1.08$ mm of Hg; 6 (◇), $p=2.31$ mm of Hg.

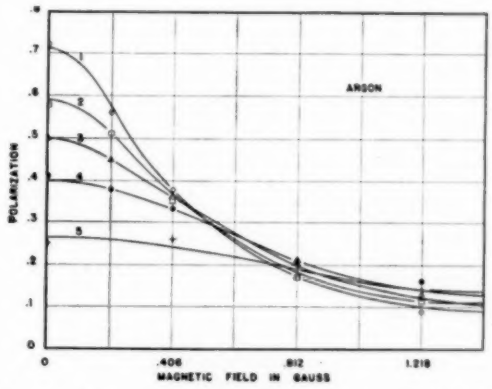

FIG. 4. Effect of magnetic fields on polarization of mercury resonance radiation at fixed argon pressures. The curves are drawn with $\alpha=0.01\times10^7$, $\alpha'=0.97\times10^7$ and $\alpha''=0.13\times10^7$. Curve 1 (○), argon pressure = 0.12 mm of Hg; 2 (□), $p=0.35$ mm of Hg; 3 (△), $p=0.67$ mm of Hg; 4 (●), $p=1.12$ mm of Hg; 5 (+), $p=2.30$ mm of Hg.

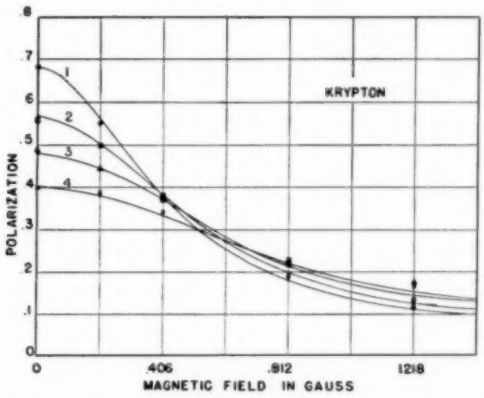

FIG. 5. Effect of magnetic fields on polarization of mercury resonance radiation at fixed krypton pressures. The curves are drawn with $\alpha=0.0$, $\alpha'=1.11\times10^7$ and $\alpha''=0.0$. Curve 1 (○), krypton pressure = 0.17 mm of Hg; 2 (□), $p=0.43$ mm of Hg; 3 (△), $p=0.75$ mm of Hg; 4 (×), $p=1.14$ mm of Hg.

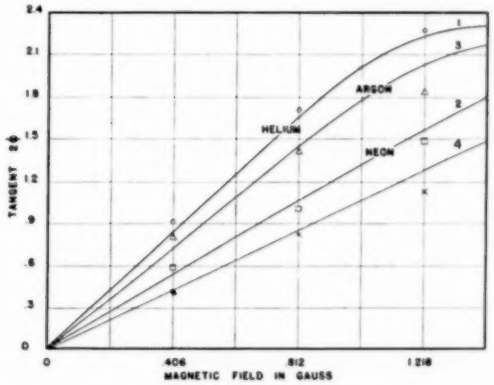

FIG. 6. Rotation of the plane of maximum polarization as a function of magnetic fields for the gases studied. The curves are drawn with the α's given in Table V. Curve 1 (○), helium at $p=0.15$ mm of Hg; 2 (□), neon at $p=1.08$ mm of Hg; 3 (△), argon at $p=0.35$ mm of Hg; 4 (×), krypton at $p=1.14$ mm of Hg.

TABLE V. *Collision probabilities* ($\times 10^{-7}$ sec.$^{-1}$) *and cross sections* ($\times 10^{16}$ cm^2).

Gas	Quenching α	Quenching σ_α^2	Non-Adiabatic Depolarizing α'	Non-Adiabatic Depolarizing $\sigma_{\alpha'}^2$	Adiabatic Depolarizing α''	Adiabatic Depolarizing $\sigma_{\alpha''}^2$	Total Depolarizing $\sigma^2\alpha'+\alpha''$
He	negligible	negligible	1.40	10.6	0.35	2.66	13.26
Ne	0.02	0.325	0.77	12.6	0.14	2.30	14.90
A	0.01	0.222	0.97	21.6	0.13	2.89	24.49
Kr	negligible	negligible	1.11	32.7	0.00	0.00	32.70

Table V displays the choices of quenching and depolarizing coefficients for each gas as well as the cross sections computed from the kinetic theory formula presented in paper I.

CONCLUSIONS

A comparison of the observed polarizations and rotations of plane of polarization with the calculated values leaves one in some doubt concerning the necessity of introducing a probability of adiabatic depolarization. As far as the polarization *vs.* magnetic field intensity is concerned, there is little difference between the calculations with α'' unequal to zero and those for which it was zero. With regard to the rotation of the plane of polarization *vs.* magnetic field data, considerably better agreement is secured in most instances by using α'' unequal to zero.

A similar comment could be made regarding the data presented for nitrogen in paper I. The necessity of introducing adiabatic depolarization is chiefly apparent in securing agreement between calculated and experimental values of the rotation of the plane of polarization, although a slight improvement is also produced in the agreement of the polarization data.

The quenching efficiencies listed in Table V range from zero for helium and krypton to 0.02×10^7 sec.$^{-1}$ for neon. These gases are thus poor quenchers, as would be expected. Probably no significance should be attached to the small variation in quenching ability which the table displays as it is undoubtedly within experimental error.

Further experimental work on additional gases will be undertaken.

It is a pleasure for the author to thank the State University of Iowa Department of Physics for a loan of the necessary optical equipment which has enabled him to carry on this work. He also wishes to express his appreciation to Dr. J. J. Nassau for placing the facilities of the photometry laboratory of the Case Warner and Swasey Observatory at his disposal. The author wishes to thank Dr. Forsythe of General Electric, Nela Park, and Mr. Fahrenthold of General Electric Wire Works for their generous cooperation in furnishing the krypton needed for these experiments.

A Discussion of the Fundamental Limit of Performance of an Electron Microscope

JAMES HILLIER
Research Laboratories, RCA Manufacturing Company, Inc., Camden, New Jersey
(Received September 20, 1941)

In the case of a given electron microscope objective the diffraction defect diffuses the image of a geometrical point over a finite area. The contrast which can be obtained in the image of a single atom is limited by this phenomenon because the actual image of an atom extends over many times the area of its geometrical image. If a ten percent change in intensity is the minimum change that can be detected in the electron image by means of a photographic emulsion, it is shown that a single atomic nucleus can produce a discernible image only if it is of atomic number greater than 25. With the optimum objective aperture the addition of the atomic electrons appears to produce only a slight change in this lower limit of atomic number. Its value is increased by the effects of neighboring atoms, non-parallel illumination, and lens aberrations.

IN discussing the practical limit of resolving power of the bright-field transmission-type magnetic electron microscope, most writers have agreed fairly well in setting that limit at approximately 10 angstrom units.[1,2] Such discussions, however, have been based on the ability (as limited by the magnitude of the lens aberrations) of a lens to form separated images of closely situated particles, and have not taken into consideration the intensity problems which may prevent the observation of images of particles of the size implied by the definition and magnitude of the limiting resolving power. While a few writers[3–5] have considered the intensity and contrast relationships in the present type of electron microscope, they have assumed that multiple scattering obtains and have been concerned mainly with the differences in thickness of a homogeneous specimen and with the differences in density of a uniformly thick specimen required to produce an observable change in intensity in the image. In the following it will be shown that even in the optimum case of minute "*free*" particles in the specimen plane, the contrast obtainable sets a lower limit to the size of particle which may be discerned with the electron microscope. (The term "free" particle is used here to describe the hypothetical case of a particle suspended in space in the object plane of the objective.)

As one criterion for the measurement of resolving power, von Ardenne[1] uses the magnitude d_H, which is defined as the half-value width of the intensity distribution, constituting the image of a point. Inherent in this definition is the assumption that the point of which an image is produced is so small that its physical extent has no effect on the value of d_H. Thus, in order to demonstrate a resolving power of 10A with an instrument of which the limiting resolving power is just 10A, it would be necessary to produce images of points that are themselves not more than 1 to 2A in diameter. From this it becomes apparent that in order to reproduce in the image the detailed structure of a specimen down to 10A the electron microscope must be capable of producing observable images of either individual atoms, or at least of very small groups of atoms.

The following approximate calculations indicate the contrast obtainable in the image of a single atom situated in the object plane of an electron-microscope objective. It will be assumed that the resolving power of the electron-microscope objective is limited only by the diffraction defect, which has the magnitude given by the familiar formula

$$d_R = 0.61\lambda/\sin\alpha_{ob}, \qquad (1)$$

where λ = wave-length associated with electron radiation used; α_{ob} = half the angle subtended by the objective aperture at the point of the specimen on the axis of the system; d_R = radius of

[1] M. von Ardenne, Zeits. f. Physik **108**, 338–352 (1938).
[2] B. von Borries and E. Ruska, Zeits. f. tech. Physik **20**, 225–235 (1939).
[3] M. von Ardenne, *Elektronen-Übermikroskopie* (Julius Springer, 1940)
[4] L. Marton, Physica **3**, 959–967 (1936).
[5] M. von Ardenne, Zeits. f. physik. Chemie **187**, 1–12 (1940).

first diffraction minimum in the circular diffraction pattern which constitutes the image of a point. The above assumptions lead to the result that d_R is approximately equal to d_H.

For the present we shall assume that the intensity distribution in the image of a point is given by a function $F(r)$ which expresses the number of electrons per second per square millimeter at a point in the image r millimeters from the position of the geometrical image of the point when the point is considered to transmit one electron per second. We shall also assume that the object plane is illuminated by a homogeneous beam of electrons of intensity I_o, and that the paths of all the electrons which constitute the illuminating beam are parallel to the optic axis of the objective. Then $I_o r_o dr_o d\theta_o$ is the number of electrons per second passing through an element of area of the object plane in the absence of a specimen, where r_o and θ_o are the plane polar coordinates of the object space referred to an arbitrary origin.[6] The electron intensity at a point in the image at a distance r_i from the geometrical image of the element of area is $F(r_i) I_o r_o dr_o d\theta_o$. The total intensity at any point in the image of a uniformly illuminated object plane is

$$I_i = I_o \int_0^{\infty} \int_0^{2\pi} F(r_i) r_o dr_o d\theta_o, \tag{2}$$

where the integration is carried out in the object space. If we choose the origin of the object space coordinates to be at the point of the object corresponding to the point of the image under consideration, r_o is always equal to r_i, and the above expression may be written

$$I_i = I_o \int_0^{\infty} \int_0^{2\pi} F(r_o) r_o dr_o d\theta_o, \tag{3}$$

but from the definition of $F(r)$ we obtain the obvious result that $I_i = I_o$ when there is no matter in the object plane.

If we have a single atom on the object plane, it will appear, from the point of view of the electron-microscope objective, as an opaque disk of radius r_a. r_a represents the radius of the apparent cross section of the atom, that is, the distance between the center of the atom and the rectilinear continuation of the path of the electron which is deflected by just the angular aperture α_{ob} of the objective. Electrons in the paths which pass closer than r_a will be deflected outside the objective aperture. The magnitude of r_a is dependent on α_{ob}. The type of atom, and the velocity of the illuminating electrons. The intensity which exists at the center of the geometrical image of such an atom is given by the expression

$$I_i = I_o \int_0^{2\pi} \int_{r_a}^{\infty} F(r_i) r_o dr_o d\theta_o, \tag{4}$$

where the origin of the object space coordinates is taken at the center of the atom so that $r_i = r_o$, and the integration is carried out in the object space as above. In the case being considered, the function $F(r)$ is the electron intensity distribution in the diffraction image of a point. As this is too unwieldy mathematically for the present rough approximation, we shall express $F(r)$ as an error function. This expression has approximately the same shape as the diffraction distribution, and by the proper choice of the constants it can be made to have the same essential values. Let

$$F(r) = a \exp(-kr^2), \tag{5}$$

where

$$a = k/\pi \tag{6}$$

by virtue of the definition of $F(r)$. Moreover, since we require that

$$F(d_H/2) = \tfrac{1}{2} F(0), \tag{7}$$

we must have

$$k = (4 \log_e 2)/d_H^2. \tag{8}$$

Substituting expressions (5), (6), and (8) in expression (4), we obtain

$$I_i = I_o \int_0^{2\pi} \int_{r_a}^{\infty} \frac{k}{\pi} \exp(-kr_o^2) r_o dr_o d\theta_o = I_o 2^{-(4r_a^2/d_H^2)}. \tag{9}$$

For a difference in intensity to be detected by a photographic emulsion, such a difference must be at least 10 percent of the original, while to be detected on a fluorescent screen, the difference must be somewhat greater. Thus,

$$2^{-(4r_a^2/d_H^2)} \gtrless 0.9 \tag{10}$$

[6] The subscript o will denote measurements in the object plane; the subscript i will denote measurements in the image plane. The magnification is considered to be unity so that the scales of the two planes will be the same.

must be true if the atom is to produce an observable change in the intensity of the recorded image. From this it can be deduced immediately that

$$r_a^2/d_H^2 \gtreqless 0.038. \quad (11)$$

If we neglect the existence of the atomic electrons, the value of r_a may be written in the form

$$r_a=(Ze^2/mv^2)(1/\tan\alpha_{ob}+1/\sin\alpha_{ob}), \quad (12)$$

which is obtained directly from classical scattering theory as first given by Rutherford. In this expression Z is the atomic number, e is the electronic charge, m the electronic mass, and v the electron velocity.

On substituting expressions (12) and (1) in (11), we obtain

$$\frac{r_a}{d_H}=\frac{Ze^2(\cos\alpha_{ob}+1)}{0.61\lambda mv^2}\gtreqless(0.038)^{\frac{1}{2}}. \quad (13)$$

We see from this that we obtain *maximum contrast* for $\alpha_{ob}=0$, and that for an electron velocity corresponding to 60 kilovolts

$$Z \gtreqless \sim 25 \quad (14)$$

must be true if the presence in the object plane of the nucleus of an atom is to be detected by an electron microscope using 60-kilovolt electrons. Thus, in the case of materials composed of the lighter elements, *viz.*, organic compounds, a particle must consist of at least several atoms if it is to be discernible in an electron microscope using electrons of this velocity.

If we consider the presence of atomic electrons, the problem becomes much more complicated. The expression for r_a must be modified to include the screening effects of the electrons, the elastic and inelastic scattering by the electrons, and the state of ionization of the atom as a whole. The value of r_a no longer increases indefinitely with decreasing value of α_{ob}, hence for any atom *the ratio r_a/d_H approaches zero as α_{ob} approaches zero.* This means that for small aperture lenses such as used in the present electron microscopes, it is probably impossible to detect a single atom of any type. An initial approximate calculation indicates that for the value of α_{ob} which gives maximum contrast the minimum value of Z is approximately the same as that given in (14).

In actual practice the contrast in the image of a given atom is reduced greatly by the presence of nearby atoms, by the use of non-parallel illumination, by the presence of a supporting membrane, and by lens aberrations. In the above discussion it has been shown that for organic material the size of the smallest particle which can be observed with an ideal electron microscope is limited by the contrast in the image rather than by the resolving power of the lens system. For heavy materials, on the other hand, the contrast in the image limits the size of the smallest particle which may be observed *only in the presence of lens errors* and other detrimental effects, all of which are amenable to control. Thus, it appears that individual atoms of heavy elements may be discernible with the electron microscope and that a magnitude of resolving power compatible with the size of the image of such atoms may eventually be demonstrated.

The author wishes to thank Dr. V. K. Zworykin and Dr. E. G. Ramberg for their very helpful discussions regarding this work.

Letters to the Editor

PROMPT publication of brief reports of important discoveries in physics may be secured by addressing them to this department. Closing dates for this departmen are, for the first issue of the month, the eighteenth of the preceding month, for the second issue, the third of the month. Because of the late closing dates for the section no proof can be shown to authors. The Board of Editors does not hold itself responsible for the opinions expressed by the correspondents.

Communications should not in general exceed 600 words in length.

Cosmic Rays and the Magnetic Disturbance of September 18, 1941

VICTOR F. HESS AND EDWARD B. BERRY, S.J.
Fordham University, New York, New York
October 21, 1941

THE "magnetic storm effect" on cosmic rays, well established and recognized as a world-wide phenomenon by S. E. Forbush, V. F. Hess, J. Clay, Th. A. Johnson and others[1] is a phenomenon which consists in a positive correlation between the horizontal magnetic intensity and cosmic-ray intensity. In the recent strong display of aurora borealis field changes of 1200 gamma (from 17,700 to 18,900 gammas) of the horizontal magnetic intensity occurred. Since we have been registering cosmic rays with different instruments in New York for a long time it seemed of interest to analyze our results and to compare them with former reports on cosmic-ray changes during aurora displays.

A large twin counter telescope has been in operation since March, 1941 at Fordham University. Designed by W. F. G. Swann it consists of two independent but interlocked triple coincident sets of counter tubes, with a total of 108 G.M. tubes. This instrument, with 22 cm of lead between the counter trays, automatically registers the number of mesotrons traversing the apparatus in bi-hourly intervals.

Another much simpler apparatus, consisting of two unshielded counters in a vertical plane, has been in operation since 1939.

Finally a large Compton model C cosmic-ray meter was set up on the upper deck of the *S. S. Santa Ana* (Grace Line) to register cosmic-ray ionization between New York and Valparaiso, Chile. As the ship happened to be in New York on the day of the aurora, the registrations of this meter (shielded with 12 cm lead-equivalent) could also be used.

All three instruments simultaneously showed a decrease of the rate of cosmic radiation after the onset of the magnetic disturbance (at approx. 2 A.M., September 18, 75th meridian time). All the rates were previously corrected for atmospheric pressure changes and for the atmospheric temperature effect, taking the average or "mass" temperature from an integration of the p, T curves as obtained from daily high altitude sounding balloon flights at Lakehurst, up to 80 percent of the atmosphere. The coefficient had been found to be -0.46 percent per degree C.[2]

The correlation between bi-hourly rates of the mesotron counting set and simultaneous mean values of H (horizontal geomagnetic component) gives a correlation coefficient of $+0.50\pm0.23$ and a magnetic storm coefficient $H\Delta I/I\Delta H=+1.3\pm0.6$ percent C.R. intensity per percent horizontal geomagnetic intensity (H) which is positive and of the same order of magnitude as found during previous magnetic storms. During the subsequent very rapid rise of H, between 8 A.M. and 4 P.M., on September 18 the mesotron rates showed a relatively small increase. During the evening when the aurora was most brilliant, H and the mesotron intensity were relatively low and showed erratic fluctuations.

The double coincidence set, which yields only daily mean values, gave a rate of 98.7 counts per hour on September 18 as compared with 105.8 on September 17 and 104.3 on September 19.

Hourly rates of the Compton meter were correlated with hourly magnetic intensities, giving a correlation coefficient of $+0.54\pm0.21$ and a magnetic storm coefficient $H\Delta I/I\Delta H=+0.72\pm0.27$ in sufficient agreement with the one found with the mesotron counter, but somewhat smaller, perhaps because of the lack of directional selectivity (the mesotron counter registers vertical rays only).

Compared with the aurora of January 25–26, 1938[3] the above cosmic-ray fluctuations are less pronounced and this is in accordance with the belief that, if electronic ring currents at distances of several earth's radii around the globe cause a diminution of incoming particles, then the radii of these currents may differ considerably from storm to storm or even during a storm.

We wish to thank the staff of the Cheltenham Observatory, U. S. Coast and Geodetic Survey, for kindly supplying us with the magnetic data.

[1] For complete bibliography, see Th. A. Johnson, Rev. Mod. Phys. **10**, 229 (1938).
[2] V. F. Hess and F. A. Benedetto, Phys. Rev. **60**, 610 (1941).
[3] V. F. Hess *et al.*, Nature **141**, 686 (1938).

Energies of Gamma-Rays from Ni^{63}, Mn^{56}, Zn^{69}, Ga^{67}

A. GUTHRIE
Department of Physics, Purdue University, Lafayette, Indiana
October 21, 1941

IN many cases, the best method available for the determination of gamma-ray energies is a study of the secondary electrons by means of a magnetic spectrograph. Perhaps the simplest and most commonly used form of this instrument is that with semi-circular focusing.

In the work here described, a semi-circular focusing spectrograph of standard design was used. Photoelectrons from a thin layer of lead (from about 5 mils to 60 mils) wrapped around the source were recorded on Eastman x-ray film and a standardized procedure was used in developing the film. The position of the high energy edge appearing on the film was determined in all those cases where it was feasible by use of a microphotometer. It was observed that the energies obtained by measuring the

TABLE I. *Energies of gamma-rays.*

ISOTOPES	PERIOD	GAMMA-RAYS (MEV)	REFERENCE
Ni^{63}	2.6 hr.	0.280±0.007 0.65 ±0.01 0.93 ±0.04	1
Zn^{69}	13.6 hr.	0.440±0.006	2, 3
Ga^{67}	83 hr.	0.292±0.006	3
Mn^{56}	2.59 hr.	0.800±0.015	4, 5

[1] J. J. Livingood and G. T. Seaborg, Phys. Rev. **53**, 765 (1936).
[2] J. W. Kennedy, G. T. Seaborg and E. Segrè, Phys. Rev. **56**, 1095 (1939).
[3] A. C. Helmholz, Phys. Rev. **60**, 415 (1941).
[4] R. H. Bacon, E. N. Grisewood, and C. W. van der Merwe, Phys. Rev. **59**, 531 (1941).
[5] M. Deutsch and A. Roberts, Phys. Rev. **60**, 362 (1941).

distance from the center of this target to the visually observed high energy edge checked within experimental error with the energy value obtained from the corresponding microphotometer trace. This method had been found to be very useful in those cases where the background of the film due to scattered electrons and to the continuous electron spectrum is too dense to permit taking useful microphotometer traces. The magnetic field strength was determined in each case by use of a mutual inductance circuit and fluxmeter. The error in the field strength is believed to be less than 1 percent. A check on these measurements was made by determining the value of the annihilation radiation from Cu^{61} and Cu^{64}. The average value of 20 measurements was found to be 0.512±0.006 Mev, (Table I).

The values tabulated are the averages of at least five separate measurements. In the case of Mn^{56} an attempt was made to find a gamma-ray of energy greater than 2 Mev as reported by Bacon *et al.* but without success because of insufficient intensity. The first two gamma-rays recorded in the case of Ni^{63} have not been previously reported. These values, together with rough intensity measurements, suggest a cascade process in which the upper state decays to the ground state by the emission of either a single 0.93 Mev gamma-ray or two gamma-rays of energies 0.280 Mev and 0.65 Mev, respectively, through an intermediate state.

All of these gamma-ray energies were obtained during the progress of some work which was completed in June, 1941 and is reported in the author's Ph.D. thesis. More recently, the values of some of these gamma-ray energies have been published (references 3 and 5 in Table I) and they agree fairly well with the values tabulated above.

Radioactive Isotopes of Mercury

C. S. WU AND G. FRIEDLANDER
Radiation Laboratory, Department of Physics and Department of Chemistry, University of California, Berkeley, California
November 3, 1941

WHEN the present investigation was started, the following mercury activities had been reported: a 43–48-minute period, produced by fast neutrons[1–4] and deuterons[4] on mercury, and variously assigned to Hg^{203} or Hg^{197}; a period of between 25 and 40 hours' half-life, produced by slow[5] and fast[3, 4] neutrons and by deuterons[4] on mercury, and by deuterons[4, 6] on gold, and assigned to Hg^{205} or Hg^{198*}; a 5.5-minute period, assigned to Hg^{205}, and a long period (about 60 days) from deuteron bombardment of mercury.[4]

Very recently, Sherr, Bainbridge and Anderson[7] reported 43-minute, 25-hour and 50-day periods, induced in mercury by fast neutrons. Our results agree in the main with theirs; but, in addition, we have found a new activity of 64 hours' half-life, isomeric with the 25-hour activity, and we have studied the x-rays from these two activities as well as from the 43-minute period by critical absorption measurements. The beta- and gamma-radiations from all activities investigated were studied by absorption methods. Chemical separations were made in all cases, except for the 5-minute period.

Hg^{197}: *25 hours and 64 hours.* Slow and fast neutron bombardments of mercury give rise to a mercury-activity whose half-life seemed to vary between 25 and 45 hours, depending on the thickness of the sample and of the window of the measuring instrument. The mercury fraction from the bombardment of gold with 16-Mev deuterons showed the same behavior; but since, in the latter case, no other periods were present, we were able to resolve the decay curve into 2 straight lines whose slopes corresponded to half-lives of 25 and 64 hours, respectively, provided thin samples and thin windows were used. The chemical identity of both periods was proved by separating gold from the active sample at various times; the gold fraction was always inactive, and the mercury fraction carried all the activity. Absorption in aluminum shows that both activities emit lines of conversion electrons, the maximum energy for the 25-hour activity being about 200 kev, that for the 64-hour activity less than 90 kev. The electron lines were kindly measured for us by Dr. A. C. Helmholz in his magnetic spectrograph; he found 6 lines decaying with a 25-hour and 2 lines decaying with a 64-hour half-life. Valley[7, 8] has also reported electron lines from mercury formed in the deuteron bombardment of gold.

Critical absorption measurements of the x-rays emitted were made with tungsten, tantalum, and lead absorbers at various intervals from the time of the chemical isolation of mercury until two weeks later; the curves remained the same at all times and agreed well with calculated curves for the absorption of the *K* radiations from gold. (*L* radiation is so soft that it is completely absorbed by the aluminum absorbers used to cut out the electrons.) The mercury fraction from neutron bombardments of mercury gave rise to the same x-ray absorption curves after the 43-minute period had decayed completely. We conclude that both the 25-hour and the 64-hour periods are due to Hg^{197} and that both decay to Au^{197} by *K*-electron capture. Both periods have complex groups of soft gamma-rays associated with them.

43-minute period. This period is induced strongly in mercury by fast neutrons. Associated with it is a line of electrons of about 460 kev, a group of several gamma-rays, and x-rays which were shown by critical absorption measurements and comparison with calculated absorption curves to be *K* radiation of mercury. Hence the 43-minute period is probably associated with an isomeric transition

in mercury. It cannot be due to Hg^{197} or Hg^{198*}, because neither the Harvard group nor we have found it in deuteron bombardments of gold; if the 43-minute activity[7] reported from alpha-particle bombardment of platinum is identical with this period, the assignment is limited to $Hg^{199 \text{ or } 201*}$. We failed to obtain a 43-minute mercury from bombardment of lead with neutrons from 16-Mev deuterons on beryllium, but this may not preclude the assignment to Hg^{201*} as Pb^{204} has an abundance of only 1.48 percent, and the cross section for an $n-\alpha$ reaction in this region may be quite small. Both Hg^{199*} and Hg^{201*} should be made by (n, γ) reactions. The yield of the 43-minute period with slow neutrons on mercury was found to be small, in agreement with the Harvard group [7]

54-day period. This activity was obtained from slow and fast neutron bombardment of mercury and is probably due to Hg^{203}. It emits negative beta-particles with an upper energy limit of 300–350 kev, and gamma-rays of about 300 kev. No x-rays are emitted.

In addition, we found a 5-minute period from slow neutron bombardment of mercury. No chemical separation was made, and the yield was so small that we cannot feel sure that the period is not due to an impurity. It may, however, be identical with the 5.5-minute mercury reported from deuteron bombardment of mercury.[4] Further work on this point is in progress.

It is a pleasure to thank Professor E. O. Lawrence for his interest. We are indebted to Professor G. T. Seaborg and Dr. E. Segrè for valuable discussions. Our thanks are also due for financial support to the Research Corporation and the Rockefeller Foundation.

[1] Heyn, Nature **139**, 842 (1937).
[2] M. L. Pool, J. M. Cork and R. L. Thornton, Phys. Rev. **52**, 239 (1937).
[3] E. McMillan, M. Kamen and S. Ruben, Phys. Rev. **52**, 375 (1937).
[4] Krishnan and Nahum, Proc. Camb. Phil. Soc. **36**, 490 (1940).
[5] Anderson, Nature **137**, 457 (1936).
[6] R. S. Krishnan, Proc. Camb. Phil. Soc. **37**, 186 (1941).
[7] R. Sherr, K. T. Bainbridge and H. H. Anderson, Phys. Rev. **60**, 473 (1941).
[8] G. E. Valley, Phys. Rev. **60**, 167 (1941).